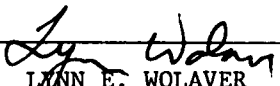MICROCOPY RESOLUTION TEST CHART
NATIONAL BUREAU OF STANDARDS-1963-A

AD-A171 284

(a Entered)

REPORT DOCUMENTATION PAGE		READ INSTRUCTIONS BEFORE COMPLETING FORM
1. REPORT NUMBER AFIT/CI/NR 86- 123D	2. GOVT ACCESSION NO.	3. RECIPIENT'S CATALOG NUMBER
4. TITLE *(and Subtitle)* A Simple Solar, Spectral Model For Studying The Effects Of Cloud Cover And Surface Albedo On The Incoming Solar Radiation		5. TYPE OF REPORT & PERIOD COVERED THESIS/DISSERTATION
		6. PERFORMING ORG. REPORT NUMBER
7. AUTHOR(s) Alfred Merrill Powell, Jr.		8. CONTRACT OR GRANT NUMBER(s)
9. PERFORMING ORGANIZATION NAME AND ADDRESS AFIT STUDENT AT: The University of Michigan		10. PROGRAM ELEMENT, PROJECT, TASK AREA & WORK UNIT NUMBERS
11. CONTROLLING OFFICE NAME AND ADDRESS AFIT/NR WPAFB OH 45433-6583		12. REPORT DATE 1986
		13. NUMBER OF PAGES 237
14. MONITORING AGENCY NAME & ADDRESS(*if different from Controlling Office*)		15. SECURITY CLASS. *(of this report)* UNCLAS
		15a. DECLASSIFICATION/DOWNGRADING SCHEDULE

16. DISTRIBUTION STATEMENT *(of this Report)*

APPROVED FOR PUBLIC RELEASE; DISTRIBUTION UNLIMITED

DTIC
ELECTE
AUG 2 3 1986

17. DISTRIBUTION STATEMENT *(of the abstract entered in Block 20, if different from Report)*

B

18. SUPPLEMENTARY NOTES

APPROVED FOR PUBLIC RELEASE: IAW AFR 190-1

LYNN E. WOLAVER
Dean for Research and
Professional Development
AFIT/NR

19. KEY WORDS *(Continue on reverse side if necessary and identify by block number)*

20. ABSTRACT *(Continue on reverse side if necessary and identify by block number)*

ATTACHED.

DTIC FILE COPY

ABSTRACT

A SIMPLE SOLAR, SPECTRAL MODEL FOR STUDYING

THE EFFECTS OF CLOUD COVER AND SURFACE ALBEDO

ON THE INCOMING SOLAR RADIATION

by

Alfred Merrill Powell, Jr

Major, U.S. Air Force

1986

Degree Awarded: Ph.D. in Atmospheric Science

Number Of Pages: 237

Institution: The University of Michigan

The effect of cloud cover and surface albedo on the solar
insolation at the surface of the Earth was investigated. The
model uses Bird's (1984) clear sky model for direct-normal
and diffuse horizontal irradiance as its basis. Bird's model
was modified to include inclined surfaces and cloud cover.
The clouds were modelled using parameterizations developed
by Welch, Cox and Davis (1980) and a weighting technique to
account for cloud shape using plane-parallel calculations. —

)

86   8   ⌐⌐   017

suggested by Welch and Wielicki (1984). The radiative
transfer in the cloud was modelled by a two stream
approximation known as the Shuster-Schwarzchild method. The
model results were compared with clear sky broadband and
spectral observations, and cloudy broadband observations.
The clear sky spectral observations were obtained from the
Solar Energy Research Institute (SERI) in Golden, Colorado.
The broadband observations were obtained from the Solar and
Meteorological Research Program at the University of
Michigan. The effects of cloud amount, cloud thickness,
cloud type, and surface albedo are demonstrated. Cloud
amount and cloud thickness are the predominant cloud factors
affecting insolation. High surface albedos tend to slow the
decrease in insolation due to increasing cloud cover; while
low surface albedos cause greater variation in insolation
under the same circumstances. The model has the capability
to simulate simple mountain obstructions. However, no cases
with obstructions are presented. The model produces
terrestrial spectra between 0.28 and 4.0 micrometers with a
resolution of approximately 10 nm. The goal of this work is
to provide researchers with the capability to calculate
spectral irradiance for different atmospheric conditions and
different collecting surface geometries.

Key Bibliography

Bird, R.E.; "A Simple Solar Spectral Model For Direct-Normal
     And Diffuse Horizontal Irradiance". Solar
     Energy, 32(4), 1984, pp. 461-471.

A SIMPLE SOLAR, SPECTRAL MODEL FOR STUDYING

THE EFFECTS OF CLOUD COVER AND SURFACE ALBEDO

ON THE INCOMING SOLAR RADIATION

by

Alfred Merrill Powell, Jr

A dissertation submitted in partial fulfillment
of the requirements for the degree of
Doctor of Philosophy
(Atmospheric Science)
in The University of Michigan
1986

Doctoral Committee:

Professor Frederick L. Bartman, Chairman
Professor S. Roland Drayson
Professor William R. Kuhn
Professor Charles E. Olson

DEDICATION

This dissertation is dedicated to my mother,
father, and sister for their support and
encouragement.

ACKNOWLEDGEMENTS

Accession For

NTIS

DTIC T

Unau

Just

By

Di

Av

Dist

A-1

iii

TABLE OF CONTENTS

LIST OF FIGURES

CHAPTER III

APPENDICES

LIST OF TABLES

LIST OF APPENDICES

CHAPTER I

INTRODUCTION

The purpose of this research is to develop a solar
spectral model that describes the instantaneous and daily
solar radiation flux for a given location on the Earth. The
model was designed so the results would be valid at the
surface of the Earth and the top of the atmosphere. The
author's desire was to construct a solar spectral model
which would compute the global, direct, diffuse, and
direct-normal radiation incident on the surface. It was also
desirable to obtain the spectral fluxes of radiation leaving
the top of the atmosphere for those individuals interested
in remote sensing applications. With this purpose in mind,
several types of models were studied.

Many of the models for solar radiation were designed
with a specific purpose in mind. A model developed by Szeicz
(1974) is specialized for use in plant growth. Other models
were designed for particular locations (Barbaro, 1979),
clear sky cases only (Bird, 1984), for slopes of different
orientation (Temps and Coulson, 1977; Sweat and Carroll,
1983), and for overcast skies only (Atwater and Ball, 1981;
Kasten and Dzeplak, 1980; Liou, 1976). Some models were
statistical correlations between observed parameters and the

solar radiation measured at the surface (Stanhill, 1983). Some models dealt only with the ultraviolet portion of the solar spectrum (Leighton, 1961; Green, 1974). There were models that used a multilayered atmosphere (Dave, 1978; Dave and Brauslau, 1974) while others used only a single layer (Bird, 1984). In some cases, the models were too restrictive to be used in a general sense and others were too difficult to be used by researchers outside the physical sciences due to their complexity.

There are many parameters and factors which should be considered when developing a general solar spectral model. Most of the essential factors are listed in Figure 1.A. The multiplicity of factors and their interaction make it difficult to maintain a simple yet realistic model of the effects of the atmosphere. However, an attempt will be made to include all of the factors listed in the figure as well as others when needed.

The intent behind developing this model is to construct a simple, solar spectral model which has the basic components so that it may be used in a general fashion by a large group of users. The primary user groups are expected to be in the fields of solar energy engineering, agriculture and plant ecology, environmental photochemistry, and remote sensing. The model should distinguish between the global, direct, and diffuse components of the solar energy incident on a surface of arbitrary orientation. Hooper and Brunger (1980) showed that the diffuse fraction of the total solar

Viewing geometry:
Solar zenith angle, θ_i
Viewing angle, θ_r
Azimuthal angle, ϕ_i or ϕ_r
Relative azimuthal angle, ψ,
  where $\psi = \phi_r - \phi_i + 180$
Altitude of sensor, H

Meteorological parameters:
Relative humidity
Cloud cover
Surface pressure

Atmospheric optical parameters:
Optical thickness, τ_A
Aerosol type (phase function)
Single-scattering albedo, ω_o

Target and background parameters:
Target size
Target reflectance, ρ_t
Background reflectance, ρ_b
Instantaneous field-of-view, IFOV

Figure 1.A

Factors Affecting Apparent Reflectance Determination

(After Bowker, Davis, Myrick, Stacy and Jones, 1985)

radiation reaching the surface is very important, especially for the more northern (southern) latitudes where the air mass path is large. They also pointed out that local climate (terrain, proximity to bodies of water, local circulation) has more effect than latitude. For tilted surfaces, Hooper and Brunger (1980) showed for 11 Cana_ian cities that about 40 percent of the annual incident short wave solar radiation on such surfaces is diffuse (sky plus ground diffuse) radiation. The surface albedo is an important factor in the radiative interaction between the atmosphere and the ground. It affects the amount of sky and ground diffuse radiation observed at a particular location.

Many models account for surface albedo in some simple form, usually with an average value near 20 percent for the entire spectrum. However, in practice the surface albedo can vary substantially with wavelength. Figure 1.B shows the variation in reflectance with wavelength for typical vegetation and soil. The differences are rather pronounced in some regions of the spectrum. The effect of different spectral albedos is not usually included in solar radiation models. The reflectances shown in Figure 1.B are hemispheric reflectances measured with a zenith angle relative to the surface of zero degrees (normal to the surface). The surface reflectance changes with the solar zenith angle and the relative orientation of the surface. These factors should be included in any general solar spectral model.
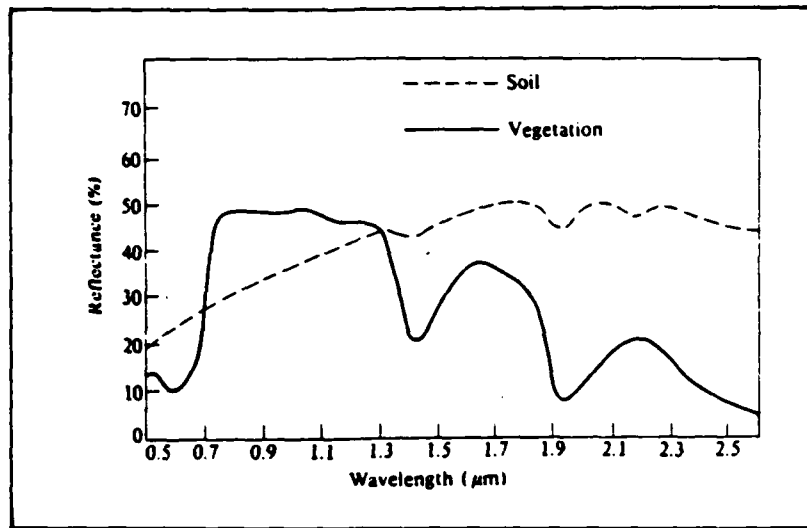
Figure 1.B

Spectral reflectance curves for healthy green vegetation and air-
dried soils. These curves represent averages of 240 spectra from
vegetation and 154 spectra from air-dried soils. The relative
differences in reflectance in the visible (0.4 to 0.7 μm), near-
infrared (0.7 to 1.3 μm), and middle-infrared (1.3 to 3.0 μm)
portions of the spectrum are clearly shown in this data.

(Adapted from Lillesand and Kiefer, 1979)

A desirable characteristic of a general solar spectral model would be to allow the user to select spectral bands from within the range of 0.28 to 4.0 micrometers. This would enhance the usefulness of the model to users who are trying to choose particular spectral bands for their application. Those users interested in remote sensing, agriculture, or solar energy engineering would be particularly interested in being able to compare the radiation available in different spectral bands on slopes of varying orientation at different solar zenith angles. Another factor which directly affects the amount of radiation reaching the surface is the cloud cover.

Clouds are not contained in many of the solar models mainly due to the complexity of the calculations, and the difficulty of obtaining the observations needed to verify the model's results. Clouds have been included so the user may obtain an idea of how clouds may affect their project. The effect of clouds is governed by the thickness of the cloud, the cloud droplet size distribution, the size and shape of the clouds, and the cloud cover. A simple spectral cloud parameterization has been included in the model.

In summary, a general spectral solar radiation model has been constructed which has the following features:

1. It covers the solar spectrum between 0.28 and 4.0 micrometers with 126 finite, non-uniform width, irregularly spaced spectral intervals.

2. It computes the global, direct, and diffuse radiation incident on a plane surface of

arbitrary orientation located at the Earth's surface. The direct-normal radiation at the surface is also computed. Computations of the radiation reaching a satellite observation point at the top of the Earth's atmosphere are made. This radiation is computed in terms of path radiance, global, direct, and diffuse. In this case, the direct radiation is the radiation arriving at the satellite observation point directly from the target. Diffuse radiation is radiation from the target which is scattered to the satellite by the atmosphere. Global radiation is the sum of the direct, diffuse, and path radiance values. The path radiance term in this model is the radiation scattered by the atmosphere to the observation point. The path radiance includes no radiation from the target.

3. The model allows the user to select any spectral band between 0.28 and 4.0 micrometers for the calculations.

4. The model uses spectral surface albedos.

5. The model includes the dependence of albedo on solar zenith angle.

6. A simple, yet quantitative, calculation of the spectral effects of clouds has been included in the model.

7. The model determines the spectral solar radiation reaching an arbitrarily oriented surface at a given location on the Earth.

8. The model adjusts for astronomical factors such as the Earth-sun distance, declination of the sun and sunrise/sunset times.

9. The model accumulates the daily solar radiation on a surface of fixed orientation.

10. The model allows the user to select simple obstructions to sunrise/sunset so that the effects of solar radiation in mountainous areas might be studied.

The model includes many of the desirable features of a general solar spectral radiation model. The criteria for selecting how a particular component or

feature would be modelled was based on computer time, how accurately the form reflected physical science, and the ease of inclusion with the other components of the model.

The unique features in this work are:

1. the inclusion of a select set of spectral surface albedos

2. the inclusion of spectral cloud parameterizations

3. the inclusion of inclined surfaces

4. the inclusion of simple obstructions to sunrise and sunset

5. the ability to obtain insolation values representative of instantaneous, hourly or daily time intervals.

The program is written in ANSI Standard (1977) FORTRAN. It is available from the Department of Atmospheric and Oceanic Science, The University of Michigan.

CHAPTER II

THE MODEL

In this chapter, the basic components of the model will
be discussed. In some instances, the model allows the user
the option of choosing which technique or parameters are to
be used in the model. These options will be outlined and
discussed where necessary. With a large number of composite
techniques being used together to form a general model,
simplicity and accuracy were the primary criteria for
choosing the basis of the model. The use of the complex and
rigorous SOLTRAN and LOWTRAN radiative codes for clear skies
seemed computationally unnecessary as we are striving for an
overall error of less than 5%. To incorporate clouds into
the more rigorous radiative transfer schemes could lead to
computer computation times much higher than would prove
economically feasible to many users. To this end, the
foundation for this model was chosen to be Bird's simple
solar spectral model for direct-normal and diffuse
horizontal irradiance (1984). Bird compared his model with
the results of the BRITE and SOLTRAN 5 models which are
believed accurate within 5% on the direct-normal and within
15% on the diffuse horizontal. Bird's model compares very

well with these model results. Comparisons of this model
with experimental data have not been published. The Bird
model was chosen for use in this study because it is simple,
accurate and has good spectral resolution (approximately 10
nm). Modifications were made to the clear sky model to
account for inclined surfaces.

2.1 Extraterrestrial Solar Spectrum

The Neckel and Labs extraterrestrial solar spectrum was
used by Bird. According to Bird, Hulstrom, and Lewis (1983),
who did a comparative study between the extraterrestrial
data sets available, the Neckel and Labs data set (1981) is
the best currently in use. This data set is designed to
reflect the extraterrestrial solar spectrum under normal
conditions at the mean Earth-sun distance. The Neckel and
Lab's spectrum has a resolution of 0.005 micrometers. This
is better resolution than the spectrum by Thekaekara which
has been used as a standard by many investigators. For the
purposes of developing a solar spectral model, the spectrum
was divided into 126 non-uniform width, spectral intervals
between 0.28 and 4.0 micrometers. With the exception of the
first four values, the values of the extraterrestrial solar
spectrum are those derived by Bird from the Labs and
Neckel's data set and are shown in Table 2.1.A. The first
four values of 0.28, 0.285, 0.290, and 0.295 micrometers
were derived from the extraterrestrial spectrum of Frolich

WAVELENGTH	EXTRATERRESTRIAL SPECTRUM				WAVELENGTH	EXTRATERRESTRIAL SPECTRUM			
(μm)	($W\ m^{-2}\ \mu m^{-1}$)	$a_{w\lambda}$	$a_{o\lambda}$	$a_{u\lambda}$	(μm)	($W\ m^{-2}\ \mu m^{-1}$)	$a_{w\lambda}$	$a_{o\lambda}$	$a_{u\lambda}$
0.280	186.2	0.0	52.0	0.0					
0.285	299.7	0.0	35.0	0.0					
0.290	309.0	0.0	18.0	0.0					
0.295	553.7	0.0	11.0	0.0					
0.300	535.9	0.0	10.0	0.0	0.980	767.0	1.48	0.0	0.0
0.305	558.3	0.0	4.80	0.0	0.9935	757.6	0.1	0.0	0.0
0.310	622.0	0.0	2.70	0.0	1.04	688.1	0.00001	0.0	0.0
0.315	692.7	0.0	1.35	0.0	1.07	640.7	0.001	0.0	0.0
0.320	715.1	0.0	0.800	0.0	1.10	606.2	3.2	0.0	
0.325	832.9	0.0	0.380	0.0	1.12	585.9	115.0	0.0	0.0
0.330	961.9	0.0	0.160	0.0	1.13	570.2	70.0	0.0	0.0
0.335	931.9	0.0	0.075	0.0	1.145	564.1	75.0	0.0	0.0
0.340	900.6	0.0	0.040	0.0	1.161	544.2	10.0	0.0	0.0
0.345	911.3	0.0	0.019	0.0	1.17	533.4	5.0	0.0	0.0
0.350	975.5	0.0	0.007	0.0	1.20	501.6	2.0	0.0	0.0
0.360	975.9	0.0	0.0	0.0	1.24	477.5	0.002	0.0	0.05
0.370	1119.9	0.0	0.0	0.0	1.27	442.7	0.002	0.0	0.30
0.380	1103.8	0.0	0.0	0.0	1.29	440.0	0.1	0.0	0.02
0.390	1033.8	0.0	0.0	0.0	1.32	416.8	4.0	0.0	0.0002
0.400	1479.1	0.0	0.0	0.0	1.35	391.4	200.0	0.0	0.00011
0.410	1701.3	0.0	0.0	0.0	1.395	358.9	1000.0	0.0	0.00001
0.420	1740.4	0.0	0.0	0.0	1.4425	327.5	185.0	0.0	0.05
0.430	1587.2	0.0	0.0	0.0	1.4625	317.5	80.0	0.0	0.011
0.440	1837.0	0.0	0.0	0.0	1.477	307.3	80.0	0.0	0.005
0.450	2005.0	0.0	0.003	0.0	1.497	300.4	12.0	0.0	0.0006
0.460	2043.0	0.0	0.006	0.0	1.520	292.8	0.16	0.0	0.0
0.470	1987.0	0.0	0.009	0.0	1.539	275.5	0.002	0.0	0.005
0.480	2027.0	0.0	0.014	0.0	1.558	272.1	0.0005	0.0	0.13
0.490	1896.0	0.0	0.021	0.0	1.578	259.3	0.0001	0.0	0.04
0.500	1909.0	0.0	0.030	0.0	1.592	246.9	0.00001	0.0	0.06
0.510	1927.0	0.0	0.030	0.0	1.610	244.0	0.0001	0.0	0.13
0.520	1831.0	0.0	0.048	0.0	1.630	243.5	0.001	0.0	0.001
0.530	1891.0	0.0	0.063	0.0	1.646	234.8	0.01	0.0	0.0014
0.540	1898.0	0.0	0.075	0.0	1.678	220.5	0.036	0.0	0.0001
0.550	1892.0	0.0	0.085	0.0	1.740	190.8	1.1	0.0	0.00001
0.570	1840.0	0.0	0.120	0.0	1.80	171.1	130.0	0.0	0.00001
0.593	1768.0	0.075	0.119	0.0	1.860	144.5	1000.0	0.0	0.0001
0.610	1728.0	0.0	0.120	0.0	1.920	135.7	500.0	0.0	0.001
0.630	1658.0	0.0	0.090	0.0	1.960	123.0	100.0	0.0	4.3
0.656	1524.0	0.0	0.065	0.0	1.985	123.8	4.0	0.0	0.20
0.6676	1531.0	0.0	0.051	0.0	2.005	113.0	2.9	0.0	21.0
0.690	1420.0	0.016	0.028	0.15	2.035	108.5	1.0	0.0	0.13
0.710	1399.0	0.0125	0.018	0.0	2.065	97.5	0.4	0.0	1.0
0.718	1374.0	1.80	0.015	0.0	2.10	92.4	0.22	0.0	0.08
0.7244	1373.0	2.5	0.012	0.0	2.148	82.4	0.25	0.0	0.001
0.740	1298.0	0.061	0.010	0.0	2.198	74.6	0.33	0.0	0.00038
0.7525	1269.0	0.0008	0.008	0.0	2.270	68.3	0.50	0.0	0.001
0.7575	1245.0	0.0001	0.007	0.0	2.360	63.8	4.0	0.0	0.0005
0.7625	1223.0	0.00001	0.006	4.0	2.450	49.5	80.0	0.0	0.00015
0.7675	1205.0	0.00001	0.005	0.35	2.5	48.5	310.0	0.0	0.00014
0.780	1183.0	0.0006	0.0	0.0	2.6	38.6	15000.0	0.0	0.0006t
0.800	1148.0	0.0360	0.0	0.0	2.7	38.6	22000.0	0.0	100.0
0.816	1091.0	1.60	0.0	0.0	2.8	32.0	8000.0	0.0	150.0
0.8237	1062.0	2.5	0.0	0.0	2.9	28.1	650.0	0.0	0.13
0.8315	1038.0	0.500	0.0	0.0	3.0	24.8	240.0	0.0	0.0095
0.840	1022.0	0.135	0.0	0.0	3.1	22.1	230.0	0.0	0.001
0.860	998.7	0.00001	0.0	0.0	3.2	19.6	100.0	0.0	0.8
0.880	947.2	0.0026	0.0	0.0	3.3	17.5	120.0	0.0	1.9
0.905	893.2	7.0	0.0	0.0	3.4	15.7	19.5	0.0	1.3
0.915	868.2	5.0	0.0	0.0	3.5	14.1	3.6	0.0	0.075
0.925	829.7	5.0	0.0	0.0	3.6	12.7	3.1	0.0	0.01
0.930	830.3	27.0	0.0	0.0	3.7	11.5	2.5	0.0	0.00195
0.937	814.0	55.0	0.0	0.0	3.8	10.4	1.4	0.0	0.004
0.948	786.9	45.0	0.0	0.0	3.9	9.5	0.17	0.0	0.29
0.965	768.3	4.0	0.0	0.0	4.0	8.6	0.0045	0.0	0.025

Table 2.1.A

The Neckel and Labs revised extraterrestrial spectrum
and atmospheric absorption coefficients at 126 wavelengths.

(Adapted from Bird, 1984)

and Werli (1981) of the World Radiation Center in Davos,
Switzerland. Bird's original clear sky model did not extend
to 0.28 micrometers and his model was extended to include
the range of 0.28 to 4.0 micrometers. The Werli and Frolich
data set was largely based on Labs and Neckel's revised
extraterrestrial solar spectrum (1981) and the two data sets
are very compatible. Also included in Table 2.1.A are the
absorption coefficients for water vapor (subscript w), ozone
(subscript o), and the uniformly mixed gases (subscript u).
The units of the absorption coefficients are square
centimeters per gram, per centimeter, and per kilometer
respectively.

2.2 Astronomical Factors

Since the orbit of the Earth is not circular, one
should adjust the values of the extraterrestrial solar
spectrum for the Earth-sun distance on a given day of the
year. Presently, the Earth's orbit is only slightly
elliptical (the eccentricity is small). However, the square
of the Earth-sun distance varies by $\pm$ 3.5 percent; hence,
the solar irradiance at the Earth varies by $\pm$ 3.5 percent
(Iqbal, 1983). Paltridge and Platt (1976) give an expression
for the square of the ratio of the mean Earth-sun distance
to the Earth-sun distance with the dependent variable being
the day of the year. The accuracy of this expression is
quoted as being better than 0.0001. The expression for the

square of the Earth-sun ratio is:

$$(Rm \ / \ R)^2 = 1.000110 + 0.034221 \cos (\ \theta_o) + 0.001280 \sin (\ \theta_o)$$
$$+ 0.000719 \cos (2\theta_o) + 0.000077 \sin (2\theta_o)$$

where

Rm = mean Earth-Sun distance

R = actual Earth-Sun distance

θ_O = an expression defined in terms of the day of the year

$$2 \pi dn \ / \ 365$$

dn = day of the year (0=Jan 1; 364=Dec 31)

In addition to the correction for the Earth-sun distance, other astronomical factors affect the solar radiation arriving at the Earth's surface. One of these factors is the declination of the sun. The declination is the angular distance, measured along an hour circle, between the sun and the celestial equator. The declination varies by day of the year and can be expressed in the following form (Spencer, 1971; Paltridge and Platt, 1976):

$$\delta = 0.006918 - 0.399912 \cos (\ \theta_o) + 0.070257 \sin (\ \theta_o)$$
$$- 0.006758 \cos (2\theta_o) + 0.000907 \sin (2\theta_o)$$
$$- 0.002697 \cos (3\theta_o) + 0.001480 \sin (3\theta_o)$$

where

δ = declination in radians

The expression for declination has a maximum error of 0.0006

radians or an error less than 3 minutes. These expressions can be found in Paltridge and Platt (1976).

Another important astronomical factor is the oblateness of the Earth. Van Hemelruck (1983) studied the effects of oblateness on the distribution of the radiation which reaches the Earth and the other planets in the solar system. Van Hemelruck found the oblateness effect on the solar radiation is a few tenths of a percent. The largest differences being decreases in solar radiation. The maximum increase was 0.1 percent while the largest decrease was 1.3 percent with most of the decreases in the range of 0.1 to 0.5 percent. The study showed the daily insolation accumulated at a given location could be decreased by 2 percent due to oblateness. The net result of oblateness is to decrease the amount of solar radiation reaching the planet. The largest losses derived from this effect occur between 55 and 85 degrees latitude on the Earth. Even though the effects of oblateness could have been included in the present model, it was neglected. While the effects of the oblateness can be determined to have an effect of a few tenths of a percent on the solar radiation, the effect was not significant enough to be included in this study.

2.3 Atmospheric Transmittance

The atmospheric transmittance is calculated for the regions of clear sky, i.e. regions without cloud, using the

formulation by Bird. Bird's model compares well with the
BRITE and SOLTRAN 5 models (See Figures 2.4.F and G). The
BRITE and SOLTRAN 5 models are believed to be accurate
within ±5% on the direct-normal radiation and within ± 15%
on the diffuse radiation (Bird, 1984). Bird uses the
multiplication technique for obtaining the transmissions.
The basic equation used for the direct-normal component of
the solar radiation is :

$$I_{d\lambda} = H_{o\lambda} T_{r\lambda} T_{a\lambda} T_{o\lambda} T_{u\lambda} T_{w\lambda}$$

where

$I_{d\lambda}$ = Direct-normal component of the solar radiation

$H_{o\lambda}$ = Extraterrestrial solar irradiance at the mean Earth-Sun
distance

$T_{r\lambda}$ = Transmittance function for Rayleigh scattering

$T_{a\lambda}$ = Transmittance function for aerosol scattering

$T_{o\lambda}$ = Transmittance function for ozone absorption

$T_{w\lambda}$ = Transmittance function for water vapor absorption

$T_{u\lambda}$ = Transmittance function for the uniformly mixed gases
(oxygen and carbon dioxide)

Bird and Hulstrom (1981) studied the equations used for computing the direct irradiance from several different models. Equations of similar structure have been referred to in the literature as forms of the transport equation. Bird and Hulstrom compared several forms of the transport equation developed by different researchers (Hoyt, Watt, Lacis and Hansen, Atwater and Ball, and ASHRAE), they concluded this form of the transport equation provided the closest agreement with the more rigorous SOLTRAN model. Based on this finding, the Bird clear sky model, which already contains this formalism, was used as the basis for this solar spectral model. An inherent assumption has been made when this form of the transport equation is used. The assumption is that the attenuation by each constituent is independent of every other constituent. Restated, this implies that the transmittance measured through pure materials can be combined in the form of the transport equation to produce the transmittance through a mixture of the materials. This is not true. With this methodology, two constituents which absorb in the same spectral region may cause over-attenuation or under-attentuation in the final results. For constituents which absorb in the same spectral region in different layers of the atmosphere, this form of the transport equation usually results in over-attenuation in the final results.

2.3.1 Scattering Processes

The scattering processes discussed throughout this paper have some underlying assumptions. All the scattering processes have been assumed to be independent scattering which occurs when the average separation between the particles is several times the particle radius (McCartney, 1976). This insures that the scattering pattern from one particle is not affected by the scattering pattern from neighboring particles. The separation criterion is satisfied in all typical meteorological conditions. Since the particles in the atmosphere are randomly arranged and randomly moving, there are no coherent phase relationships between the separately scattered radiation. This implies that there are no discernible interference patterns. The resultant simplification is that the intensities of the scattered waves rather than their amplitudes are additive. This type of scattering is called incoherent scattering.

It was assumed that the particles are exposed only to the light of an incident or direct beam. This assumption is referred to as single scattering. Hence, there will be references to single scattering ratios and cross sections. "No account has been taken of the fact that each particle in a scattering volume is exposed to and also scatters a small amount of the light already scattered by the other particles. Processes which account for the rescattered light are referred to as multiple or secondary scattering

processes." (McCartney, 1976). A form of multiple scattering has been included in the model, however. The multiple reflections between layers of atmosphere is a form of multiple scattering. The adding technique is used to combine the atmospheric layers in this model and is a series approximation to account for the multiple reflections between the layers. In this sense, some multiple scattering is accounted for in this model. The adding method was developed without regard for the thickness of the layers to be combined. The only requirement is that the total transmittance and total reflection for each layer be known. Since the single scattering approximation is used in the model, each initial layer should be thin enough that the single scattering approximation for the reflection and transmission be valid.

Scattering processes are dependent upon the ratio of the particle size to the wavelength of the light. The two primary scattering solutions are Rayleigh and Mie scattering and the model distinguishes between the two cases. The effects of polarization have been neglected since Hansen (1971) has shown that the values computed from exact theory including polarization differ by less than 0.1 percent from the scalar approximation in which polarization is neglected.

Hansen (1969) demonstrated that it was not necessary to use the complete cloud phase function to determine the results of the scattering processes. He showed that the truncated phase functions, while giving errors in the

angular distribution for scattering were accurate for most practical applications. In Hansen's model for multiple scattering in cloudy and hazy atmospheres, he performs his calculations using only the forward to backward scattering ratio, a procedure that is adopted here.

2.3.2 Rayleigh Scattering

Bird used an expression adapted from the LOWTRAN 5 atmospheric transmittance model to compute the transmittance due to Rayleigh scattering. The results agree well with Pendorf's data on the refractive indices of standard air and the Rayleigh scattering coefficients. The expression for the Rayleigh scattering transmittance is :

$$T_{r\lambda} = \exp\left(-M'\big/[\lambda^4 (115.6406 - 1.335/\lambda^2)]\right)$$

where

M' = Pressure corrected air mass

λ = Wavelength in micrometers

To obtain the pressure corrected air mass, one must first obtain the relative air mass. Bird elected to use the formulation for the relative air mass derived by Kasten. Kasten's expression for the relative air mass is:

$$M = [\cos(Z) + 0.15 (93.885 - Z)^{-1.253}]^{-1}$$

where

M = Relative air mass in atmospheres

Z = Apparent solar zenith angle in degrees

To obtain the pressure corrected air mass, multiply the relative air mass, M, by the ratio P / P_o.

$$M' = M \left(\frac{P}{P_o} \right)$$

where

P = surface pressure in millibars (mb)

P_o = 1013 mb

2.3.3 Aerosol Scattering And Absorption

Aerosols are solid or liquid particles that remain suspended in the air and tend to follow the motion of the air. The typical meteorological precipitates (rain, snow and hail) are not aerosols. Natural aerosol particles range in size from 10^{-3} to 10^{2} micrometers (Iqbal, 1983). The sources of these particles include smoke, haze, clouds, pollen, pollution, volcanic eruptions, sandstorms, forest fires,

agricultural burning, meteoric dust, and marine based particulates to include salt crystals and ocean spray. The degree of turbidity is based on the number of aerosol particles per cubic centimeter and the distribution of the particle sizes. One of the biggest problems in calculating solar irradiance at the surface is accounting for the effects of aerosols. Part of the difficulty is specifying the properties associated with the aerosols. The properties include their size distribution, number, and optical characteristics.

The aerosols produce Mie scattering which is dependent on the ratio of the particle size to the wavelength of the incident radiation. The amount of scattering will also be dependent on whether the dust particles are wet or dry. The optical properties of the particles can change with the degree of 'wetness'. The more detailed treatments of turbidity consider whether the particles are wet or dry, as well as their variability in form, size, distribution and nature of the particles. Techniques for handling aerosols can be reviewed in van de Hulst (1957) and Iqbal (1983). A simple technique for quantifying the effects of aerosols was developed by Angstrom.

Angstrom's technique is not only simple in form, but the attenuation effects (whether absorption or scattering) are included simultaneously. In practice, it is difficult to separate the attenuation effects of scattering and absorption by dust. This technique includes the effects of

both wet and dry particles; i.e. all aerosols. Angstrom
assumed a dependence of the attenuation coefficient of the
form:

$$K_a = \beta \lambda^{-\alpha}$$

where

K_a = attenuation coefficient

β = turbidity coefficient

α = turbidity exponents

The turbidity coefficient is an index representing the
amount of aerosols present while the turbidity exponent is
related to the size distribution of the aerosol particles. A
more detailed discussion of this technique can be found in
other sources (Angstrom 1961, 1964). The turbidity
coefficient and exponent can be determined simultaneously
with a dual wavelength sun photometer. The wavelengths
usually chosen for the sun photometer are 0.38, 0.5, and
0.88 micrometers. The model uses the value of turbidity at
0.5 micrometers as its definition of turbidity.

In the more rigorous atmospheric transmission models,
both the scattering and extinction by aerosols is computed
using Mie scattering theory. Calculations of this sort
require a knowledge of the aerosol particle size
distribution, the complex index of refraction with

wavelength, and the scattering phase function. These
variables are not readily available for each individual
scenario. As a consequence, a typical aerosol distribution
is usually chosen for study purposes. Bird chose to use the
rural aerosol distribution adopted by Shettle and Fenn
(1975) with the particle size distribution shown in Figure
2.3.3.A. Two aerosol distributions are combined to form the
rural aerosol model. To describe this distribution, Leckner
(1978) used an approximate expression of the Angstrom
formalism to determine the turbidity or aerosol optical
depth as a function of wavelength. This technique assumes
that the plot of turbidity versus wavelength on a log-log
scale will be linear. The rural aerosol distribution in this
model shows curvature when plotted on a log-log scale. To
compensate for this, Bird used the multiterm Angstrom
formalism as follows:

$$\tau_{a\lambda} = \beta_n \lambda^{-\alpha_n}$$

$$n=1 \text{ for } 0.28 \leq \lambda \leq 0.5 \ \mu m$$

$$n=2 \text{ for } 0.50 < \lambda \leq 4.0 \ \mu m$$

where

$\tau_{a\lambda} =$ turbidity

$\beta_n =$ turbidity coefficients directly proportional
to the turbidity

$\alpha_n =$ turbidity exponent related to the aerosol size
distribution
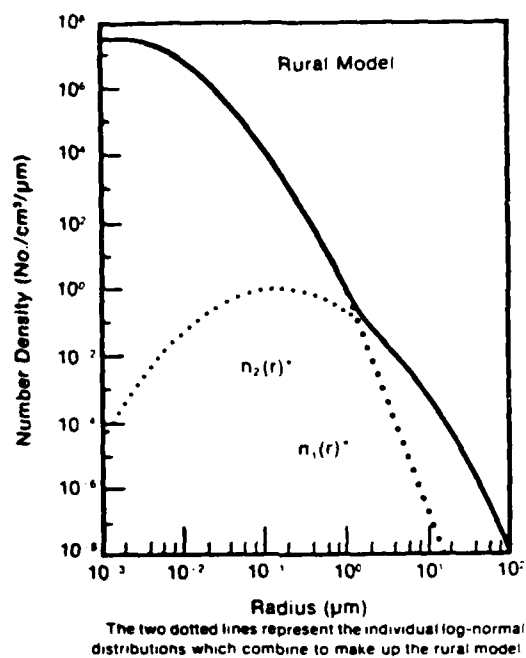
Figure 2.3.3.A

Aerosol particle size distribution for rural aerosol model.

(After Bird, 1984)

τ_a (0.5 μm)	β_1	β_2
0.1	0.0490	0.0433
0.27	0.1324	0.1170
0.37	0.1814	0.1603
0.51	0.2501	0.2210

Table 2.3.3.B

Angstrom turbidity coefficients for several turbidities
in the rural aerosol model (After Bird, 1984).

The exponents are determined by the slope of the line on a
log-log plot of turbidity versus wavelength. To approximate
the rural distribution shown in Figure 2.3.3.A, two straight
line segments were used. The values of the turbidity
coefficient and the turbidity exponent have been determined
based on these two line segments. Table 2.3.3.B shows the
Angstrom turbidity coefficients for several turbidities
using the rural aerosol model. The turbidity coefficients in
the table can be used to generate coefficients for other
turbidities by the expression:

$$\beta_n = \beta_o \left(\frac{\tau_n}{\tau_o}\right)$$

where

β_n = new turbidity coefficient

β_o = old turbidity coefficient

τ_n = new turbidity value

τ_o = old turbidity value

The turbidity coefficients and turbidity exponents are valid
for two different regions of the rural aerosol distribution,
each represented by a straight line. The subscripts 1 and 2
represent the two line segments or regions of the rural
aerosol model. The coefficient and exponent with the

subscript 1 are valid between 0.28 and 0.5 micrometers. The coefficient and exponent with the subscript 2 are valid between 0.5 and 4.0 micrometers. The values of the turbidity exponents are:

$$\alpha_1 = 1.0274$$

$$\alpha_2 = 1.2060$$

The turbidity at 0.5 micrometers is the input to calculate the turbidity coefficients and exponents by wavelength. The transmittance function for the aerosols is given by:

$$T_{a\lambda} = \exp\left[-\beta\lambda_n^{-\alpha_n} M\right] \qquad (\text{for } n = 1 \text{ or } 2)$$

where

M = Relative air mass in atmosphere

2.3.4 Water Vapor Absorption

There are several atmospheric constituents which affect the absorption of the incoming solar radiation. Figure 2.3.4.A shows the regions of the solar spectrum most affected by absorption. The four primary absorbing constituents are water vapor (H_2O), ozone (O_3), oxygen (O_2), and carbon dioxide (CO_2). The last two constituents are often called the uniformly mixed gases because their mixing
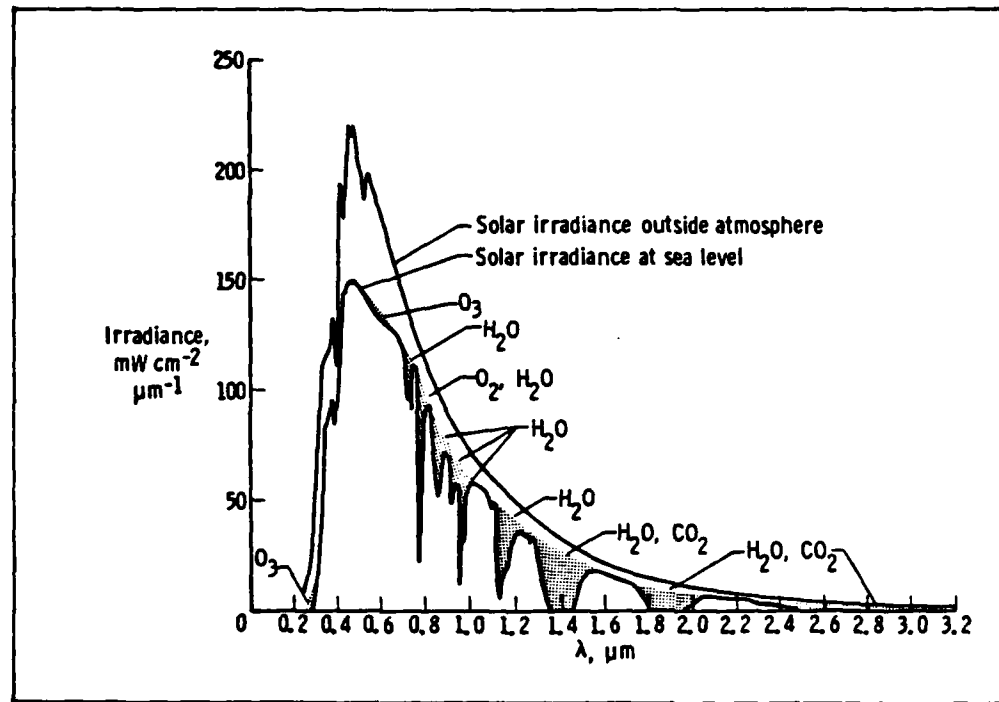
Figure 2.3.4.A

Solar spectral irradiance outside the atmosphere and at the surface, for a solar zenith angle of 0°. Features due to principal absorbers are identified.

(From Bowker, Davis, Myrick, Stacy and Jones, 1985)

ratio is nearly constant to a height of 100 kilometers. Bird
uses expressions developed by Leckner to approximate the
influence of the absorbing gases. In each case, one must
know the integrated amount of each gas in a vertical column.
Since the calculations are based on a vertical column, the
accuracy of the calculated absorption will decrease with
increasing path distance through the atmosphere (or
increasing zenith angle). The discrepancies are usually
attributed to the variation in the integrated vertical
amount of each gas with distance from the initial region
(Leckner, 1978). Usually the deviations from the calculated
values are small with oxygen and carbon dioxide. Water vapor
has the most variable effect on the absorption of the
incoming solar radiation.

Bird used a modified expression of Leckner's in his
model to compute the absorption by water vapor. The
transmittance function for water vapor used in Bird's model
was:

$$T_{w\lambda} = \exp (-0.3285\ a_{w\lambda}[w + (1.42 - w)0.5]\ M$$

$$/\ (1.0 + 20.07\ a_{w\lambda}\ M)^{0.45}\ )$$

where

$a_{w\lambda}$ = water vapor absorption coefficient

w = precipitable water in a vertical path in cm

2.3.5 Ozone Absorption

The ozone transmittance equation of Leckner was used in Bird's model. The expression follows:

$$T_{o\lambda} = \exp [-a_{o\lambda} O_3 M_o]$$

where

$a_{o\lambda}$ = Ozone absorption coefficient

(See Table 2.1.A)

O_3 = Ozone amount in a vertical path cm (NTP)

M_o = Air mass expression for ozone

The air mass expression for ozone is given by Paltridge and Platt as :

$$M_o = 35.0 / [1224.0 \cos^2 (z) + 1]^{0.5}$$

where

z = zenith angle of the sun.

If the ozone amount or ozone data are not available, the model by Van Heuklon can be used to determine the ozone amount for a vertical column. The model by T.K. Van Heuklon is a global model for calculating the amount of ozone in a vertical column at a particular location. The information required to determine an ozone amount are latitude, longitude, and day of the year. Van Heuklon used the observed distribution of ozone in a correlative type expression which calculates the ozone content of the atmosphere for any place in the world. The expression for

the ozone content is:

$$O_3 = J + (A + C \sin [D(E+F)] +$$

$$G \sin[H(\lambda + I)]) \sin^2 (\beta\varphi)$$

where

φ = latitude in degrees

λ = longitude in degrees

The other parameters (A thru I) are shown in Table 2.3.5.A. The values of the parameters vary depending on the hemisphere. Parameter E is the day of the year and has the same formulation regardless of hemisphere. Deviations in the daily ozone amount as high as thirty percent can occur (Hammond and Maugh, 1974). This model primarily predicts the influence of the seasonal effects of the general circulation on the ozone amount rather than the effects of diurnally controlled forcing functions. This empirical model is accurate within 5 percent for most areas of the world. The model values typically range from a 1 percent underestimation to a 5 percent overestimation. In the higher latitudes (above 80 degrees), the model is believed to be fairly accurate. However, the lack of observed values for comparison prohibit a statement about the accuracy of the model for latitudes greater than 80 degrees. Figure 2.3.5.B shows of the deviation between the calculated and observed annual averages for North America (Van Heuklon, 1979).

31

Parameter	N. hemisphere	Value of parameter both hemispheres	S. hemisphere
A	150.0	—	100.0
β	1.28	—	1.5
C	40.0	—	30.0
D		0.9865	
E		Jan. $1 = 1.0$, $2 = 2.0$, etc.	
F	-30.0	—	152.625
G		20.0	
H	3.0	—	2.0
I	20.0 if $\lambda = +$ / 0.0 if $\lambda = -$	—	-75.0
J		235.0	
φ	$N = +$		$S = -$
λ		$E = +$, $W = -$	

Table 2.3.5.A

Values of parameters in the ozone model

(After Van Heuklon, 1979)
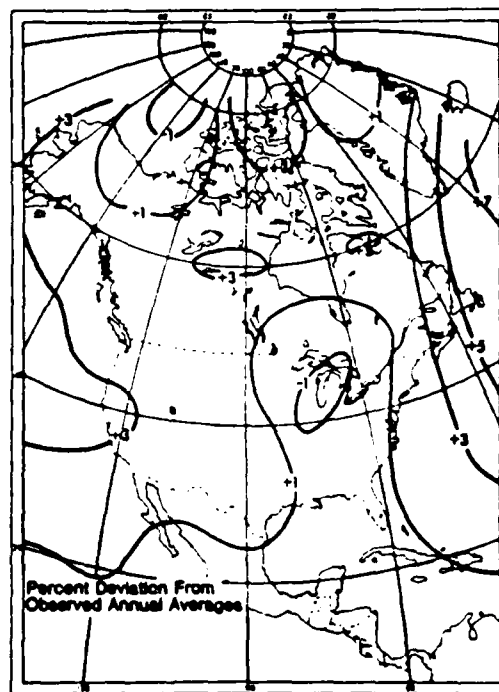
Figure 2.3.5.B

Comparison calculated vs observed annual averages of atmospheric ozone for North America

(After Van Heuklon, 1979)

The solar spectral model developed by this author contains an option where the user may elect to use Van Heuklon's model for estimating the ozone amount or enter the ozone amount of his choice in atm-cm.

2.3.6 Absorption By The Uniformly Mixed Gases

Bird used Leckner's expression to compute the transmittance function for the uniformly mixed gases. The uniformly mixed gases in this model are oxygen and carbon dioxide. The transmittance function for the uniformly mixed gases was:

$$T_{u\lambda} = \exp\left[-1.41\ a_{u\lambda} M' / \quad (1 + 118.93\ a_{u\lambda} M')^{0.45} \right]$$

where

$a_{u\lambda}$ = Absorption coefficients for the uniformly mixed gases (See Table 2.1.A)

M' = Pressure corrected air mass.

2.4 Diffuse Horizontal Irradiance

The diffuse irradiance is hard to simply quantify. The distribution of the diffuse component is non-uniform over the sky and changes with the zenith angle of the sun. Brine and Iqbal (1983) developed a method of computing the diffuse radiation based on the broadband work of Davies and Hays. Bird used the equations of Brine and Iqbal except that he
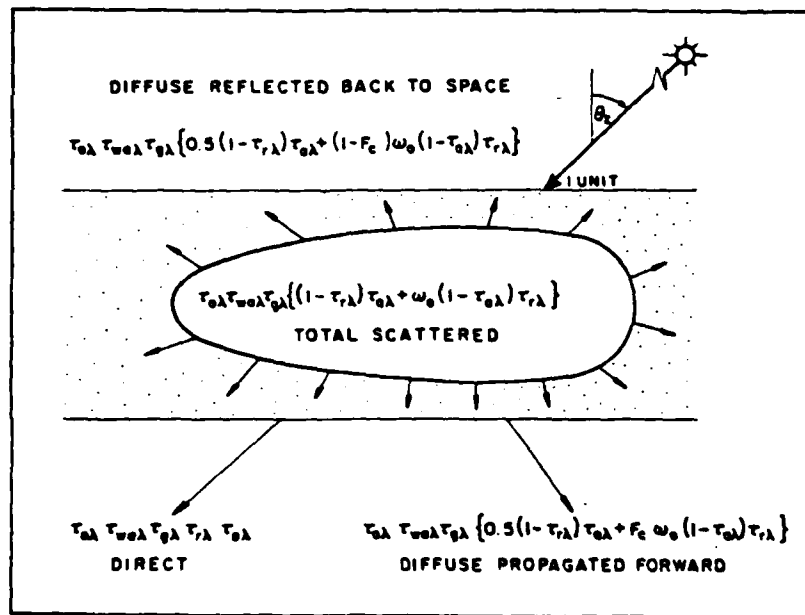
Figure 2.4.A

Partition of radiation into direct, diffuse propagated forward, and diffuse reflected back to space.

(From Iqbal, 1983)

added a correction factor. Figure 2.4.A from Iqbal (1983) shows the direct radiation, total scattered radiation, the diffuse radiation propagated forward and the diffuse radiation relected back to space. The equations used by Bird to express the diffuse radiation make use of the radiation components shown in the figure to compute the diffuse radiation on a horizontal surface. The equations for the diffuse components of radiation are:

$$I_{s\lambda} = (I_{r\lambda} + I_{a\lambda}) \, C_{\lambda} + I_{g\lambda}$$

$$I_{r\lambda} = H_{o\lambda} \cos(Z) \, T_{o\lambda} T_{u\lambda} T_{w\lambda} T_{a\lambda} (1 - T_{r\lambda}) \, W_o \, F_a$$

$$I_{a\lambda} = H_{o\lambda} \cos(Z) \, T_{o\lambda} T_{u\lambda} T_{w\lambda} T_{r\lambda} (1 - T_{a\lambda}) \, W_o \, F_a$$

$$I_{g\lambda} = [\, I_{d\lambda} \cos(Z) + (I_{r\lambda} + I_{a\lambda}) \, C_{\lambda}] \, \rho_g \rho_s / (1 - \rho_g \rho_s)$$

$$\rho_s = T'_{o\lambda} T'_{u\lambda} T'_{w\lambda} [\, T'_{a\lambda} (1 - T'_{r\lambda}) \, 0.5 +$$

$$T'_{r\lambda} (1 - T'_{a\lambda}) (1 - F_a) \, W_o \,]$$

where

$I_{s\lambda}$ = Scattered components on a horizontal surface

$I_{g\lambda}$ = Ground / atmosphere irradiance on a horizontal surface at wavelength, λ.

$I_{r\lambda}$ = Rayleigh scattered component on a horizontal surface at wavelength, λ.

$I_{a\lambda}$ = Aerosol scattered component on a horizontal surface at wavelength, λ.

$H_{o\lambda}$ = Solar irradiance at the top of the atmosphere corrected for Earth-sun distance

W_o = Single scattering albedo

F_a = Forward to total scattering ratio of the aerosol

C_λ = Correction factor by wavelength

ρ_s = Albedo of the air (sky)

ρ_g = Albedo of the ground

The primed transmittance functions indicate the values are calculated using an air mass value of 1.9. A value of 1.9 air masses produces the closest agreement for the diffuse irradiance when compared to the BRITE model. Bird used a value of 0.928 for the single scattering albedo and a value of 0.82 for the forward to total scattering ratio. The model defaults to these values for the single scattering albedo,

forward to total scattering ratio, and the air mass for the primed transmittance quantities unless the user elects to enter his own values for these quantities or use the spectral values of these parameters coded into the model.

A correction factor was needed to fit the equations to Bird's data for several turbidity and zenith angle combinations. Bird found it impossible to take the equations of this general form and get them to accurately represent a variety of conditions. These simple equations exhibit several problems:

1. the cos(Z) terms apply only to direct irradiance

2. the transmittance terms apply to direct irradiance only and are not expected to apply to scattered irradiance

3. W_o and F_a are wavelength dependent

Attempts by Bird to use a variable metric minimization method to allow modified forms of the equations were unsuccessful. The correction factor was computed for several wavelengths as a function of turbidity and zenith angle. Bird assumed that linear interpolation could be used between the tabulated wavelengths to obtain the proper correction factors. Tables 2.4.B thru E show the correction factor as a function of wavelength, turbidity, and zenith angle. Bird assumed a linear interpolation scheme could be used to compute the correction factors. Figures 2.4.F and G compare

λ	0°	37°	48.19°	60°	70°	75°	80°
0.30	0.75	0.75	0.76	0.85	1.20	1.30	1.4
0.35	0.99	0.98	0.99	1.01	1.08	1.17	1.4
0.40	1.1	1.11	1.11	1.12	1.20	1.27	1.52
0.45	1.04	1.06	1.06	1.06	1.11	1.16	1.34
0.50	1.08	1.06	1.05	1.04	1.09	1.11	1.23
0.55	1.04	1.02	1.00	1.00	1.04	1.04	1.13
0.71	1.29	1.19	1.17	1.09	1.04	0.97	0.93
0.78	1.2	1.11	1.08	1.01	1.00	0.93	0.94
0.9935	1.06	0.98	0.95	0.86	0.86	0.80	0.83
2.1	0.69	0.73	0.75	0.68	0.72	0.65	0.68
4.1	0.69	0.73	0.75	0.68	0.72	0.65	0.68

Table 2.4.B

Diffuse correction factor for $\tau_a(0.5) = 0.1$

(From Bird, 1984)

λ	0°	37°	48.19°	60°	70°	75°	80°
0.30	0.88	0.93	1.02	1.23	2.00	4.00	6.3
0.35	1.08	1.07	1.11	1.19	1.51	1.97	3.76
0.40	1.11	1.13	1.18	1.24	1.46	1.70	2.61
0.45	1.04	1.05	1.09	1.11	1.24	1.34	1.72
0.50	1.15	1.00	1.00	0.99	1.06	1.07	1.22
0.55	1.12	0.96	0.96	0.94	0.99	0.96	1.04
0.71	1.32	1.12	1.07	1.02	1.10	0.90	0.80
0.78	1.23	1.09	1.05	1.07	1.00	0.85	0.78
0.9935	0.98	0.94	0.91	0.83	0.90	0.79	0.74
2.1	0.69	0.68	0.71	0.64	0.70	0.59	0.52
4.1	0.69	0.66	0.71	0.64	0.70	0.59	0.52

Table 2.4.C

Diffuse correction factor for $\tau_a(0.5)=0.27$

(From Bird, 1984)

λ	0°	37°	48.19°	60°	70°	75°	80°
0.3	0.88	0.89	0.94	1.11	1.84	3.96	12.2
0.35	1.16	1.00	1.09	1.23	1.65	2.40	5.47
0.4	1.13	1.19	1.41	1.30	1.51	2.03	2.87
0.45	1.08	1.10	1.30	1.16	1.26	1.34	1.72
0.5	1.18	1.04	1.03	1.01	1.13	1.12	1.27
0.55	1.15	1.01	0.99	0.96	1.06	1.02	1.07
0.71	1.33	1.12	1.06	1.02	1.00	0.88	0.80
0.78	1.05	1.03	0.98	0.89	0.92	0.79	0.75
0.9935	0.94	1.00	0.88	0.82	0.90	0.80	0.77
2.1	0.76	0.78	0.84	0.70	0.77	0.69	0.57
4.1	0.76	0.78	0.84	0.70	0.77	0.69	0.57

Table 2.4.D

Diffuse correction factor for $\tau_a(0.5)=0.37$

(From Bird, 1984)

λ	0°	37°	48.19°	60°	70°	75°	80°
0.3	0.88	0.99	1.02	1.22	2.26	5.17	31.3
0.35	1.08	1.11	1.28	1.27	1.80	2.76	7.48
0.40	1.06	1.09	1.29	1.12	1.36	1.67	2.78
0.45	1.01	1.03	1.20	1.00	1.11	1.20	1.57
0.5	1.21	1.06	1.01	0.99	1.04	1.02	1.17
0.55	1.20	1.02	0.97	0.95	0.97	0.92	0.98
0.71	1.21	1.09	1.04	0.95	0.94	0.82	0.71
0.78	1.14	0.97	0.96	0.88	0.92	0.77	0.68
0.9935	0.98	0.99	0.93	0.84	0.89	0.73	0.69
2.1	0.69	0.63	0.71	0.73	0.81	0.72	0.78
4.1	0.69	0.63	0.71	0.73	0.81	0.72	0.78

Table 2.4.E

Diffuse correction factor for $\tau_a(0.5)=0.51$

(From Bird, 1984)

Bird's clear sky spectral model (SPECTRAL) against the more rigorous BRITE model. Because of the close comparison, Bird's clear sky is expected to be within the same accuracy range as the BRITE model.

In the model developed for this research, several changes were made which happen to coincide with changes Bird made in his most recent model (Bird and Riordan, 1984). The single scattering albedo (W_o) and the forward to total scattering ratio (F_a) have been made spectrally dependent based on the rural aerosol distribution. Plots of the spectral values of the single scattering albedo and the forward to total scattering ratio for a clear sky based on the rural aerosol distribution used by Bird are shown in Figure 2.4.I. The spectral values are interpolated from data provided by Bird (1984). After reviewing Bird's data and the information in Kerker (1969) concerning scattering ratios, it was demonstrated that the parameters varied slowly enough so that linear interpolation of the single scattering albedo and the forward to total scattering ratio could be used over the wavelength range of interest. If the user desires, the model gives the option of choosing constant values for both of the parameters. The model also allows the choice of whether to use Bird's correction factor. These two options give the user the flexibility to compare results using slightly different techniques. With the correction factor, the equations represent Bird's clear sky model (1984). Without the correction factor, the equations represent Brine
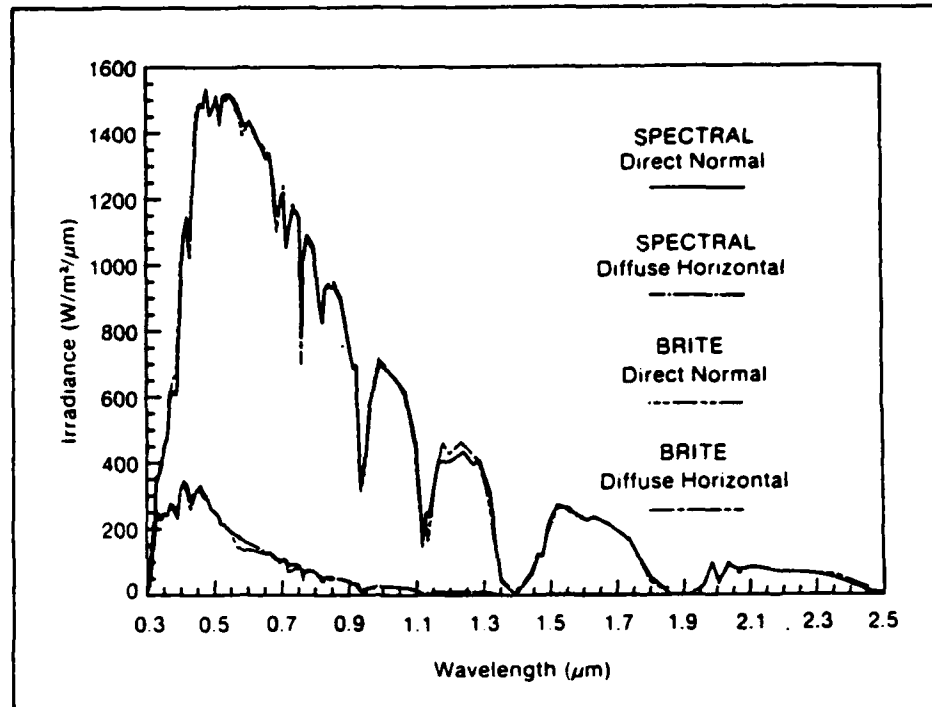
Figure 2.4.F

Comparison of SPECTRAL and BRITE spectra for USS atmosphere, $\tau_a(0.5)=0.1$, ALB=0.0 and AM1.

(From Bird, 1984)
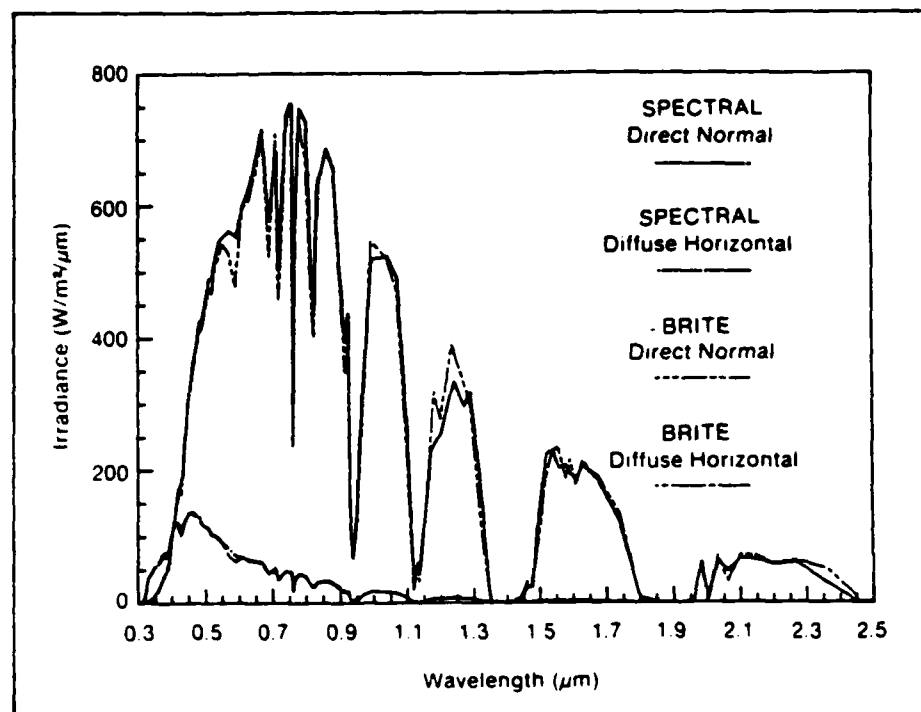
Figure 2.4.G

Comparison of SPECTRAL and BRITE spectra for USS atmosphere, $\tau_a(0.5)=0.1$, ALB=0.0 and AM 5.6

(From Bird, 1984)

WZERO AND FSUBA
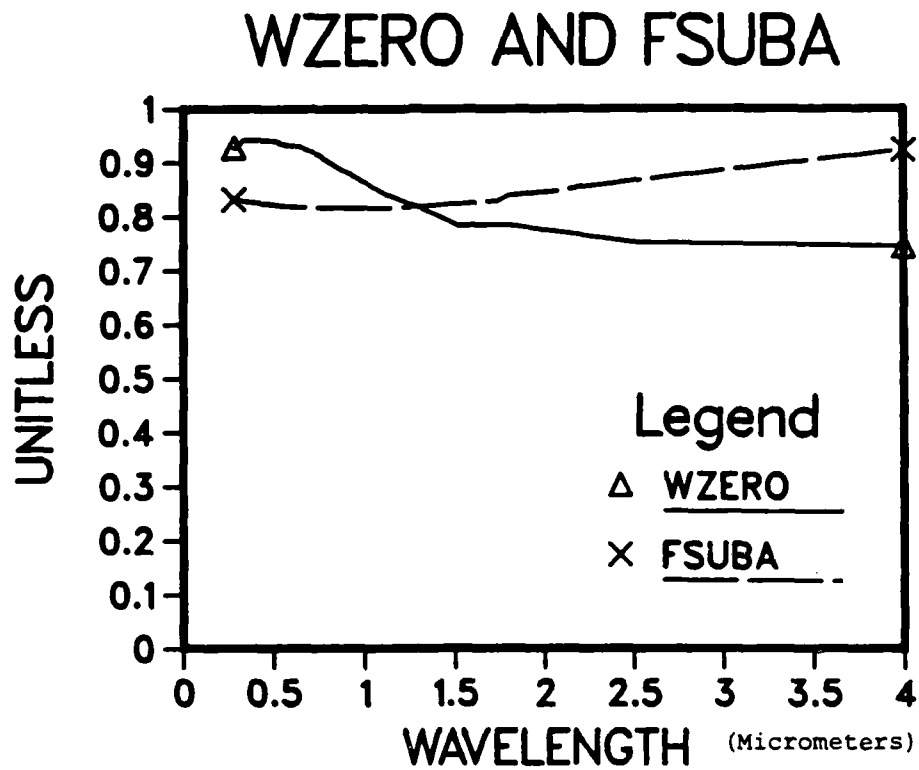
Figure 2.4.H

Spectral single scattering albedo (W_o) and the spectral forward to total scattering ratio (F_a) for a clear sky based on the rural aerosol distribution.

and Iqbal's clear sky formulation (1983).

2.5 Model Geometry

Most of the geometrical quantities needed for the model
were calculated from equations developed by Enrico Coffari
which were published in Solar Energy Engineering edited by
A.A.G. Sayigh (1977). While the coordinate system used in
somewhat unconventional, it has the advantage of producing
an analytic set of equations which minimizes the number of
computational checks needed to verify whether an angle is in
a particular quadrant or it is in front or behind a plane.
The equations are based on the use of vectors and the
direction cosines of the vectors combined with straight
forward principles of solid geometry. The equations allow
the computation of the following quantities:

(1) Solar quantities

a. Solar altitude

b. Solar azimuth

c. Sunrise time

d. Sunrise azimuth

e. Sunset time

f. Sunset azimuth

(2) Angle of incidence of direct radiation on an

inclined plane

(3) Zero-irradiation solar times (Planerise and planeset times; or times when the sun rises and sets on an inclined plane)

    a. Solar altitude and azimuth at planerise

    b. Solar altitude and azimuth at planeset

A list of the equations used to compute these quantities is contained in Appendix C. To calculate the amount of radiation arriving on an inclined plane surface one must be able to determine whether:

    a. Only diffuse radiation is reaching the inclined plane

    b. Both diffuse and direct radiation are reaching the inclined plane

A comparison of the sunrise/sunset times with the planerise/planeset times allows the determination of whether any radiation, diffuse radiation only, or both diffuse and direct radiation are reaching the inclined plane surface. In the more northern and southern latitudes it is possible to have an inclined plane orientation so that the sun will

begin and end shining on the inclined plane twice in one day. In the polar regions, the sun may not rise or set during a twenty-four hour period; the sun either shines all day or not at all. Outside the polar regions, there is always one sunrise/sunset at a particular location on the Earth. The orientation of the inclined plane and its location on the Earth determine whether one or two planerise/planeset combinations will occur.

The angle of incidence of direct radiation on a horizontal surface at the same location as the inclined plane is also important. The radiation reaching the area surrounding the inclined plane is used for computing the diffuse component of the radiation. The solar zenith angle relative to a horizontal surface allows the model to compute the radiation from the surrounding area and determine the diffuse radiation reaching the inclined plane. The ground diffuse radiation from the vicinty is assumed to be from horizontal or flat terrain.

Both the angle of incidence of direct radiation on a horizontal surface and on an inclined plane affect the albedo of their respective surfaces. These angles are used to modify the surface albedo.

2.6 Surface Albedo

The bidirectional reflectance varies with the angle of

incidence and the angle of observation.
In this model, bidirectional reflectance is constant.
The ground (surface) is assumed to be a diffuse or
Lambertian reflector.

Paltridge and Platt (1976) developed an expression for
the variation of albedo with the angle of incidence. Figure
2.6.A shows the typical variation with the angle of
incidence (elevation angle) of the radiation source. The
figure demonstates how a change in solar altitude can affect
the albedo of a surface. This variation has been included
using the simple form developed by Paltridge and Platt. The
expression used by Paltridge and Platt to compute the change
in albedo with angle is:

$$\rho_g(\theta_2) = \rho_g + (1 - \rho_g) \exp[-k(90 - \theta_2)]$$

where

ρ_g — Hemispheric reflectance of the surface or the albedo
of the surface with the source at an elevation angle
of 90 degrees with respect to the surface.

$\rho_g(\theta_2)$ — Albedo or reflectance of the surface as a function of
the solar zenith angle

k — A constant parameter whose value is of order 0.1

θ_2 — Solar zenith angle relative to an arbitrarily oriented
surface (See Figure A.1 in Appendix A)

A value of k equal to 0.1 was used in this model. It is the
value of k suggested for use by Paltridge and Platt.
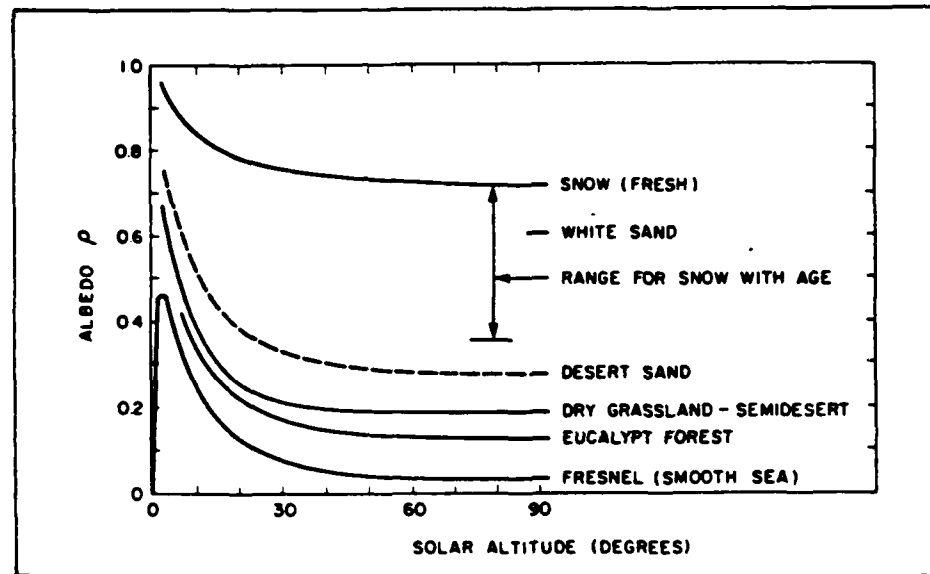
Figure 2.6.A

Angular variation of the albedo for various ground
covers (From Paltridge and Platt, 1976).

In addition to the variation of the albedo with angle of incidence, the albedo varies by wavelength. This variation is often neglected. Most models assume an albedo which is constant with wavelength. A glance at some of the reflectance curves for typical materials shows the degree of spectral variability. Seven typical spectral surface albedos have been installed in the model and the user selects the surface albedo of his choice. The model also gives the option of selecting a constant spectral surface albedo or the option of entering a spectral albedo of the users choice. In summary, the model allows the user to choose a spectral surface albedo from the following:

1. Fresh snow

2. Clay (5% moisture by weight)

3. Dry bare soil

4. Dry sand

5. Wet sand (25% moisture by weight)

6. Typical vegetation

7. Turbid water

8. A constant spectral albedo of the user's choice

9. A spectral albedo of the user's choice

Figure 2.6.B shows plots of the first seven categories of hemispheric reflectance listed immediately above. The seven categories were chosen to represent a variety of surface

HEMISPHERIC REFLECTANCE

Legend
△ FRESH SNOW
✕ BARE SOIL
□ VEGETATION

HEMISPHERIC REFLECTANCE

Legend

△ DRY SAND   □ CLAY

✕ WET SAND   ⊠ TURBID WATER
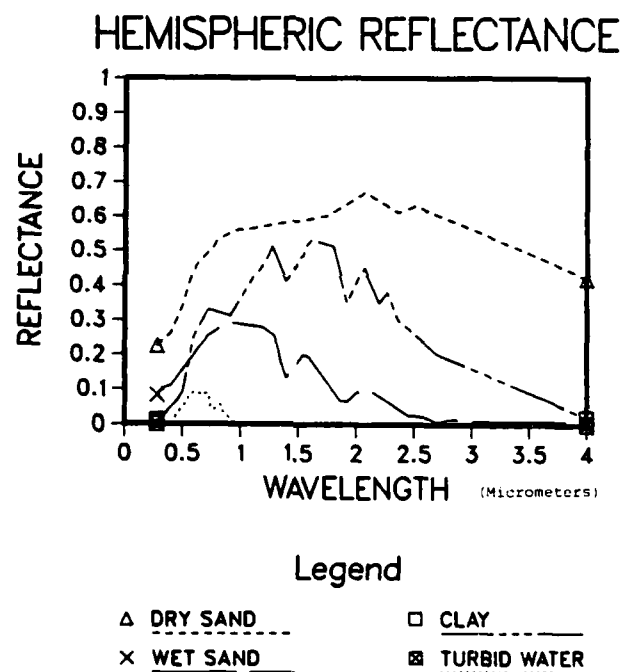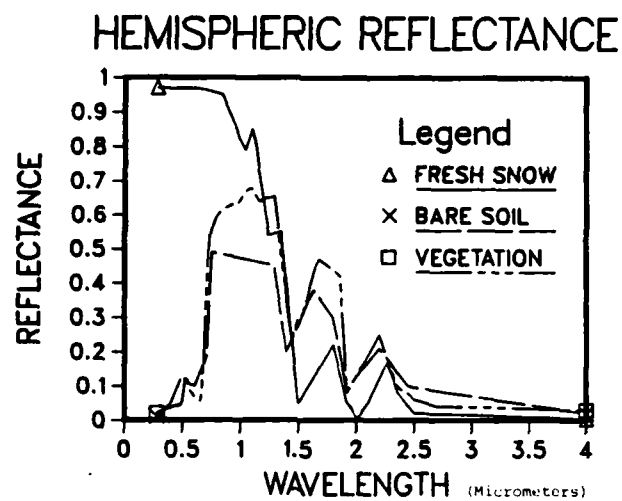
Figure 2.6.B

The figures show the seven spectral reflectance curves used in the model.

reflectances to give the user the opportunity to make model calculations and see the effects different spectral albedos make.

A water surface was included in the list of modelled albedos even though it violates the assumption that the surface is a diffuse (Lambertian) reflector. A water surface was included because most of the surface of the Earth is covered by water. Water surfaces have specular properties which means they tend to act like mirrors at certain zenith angles. The albedo of water surfaces is also affected by wind and wave disturbances. The wind and waves determine the wave structure or 'choppiness' of the water surface which has a direct effect on the albedo of a water surface. In addition, the degree of pollution affects the observed albedo of a water surface. For these reasons, a water surface may have an albedo very different from the one included with this model. The turbid water included in this model has a low albedo and is assumed to be under non-specular conditions. The low albedo of water is typical of most water surfaces in the natural environment.

The effects of surface albedo are complex. There are models to determine the albedo of a particular surface or plant canopy. Due to the influence of other parameters which affect the albedo, more information is required by these models than the solar zenith angle. Some of these additional factors are:

(a) Season

(b) Recent rainfall

(c) Leaf orientation or surface structure

(d) Composite albedo (i.e. bare soil showing through a plant canopy)

It should be obvious that these factors are interrelated. For example, the season will determine the degree of foliation which will affect the amount of bare soil showing through the plant canopy. The surface structure or leaf orientation may be dependent on the wind, type of plant, season, or rainfall. The amount and frequency of rainfall is dependent on season. The degree of complexity in computing albedo can become great quickly.

For this model, the surface is assumed to be uniformly made of the material chosen by the user. In other words, there are no assumptions concerning the amount of bare soil, grass, etc. that could be showing through the vegetation canopy. The surface is assumed to consist of a material which is uniform in texture and has the spectral reflectance of the chosen category. The spectral reflectance is modified at each wavelength interval by the effect of the solar zenith angle.

Although this model does account for changes in the reflectance of the surface due to the solar zenith angle, it does not strictly account for bidirectional reflectance. In practice, the observed reflectance depends on the angle from

which the material is viewed. Since every material has different characteristics, it is not feasible in a simple model to adequately represent the anisotropic scattering of radiation by a surface. Most surfaces reflect radiation in an anisotropic sense which is the reason one should account for bidirectional reflectance. Since the surfaces in this model are assumed to be Lambertian (perfectly diffuse reflectors), this means that the radiation reflected off the surface is isotropic and the bidirectional reflectance is constant.

2.7 Clouds

Clouds present a number of problems. The first and foremost of these problems is the complexity and detail needed to do an accurate job of computing their effects. It would be unsuitable to include all the aspects of clouds theorized in the more current cloud models. Due to their complexity, the amount of computation time needed for some of these models would be prohibitive. A simple, accurate accounting of the effects of cloud cover on the incoming and outgoing solar radiation is desired. Several parameters important to cloud modelling are listed below:

1. Cloud geometry

    a. Shape of the cloud
    b. The cloud's proximity to other clouds
    c. The height of the cloud base
    d. The dimensions of the cloud

2. Cloud droplet size distribution

3. Mie scattering

4. Multiple scattering

5. Atmospheric water vapor profile and cloud liquid
   water content

6. Temperature structure in the cloud

These aspects will be discussed in relation to the cloud
model that was developed for this solar radiation model.

2.7.1 Cloud Characteristics

Finding a simple, accurate cloud model, proved to be an
impossible task. The cloud models available were either very
complex in terms of the radiative transfer scheme, were
broadband versus spectral in nature, geometrically complex,
or required data not readily available to most users. Since
this model is intended to be spectral, the first priority
was to find a cloud study or cloud model which is either
spectral in nature or could be expressed in spectral terms.
The cloud characteristics described by Welch, Cox, and Davis
(1980) were spectral. The solar spectrum was divided into
eight regions. The center wavelengths of the eight regions
were 0.765, 0.950, 1.15, 1.40, 1.85, 2.80, 3.35, and 6.30
micrometers. The study used a variety of cloud types. Of the
cloud types listed in the paper, four were chosen for their
diversity in covering the range of the most commonly

reported low clouds. The low cloud types chosen were stratocumulus, stratus, nimbostratus, and cumulus.

The data used by Welch, Cox, and Davis includes specific details about the clouds. One of the primary considerations is the cloud droplet size distribution. The drops are assumed to be liquid; no ice is contained in these clouds. Ice clouds will have different characteristics from water droplet clouds. Using this model for ice clouds, without modification, will result in large errors. Welch and Cox used the drop size distribution functions of Best (1951) and Deirmendjian (1975). The drop size distribution varies with the height in the cloud. As a consequence, Welch and Cox list the droplet size distributions for the base and the top of the clouds. The drop size distribution for the four cloud types used in this model are given in terms of the modified gamma size distribution function developed by Deirmendjian. The modified gamma distribution function has the following form:

$$n(r) = a\ r\alpha \exp[-(\alpha/\varepsilon)\ (r/r_c)^{\varepsilon}]$$

where

$n(r)$ — Number density of droplets with radius, r, expressed in number by cubic centimeter per micrometer

r — Droplet radius in micrometers

r_c — Modal radius of the distribution in micrometers

Table 2.7.1.A (From Welch, Cox, and Davis 1980)

Cloud Droplet Size Distribution Parameters

Type	a	α	δ	r_c (μm)	W_L (g/m^3)	N (cm^{-3})
Stratocumulus base	2.8230	5	1.19	5.33	0.141	100
Stratocumulus top	1.9779	2	2.46	10.19	0.796	100
Stratus base	9.7923	5	1.05	4.70	0.114	100
Stratus top	3.8180	3	1.30	6.75	0.379	100
Nimbostratus base	8.0606	5	1.24	6.41	0.235	100
Nimbostratus top	1.0969	1	2.41	9.67	1.034	100
Cumulus	0.5481	4	1.00	6.00	0.297	100

a, α, δ — Empirically derived cloud droplet distribution constants

r_c — Modal radius of the cloud droplet distribution

W_L — Cloud liquid water content

N — Number of cloud droplets per cubic centimeter
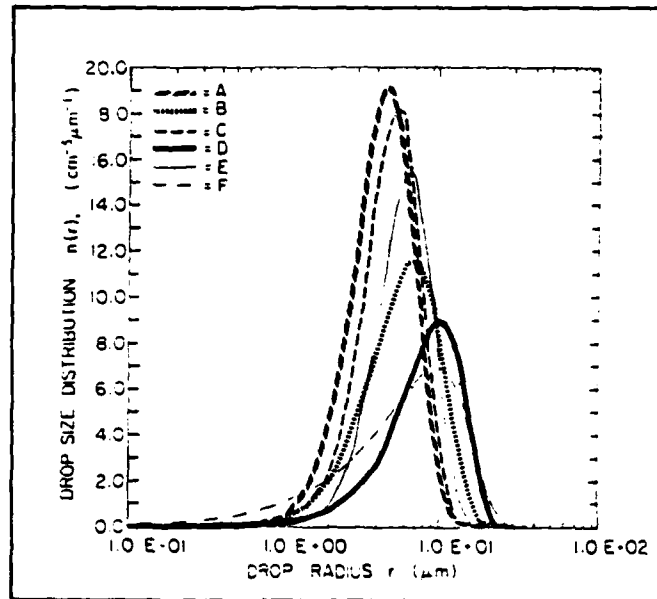
Figure 2.7.1.B

Drop size distributions n(r) for various cloud cases:
A. stratus base. B. stratus top. C. stratocumulus base.
D. stratocumulus top. E. nimbostratus base. F. nimbostratus top.

(After Welch, Cox, and Davis, 1980)

The other parameters are empirically derived constants. Table 2.7.1.A gives the original values of the parameters used by Welch and Cox. Figure 2.7.1.B shows the shape of the distributions used by Welch and Cox. The cumulus cloud formulation was taken from Deirmendjian and has just one droplet distribution throughout the cloud, rather than a different droplet distribution at the top and base of the cloud.

Other characteristics of the clouds used by Welch and Cox which should be noted. The clouds are assumed to have the temperature structure of the standard atmosphere. The clouds are also assumed to be saturated at each level within the cloud. For this research, the user is given the option of choosing the surface temperature. This option does not directly affect the modelling of the clouds or the assumptions concerning their use.

I have defined the cloud model by establishing the temperature of the cloud, the water vapor content, and the drop size distributions. Next we must consider the effects of Mie scattering and geometry.

2.7.2 Mie Scattering

Mie scattering defines a scatter process which relates the intensity of the scatter to the size parameter. The size parameter is proportional to the ratio of the drop radius divided by the wavelength of light. When Welch and Cox

(1980) developed the cloud droplet extinction and absorption coefficients for the clouds modelled in their study, they used a wavelength dependent Mie efficiency factor and the pertinent cloud drop size distribution. However, these factors were computed at only eight wavelengths. The cloud droplet extinction coefficients are needed at 126 non-uniform width, irregularly spaced intervals across the region of 0.28 to 4.0 micrometers. Deirmendjian showed that the droplet absorption, scattering, and extinction parameters are relatively slowly varying functions of wavelength. The droplet extinction and absorption coefficients for three different types of clouds have been plotted by Deirmendjian. Figure 2.7.2.A shows the plot of the droplet extinction and scattering coefficients for various clouds. Because the coefficients are slowly varying, it was assumed that linear interpolation could be used to obtain the values of the droplet extinction and absorption coefficients between the wavelengths where Welch and Cox rigorously computed their values. Linear interpolation and extrapolation was used to determine the 126 droplet extinction and absorption coefficients.

Welch and Cox have two droplet size distributions for some of the clouds. They generated different droplet extinction and absorption coefficients at the base and the top of the clouds. For simplicity, it was desirable to obtain only one set of coefficients to represent each cloud. To obtain a single droplet absorption or extinction
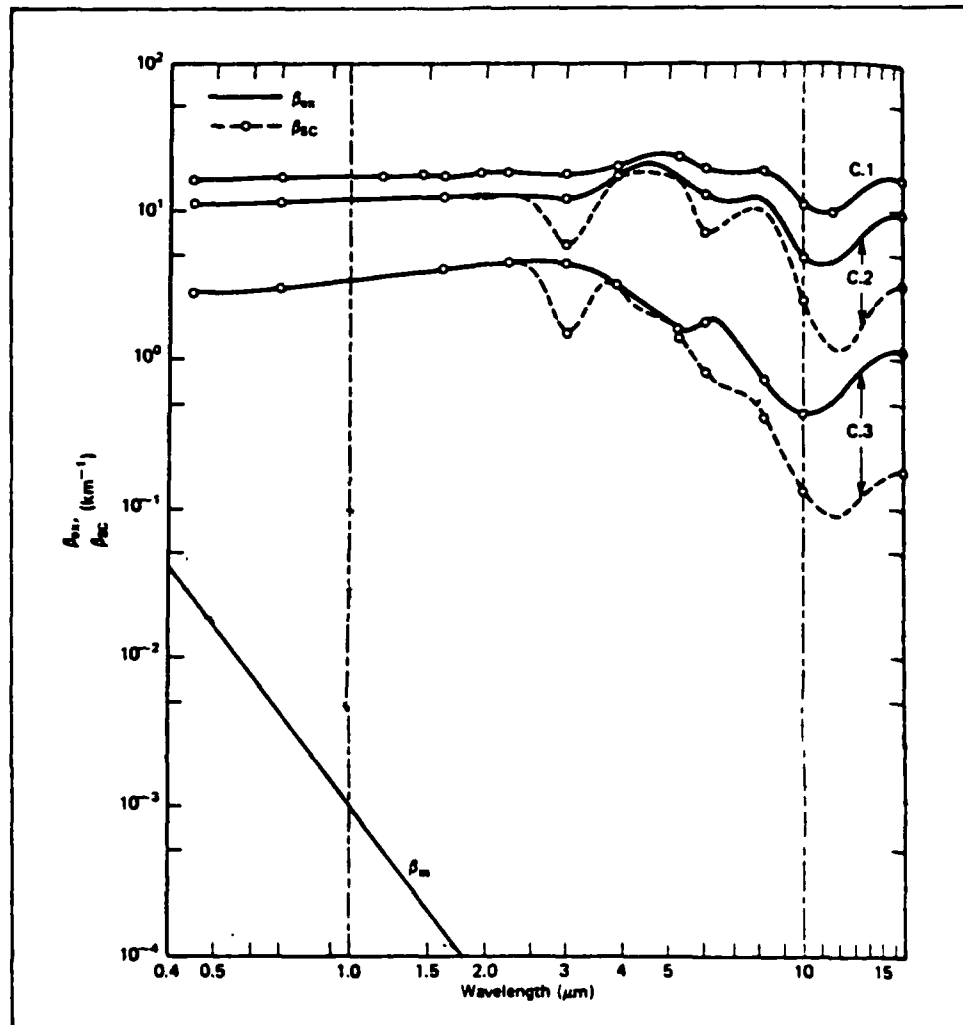
Figure 2.7.2.A

Extinction and scattering coefficients versus wavelength for cloud models.

β_m = Molecular scattering coefficient

β_{sc} = Cloud scattering coefficient

β_{ex} = Cloud extinction coefficient

C.1 = Cumulus cloud

C.2 = Corona cloud

C.3 = Mother of Pearl cloud

(Adapted from McCartney, 1976)

coefficient, the values of the droplet coefficients at the base and top of the cloud were averaged. It was assumed the average droplet extinction and absorption coefficients would sufficiently represent the entire cloud. Table 2.7.2.B shows the values computed by Welch and Cox. Table 2.7.2.C shows the averaged values used for this model.

Mie scattering affects the amount of radiation forward scattered and backward scattered. Welch and Cox (after Zdunkowski, 1967) determined phase function expansion coefficients for a series of Lengendre polynomials which represent the proportion of total energy scattered in a particular direction. Assuming single scattering and approximating the scattering phase function by a Dirac delta function for the forward scattering peak (Joseph, Wiscomb, and Weinman, 1976; Wiscomb, 1977), it can be shown that the fourth Legendre coefficient divided by 9.0 is a representation of the total amount of energy forward scattered. The value, 9.0, results from the use of the fourth term (n=4) of the approximate expression which contains the factor (2n+1). Based on the study by Hansen (1969) and for simplicity, only two components of the scattered radiation, the forward scattered and the backward scattered components will be considered. Scanning the table of expansion coefficients of Welch and Cox, one can see the expansion coefficients are slowly varying just like the droplet extinction and absorption coefficients. Using the same reasoning as with the droplet extinction and absorption

Table 2.7.2.B   (After Welch, Cox, and Davis, 1980)

Droplet Extinction Coefficients (Per Kilometer)

Wavelengths (μm)

	0.95	1.15	1.4	1.85	2.8	3.35	6.3
SC base	29.02	29.44	29.80	30.20	31.34	31.69	34.92
SC top	90.13	91.13	91.59	92.90	94.58	95.83	105.10
NS base	40.82	41.22	41.58	42.30	43.41	44.05	50.38
NS top	101.80	102.80	103.20	104.60	106.40	107.70	115.90
ST base	24.35	24.68	25.02	25.63	26.61	26.81	28.46
ST top	53.51	54.06	54.49	55.23	56.54	57.32	64.39
CU	45.17	45.41	45.95	46.55	47.97	48.61	54.51

Droplet Absorption Coefficients (Per Kilometer)

Wavelengths (μm)

	0.95	1.15	1.40	1.85	2.8	3.35	6.3
SC base	0.004	0.011	0.204	0.566	15.18	15.25	11.91
SC top	0.022	0.062	1.090	2.960	46.88	46.27	45.68
NS base	0.008	0.019	0.369	0.940	21.44	21.35	18.06
NS top	0.028	0.077	1.390	3.73	52.46	51.74	52.34
ST base	0.0033	0.0095	0.162	0.45	12.66	12.80	9.64
ST top	0.0121	0.037	0.581	1.45	27.94	27.72	25.21
CU	0.008	0.028	0.406	1.12	23.61	23.49	20.69

SC = Stratocumulus
ST = Stratus
NS = Nimbostratus
CU = Cumulus

Table 2.7.2.C

Average Droplet Extinction Coefficients (Per Kilometer)

Wavelengths (μm)

	0.95	1.15	1.40	1.85	2.80	3.35	6.30
SC	59.575	60.285	60.695	61.550	62.96	63.839	70.01
NS	71.31	72.01	72.44	73.45	74.905	75.875	83.14
ST	38.93	39.37	39.755	40.43	41.575	42.065	46.42
CU	45.17	45.41	45.95	46.55	47.97	48.61	54.51

Average Droplet Absorption Coefficients (Per Kilometer)

Wavelengths (μm)

	0.95	1.15	1.40	1.85	2.8	3.35	6.30
SC	0.013	0.0365	0.647	1.763	31.03	30.26	28.795
NS	0.018	0.048	0.8795	2.335	36.95	36.545	35.200
ST	0.00765	0.02325	0.3715	0.95	20.3	20.26	17.425
CU	0.008	0.028	0.406	1.120	23.61	23.49	20.69

SC = Stratocumulus
ST = Stratus
NS = Nimbostratus
CU = Cumulus

Table 2.7.2.D   (After Welch, Cox, and Davis, 1980)

Droplet Phase Function Expansion Coefficients

	Wavelengths (μm)							
	0.765	0.95	1.15	1.40	1.85	2.80	3.35	6.3
SC base	5.305	5.250	5.179	5.133	5.051	7.199	6.926	5.762
SC top	5.413	5.395	5.362	5.362	5.372	8.074	7.746	6.670
NS base	5.337	5.294	5.248	5.205	5.169	7.555	7.258	6.066
NS top	5.419	5.399	5.379	5.384	5.420	8.123	7.806	6.892
ST base	5.268	5.206	5.149	5.096	4.999	7.016	6.713	5.596
ST top	5.367	5.339	5.300	5.275	5.253	7.789	7.466	6.310
CU	5.360	5.305	5.269	5.243	5.209	7.661	7.346	6.186

Table 2.7.2.E

Average Droplet Phase Function Expansion Coefficients

	Wavelengths (μm)							
	0.765	0.95	1.15	1.40	1.85	2.80	3.35	6.30
SC	5.359	5.3225	5.2705	5.2475	5.2115	7.6365	7.336	6.216
NS	5.378	5.3465	5.3135	5.2945	5.2945	7.839	7.532	6.479
ST	5.3175	5.2725	5.2245	5.1855	5.126	7.4025	7.0895	5.953
CU	5.360	5.305	5.269	5.243	5.209	7.661	7.346	6.186

SC = Stratocumulus
ST = Stratus
NS = Nimbostratus
CU = Cumulus

CLOUD DROPLET
EXTINCTION COEFFICIENTS

Legend △ ST □ NS
× SC ⊠ CU

EXTINCTION COEFFICIENTS

WAVELENGTH (Micrometers)

CLOUD DROPLET
ABSORPTION COEFFICIENTS

ABSORPTION COEFFICIENTS

Legend
△ ST
× SC
□ NS
⊠ CU

WAVELENGTH

CLOUD DROPLET
FORWARD SCATTERING
PERCENTAGE

FORWARD SCATTERING PERCENTAGE

Legend
△ ST
× SC
□ NS
⊠ CU
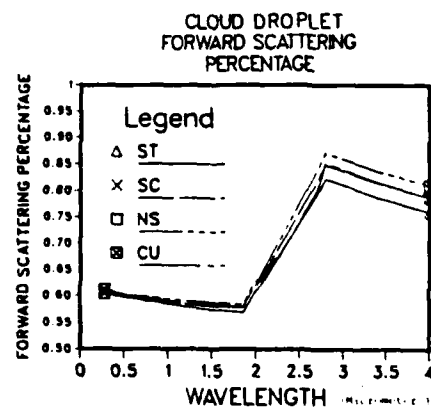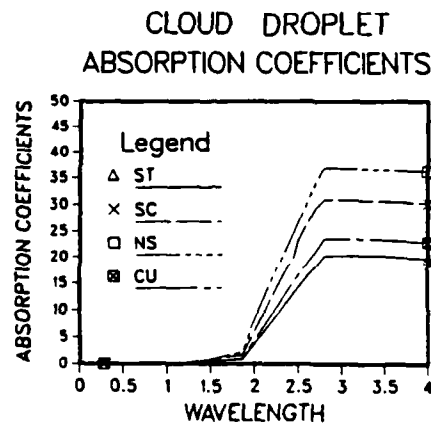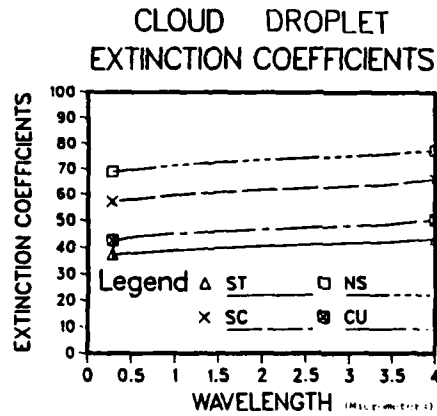
WAVELENGTH

Figure 2.7.2.F

The spectral cloud droplet extinction, absorption, and
forward scattering percentage as interpolated and extrapolated
from Welch, Cox, and Davis (1980). The wavelength is in
micrometers.

ST - Stratus   NS - Nimbostratus
SC - Stratocumulus   CU - Cumulus

coefficients, linear interpolation and extrapolation was used to determine the expansion coefficients at wavelengths not computed by Welch and Cox. An average of the expansion coefficients at the top and base of the cloud was used to represent the expansion coefficient for the entire cloud. Since only the forward and backward scatter is being considered, only the fourth Legendre phase function expansion coefficient was interpolated. Table 2.7.2.D shows the original values of the fourth phase function coefficient used by Welch and Cox. Table 2.7.2.E shows the averaged values of the fourth phase function coefficient which is used to represent the overall cloud. The amount of backward scattered radiation was determined by subtracting the amount of forward scattered radiation from 1.0. The spectral cloud droplet absorption coefficients, cloud droplet extinction coefficients, and cloud droplet forward scattering percentage as linearly interpolated and extrapolated from the data of Welch, Cox, and Davis (1980) are plotted in Figure 2.7.2.F.

2.7.3 Cloud Geometry

The radiative properties of clouds are deeply intertwined with the geometry of the cloud field. A number of authors have studied the effects of cloud geometry and shape on the radiative characteristics of the clouds. One of the more frustrating aspects of dealing with this problem is

the lack of a convenient way of handling complicated cloud geometries. Studies with rectangular clouds have been performed (Aida, 1977; Welch and Zdunkowski, 1980) and as a result of the relatively poor performance of rectangular type cloud geometries, some researchers have compared the effects of clouds of different shapes (Welch and Zdunkowski, 1981; Welch and Wielicki, 1984).

A number of interesting conclusions have been drawn from the studies. Aida (1977) demonstrated that the importance of cloud shape increases with increasing solar zenith angle and that clouds which are separated by more than 5 times their diameter do not alter the scattering pattern from a single cloud. Aida further concluded that the surrounding clouds increase the fraction of reflection as the distance between the clouds decreases. This effect becomes particularly evident at about two cloud diameters separation, roughly equivalent to a cloud amount of 25 percent. Welch and Zdunkowski (1980) studied the cloud size distribution in comparison to cloud reflectivity. They found that the cloud size which contributes most to the cloud field reflectivity is near the cloud size which contributes most to the total sky cover. This indicates that describing a field of clouds as one where all the clouds have the same dimensions may produce accurate results if the cloud dimensions are carefully chosen. This study did not include cloud-cloud radiative interactions. However, the result suggested cloud-cloud interactions may be neglected for

cloud fields with 30 percent or less cloud cover. Welch and Zdunkowski (1980) found that cloud droplet number density has a large influence on cloud reflectivity and transmissivity and a minimal effect on cloud absorptivity. For very large cumulus clouds, a significant fraction of the incident radiation exits the cloud sides with a majority in the downward direction. At all but the largest solar zenith angles, the radiation exiting the cloud sides is anisotropic. Welch and Zdunkowski (1981) studied the effects of several cloud shapes and concluded that rectangular geometries produce results which are marginally accurate for cylindrically shaped clouds. They also showed that the exact geometry should be taken into account to obtain accurate radiative characteristics.

Wendling (1977) studied the effects of striated cloud fields and his conclusions indicated the effects were primarily geometry dependent. The radiance emerging from striated clouds can be greater than that reflected from a plane-parallel cloud with a thickness equal to the thickness of the striated cloud. This is due to the backscattering from the vertical walls of the cloud columns occurring at intermediate sun elevation angles. By the same token, the radiance reflected from the striated clouds is reduced compared to that of a plane-parallel cloud when shadowing occurs. Wendling pointed out that plane-parallel cloud albedos are a good approximation for striated cloud albedos only when the striations are not too deep and the sun

illuminates the clouds at low angles.

Welch and Wielicki (1984) compared the effect of cloud shape on the reflected flux differences between broken and plane-parallel cloudiness. The results indicated plane-parallel cloud calculations are not accurate at most values of cloud cover, particularly those with cloud cover between 10 and 90 percent. They also found the choice of cloud shape led to large differences in the reflected fluxes. The differences were attributed to the anisotropic intensity pattern out of the cloud sides, the shape of the holes (spaces) between the clouds, and to variations in cloud area as viewed from the solar direction. Based on this finding, Welch and Wielicki were able to develop an expression for the effective cloud cover for a zenith angle of 60 degrees. Using this, they computed the broken field reflected fluxes from plane-parallel calculations. They were able to make these calculations regardless of the assumed cloud shapes. This information gives credence to the techniques which weight the areas of the clouds by the relative proportions which have been illuminated by the sun.

Based on the study by Welch and Wielicki (1984), the decision was made to use a simple cloud geometry and adjust the effective cloud cover based on solar zenith angle in an attempt to obtain cloud fluxes which represent broken cloud fields using plane-parallel calculations. Based on the study by Welch and Zdunkowski (1980), cloud fields containing a single cloud size will be used.

2.7.4. The Cloud Model

Based on the paper by Welch and Wielicki (1984), the simplest cloud geometry possible is used. The clouds in this model are rectangular in shape. I believe that adjusting or weighting the areas of the top of the cloud, the side of the cloud and the clear sky with the amounts of radiation from plane-parallel calculations it is possible to obtain accurate answers regardless of the cloud shape and geometry. A description of the cloud model I developed follows.

The clouds are basically rectangular. For rectangular clouds, the base of the clouds are assumed to have the same dimensions in both length and width (a square base). The height of the cloud base and the separation between the sidewalls of the clouds are determined by the user. The cloud separation is assumed to be uniform in the directions perpendicular to the sidewalls of the clouds. When the length of the cloud base, the height of the cloud, the separation between the clouds, and the height of the cloud base are specified, the geometry associated with an array of rectangular clouds is determined. In addition to an array of rectangular clouds (which has the flavor of a typical cumulus field), the model allows for a striated cloud field. In this geometry, the clouds are formed in infinite bands whose width and separation between the bands is defined by the user. This model is capable of handling four distinctly

different geometries:

1. Clear sky (no clouds)

2. Rectangular array of clouds

3. Striated array of Clouds

4. Overcast sky (100 percent cloud
    cover)

For geometric simplicity, the sun's rays are assumed to be parallel. Only one face (side) of the rectangular cloud is illuminated. It is assumed that this cloud orientation is maintained throughout the day when the model computes daily values. The top of the cloud is always illuminated between sunrise and sunset. The portion of the side of the cloud which is directly illuminated by the sun is determined by the solar zenith angle. Shadowing of the sides of the clouds is allowed.

2.7.4.1 Cloud Model Geometry

One of the critical factors which must be determined is the path distance that radiation must travel through the cloud. The cloud has two distinct components to its radiation field. One of the components consists of radiation which first passes through the top of the cloud and eventually emerges at the level of the cloud base through either the side or bottom of the same (or another) cloud.

The second component consists of radiation which first passes through the side of the cloud and eventually emerges at the level of the cloud base. The geometric light ray, which would travel the paths described, may cut through any number of individual clouds and spaces between the clouds depending on the solar zenith angle and the dimensions of the clouds. The average equivalent path distances through the cloud only are computed numerically.

The definition of average equivalent path distance is the distance through cloud that a light ray would travel beginning at the level of the top of the cloud and exiting at the level cloud base. The path distances will vary depending on whether the top of the cloud is entered first or whether the side of the cloud is entered first. It will also be dependent on the solar zenith angle. The solar zenith angle and the dimensions of the clouds will determine how much shadowing of the cloud sides will occur, how many complete clouds are intersected by the path, and whether the path through the top of the cloud is longer or shorter than the path through the side of the cloud. Obviously, there are many possible paths through the clouds in the manner described. The average path distances were computed by calculating 100 distinct paths (50 through the cloud top, and 50 through the cloud side) and averaging the path distances for the respective parts of the cloud. Figures 2.7.4.1.A and B show the two possible average equivalent path distances computed by the model. The transmission and
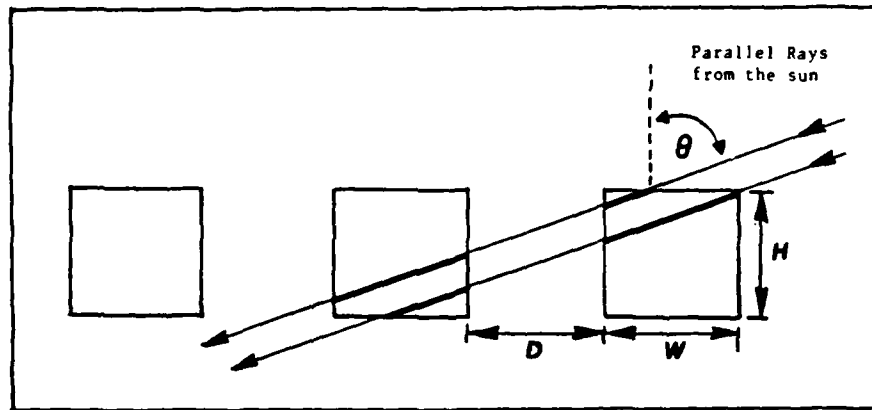
(A)
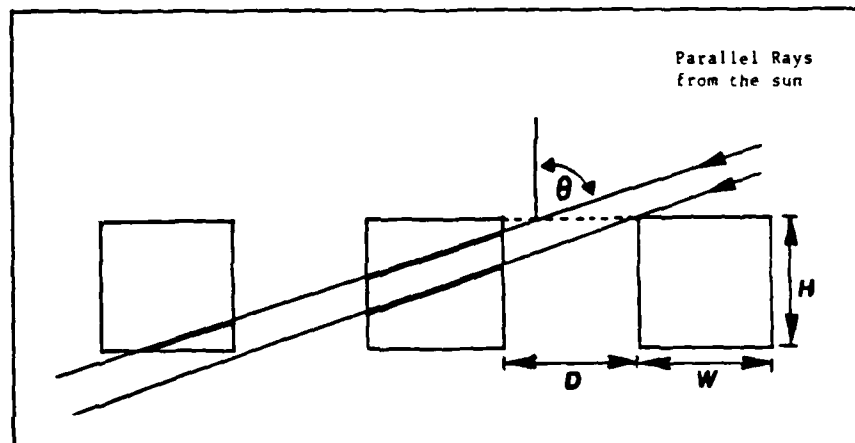
(B)

Figure 2.7.4.1

The equivalent path distances for rays entering the side and the
top of the cloud are indicated by the bold lines inside the
cloud borders. An average equivalent path distance is used in the
model.

reflection from the clear sky area between the clouds will be determined by the clear sky portion of the model.

2.7.4.2 Cloud Model Radiative Transfer

Multiple scattering contributes to both the upward and downward radiation fluxes. Neglecting multiple scattering leads to an underestimate of the radiation leaving the cloud base and ultimately an underestimate of the radiation reaching the surface of the Earth. The same is true of the cloud reflectivity.

The necessity of including multiple scattering led to the review of solutions to the basic radiative transfer equation. A simple, analytic solution to the equation of radiative would conform with the original intent of developing this model. After reviewing the solutions in the literature, two techniques produce simple, analytic solutions, the two stream technique and the Eddington technique. Both solutions handle optically thin cases and large absorption poorly. I chose the solution developed by Chu and Churchill published by the Radiation Commission (1975) in Standard Procedures To Compute Atmospheric Radiative Transfer In a Scattering Atmosphere ; the solution was recommended by Paltridge and Platt (1976). This solution uses the two stream technique of decomposing the radiation field into components (one upward; one downward) to arrive at an approximate solution for radiation passing through a

plane-parallel slab of a given thickness. The solutions
allow for the computation of the reflectivity or albedo at
the top of the plane-parallel layer and the transmission
through the plane-parallel layer. The solutions for the
albedo and transmission of the layer are:

$$\text{Albedo} = \frac{G (1.0 - e^{-2Kt})}{1.0 - G^2 e^{-2Kt}}$$

$$\text{Transmission} = \frac{(1.0 - G^2) e^{-Kt}}{1.0 - G^2 e^{-2Kt}}$$

where

$$G = (r - s) / (r + s)$$

$$r = 1.0 - W_o f + W_o b$$

$$K = s / \mu_o$$

$$s = [(1.0 - W_o f)^2 - W_o^2 b^2]^{1/2}$$

f – percentage of radiation forward scattered

b – percentage of radiation backscattered

W_o – single scattering albedo

μ_o – t cos(solar zenith angle)

t – thickness of the layer

The use of this solution was suggested by Paltridge and
Platt (1976). The two stream approximation is generally used
in applications where the scatter is not highly anisotropic.
However, the solutions are very valuable because of the

simplicity of the analytic solution. In addition, this approach can be justified within the accuracy of the model. According to Paltridge and Platt (1976), "a method of parameterizing cloud-radiation interaction on the basis that the prediction or observation of cloud amount and cloud character is inherently inaccurate to much worse than 10 percent. Generally they (the solutions) give answers to better than about 5 percent for quite anisotropic scattering when absorption is negligible and when the layer optical depth is greater than about 5. This last is usually the case for water clouds in the low atmosphere, but it is certainly not true for aerosol layers and thin cirrus." The solutions assume a non-reflecting surface or layer immediately below the atmospheric layer in question. To account for a non-black surface below the layer requires an additional technique. The complete radiative transfer problem and its solution for the plane-parallel case is reproduced from the Radiation Commission (1975) in Appendix D.

In addition to multiple scattering within the cloud itself, multiple scattering (reflections) between the cloud, atmosphere, and ground are important. The multiple reflections play a key role in determining the intensity of the radiation which reaches the surface of the Earth. Neglecting multiple reflections between the clouds and the Earth's surface will lead to an underestimate of the downward flux of solar radiation reaching the Earth's surface (Schneider and Dickinson, 1976). According to

Schneider and Dickinson, the underestimate would be most
pronounced in regions of persistent cloud cover and high
surface albedos. To include the effect of the multiple
reflections between the surface, the clouds and the
atmospheric layers, the adding technique was used (Appendix
B). The adding technique (Liou, 1980) combines two layers of
known reflectivity and transmissivity through a series
approximation of the multiple reflections which occur
between the layers.

2.7.4.3 The Atmospheric Layers

The atmosphere will be divided into three layers plus the
surface (the fourth layer). The layer above the clouds will
be treated as clear sky. The second layer will contain the
clouds. The layer below the clouds and treated as clear sky.
The bottom layer will be the ground or surface. The
transmissivity and reflectivity of the second or cloudy
layer will be computed as described in the cloud radiative
transfer section. The transmissivity and reflectivity of the
clear sky layers above and below the clouds must be computed
separately.

The amount of atmosphere in the layers above and below
the clouds affects the transmissivity and reflectivity of
the individual layers. The temperature, the pressure at the
top of the cloud, and the pressure at the base of the cloud
affect the amount of atmosphere in each layer. The user

determines the surface temperature, surface pressure, height of the cloud base, and the thickness of the cloud for the model. From these values, the atmospheric pressure at the base and top of the cloud layer is computed. Based on these reference pressures, the transmissivity and reflectivity of the atmospheric layers are determined. The calculation of the reference pressures is performed via the formula for constant lapse rate atmospheres (Hess, 1959; Iribarne and Godson, 1973).

$$P = P_o (T / T_o)^{(g/R\approx)} = P_o [(T_o - \approx z)/T_o]^{(g/R\approx)}$$

where

g   -- Gravitational constant

P   -- Pressure at height z above the surface

P_o -- Pressure at the surface

T   -- Temperature at height z above the surface

T_o -- Temperature at the surface

R   -- Universal Gas Constant

z   -- Height above the surface

$\approx$ -- Constant atmospheric lapse rate

Some assumptions are implicit in the model, when using this formula. First, the U.S. Standard Atmosphere tropospheric lapse rate (-6.5 degrees Kelvin / Km) is used. This agrees with the assumed lapse rate in the cloud parameterizations of Welch, Cox, and Davis (1980). The atmosphere is assumed

to have a constant lapse rate to the tropopause. Second, it is assumed that the clouds exist below the tropopause. This model is not designed for clouds which break through the tropopause as can be the case in some thunderstorm situations or with noctilucent clouds. Both of these assumptions are very good for most of the usual atmospheric conditions encountered.

Since the transmission for an atmospheric layer is computed using an exponential function, the exponent of each transmission function was weighted by a ratio of the pressures to give the correct exponent. For example, the total transmission through three atmospheric layers might be written as an exponential function whose exponent includes the product of an extinction coefficient (k) and an atmospheric path distance (M). The total transmission (T) for an atmospheric layer could be written as :

$$T = e^{-KM}$$

This single layer could be broken down into component layers if we assume that the product of the transmittances gives the total transmittance. While this technique could be very poor for molecular absorption and scattering, it is often used. Iqbal summarized the reasoning very succinctly. "In order to compute the direct spectral irradiance on the Earth, we need the values of the monochromatic transmittances due to the various molecular absorbers.

Molecular scattering depends primarily on the number density of molecules in the path, whereas the molecular absorption is a function of local pressure and temperature as well. The wavelength dependence of molecular (Rayleigh) scattering is very nearly proportional to λ^{-4}. On the other hand, the spectral variation of the molecular absorption coefficient is a highly oscillatory function of wavelength. For molecular absorption, it is necessary to know the frequencies, intensities, shapes, and widths of spectral lines in the region of interest in order to be able to evaluate the spectral transmittance. The simple Bouguer's law does not apply in this case. Nevertheless, since elaborate procedures require a great deal of computer time, it is quite common to apply this law or a variation of it to compute molecular absorption." (Iqbal, 1983). Bird made this assumption in choosing the form of the transport equation for his clear sky model. In a similar fashion, each layer will be formulated using this assumption. If each layer is represented by T_x then the total transmittance for the atmosphere could be represented by:

$$T = T_1 \, T_2 \, T_3$$

Each layer can be represented by:

$$T_1 = e^{-(P_{ct}/P_o)KM}$$

$$T_2 = e^{-[(P_{cb}-P_{ct})/P_o]KM}$$

$$T_3 = e^{-[(P_0-P_{cb})/P_o]KM}$$

where

T_x - Transmittance of each layer   (x = 1, 2, 3)

P_{cb}- Pressure at the cloud base

P_{ct}- Pressure at the cloud top

P_o - Pressure at the surface

Since the exponents in a product are additive, the product of the resultant layer transmissivities yields the original total transmissivity for the entire layer.

$$T = T_1 \, T_2 \, T_3 = e^{-KM}$$

This is the procedure used to compute the atmospheric transmissivities for the individual layers of the atmosphere. This technique is applied to each atmospheric absorber, scattering process, or constituent in turn. For example, the transmission for aerosols was computed by layer, the transmission by the uniformly mixed gases was computed by layer, etc. The transmission for water vapor was accomplished in an identical fashion except that only two atmospheric layers were used. It was assumed that the water vapor in the atmosphere exists below the tropopause or the top of the cloud (whichever is lower). This is a good
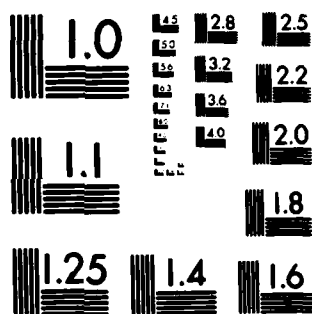
assumption under most of the normal meteorological conditions. Making this assumption means that the highest of the three component atmospheric layers used in this model has its base at the top of the tropopause or at the top of the cloud. Another assumption is that all the absorption by ozone takes place above the tropopause or the top of the cloud. This means the terms which account for the effects of ozone will be in the top layer and the terms which account for the effects of water vapor will only be in the lower two layers. Once the transmission for each of the components has been broken down by layer, the resultant layer transmission was computed by multiplying the individual layer components together in the formulation devised by Iqbal (See Figure 2.4.A). Iqbal's formulation was modified slightly by layer depending on the assumptions mentioned above. The resultant transmission calculations for the clear sky layers are:

Layer Above The Clouds:

$$T_1 = T_{r\lambda 1} \, T_{a\lambda 1} \, T_{o\lambda 1} \, T_{u\lambda 1} \; + \; T_{a\lambda 1} \, T_{o\lambda 1} \, T_{u\lambda 1} \, (1.0 - T_{r\lambda 1}) \; 0.5$$

$$+ \; T_{o\lambda 1} \, T_{r\lambda 1} \, T_{u\lambda 1} \, (1.0 - T_{a\lambda 1}) \, W_o \, F_a$$

Layer With The Clouds (Clear Air Portion Only):

$$T_2 = T_{r\lambda 2} \, T_{a\lambda 2} \, T_{w\lambda 2} \, T_{u\lambda 2} \; + \; T_{a\lambda 2} \, T_{u\lambda 2} \, T_{w\lambda 2} \, (1.0 - T_{r\lambda 2}) \; 0.5$$

$$+ \; T_{r\lambda 2} \, T_{u\lambda 2} \, T_{w\lambda 2} \, (1.0 - T_{a\lambda 2}) \, W_o \, F_a$$

Layer Below The Clouds:

$$T_3 = T_{r\lambda 3} T_{a\lambda 3} T_{w\lambda 3} T_{u\lambda 3} + T_{a\lambda 3} T_{u\lambda 3} T_{w\lambda 3} (1.0 - T_{r\lambda 3}) 0.5$$

$$+ T_{r\lambda 3} T_{a\lambda 3} T_{w\lambda 3} (1.0 - T_{a\lambda 3}) W_o F_a$$

All of the quantities in the above equations have been previously defined with the exception of the additional subscript to indicate the level of the atmosphere and will not be redefined here.

The reflectivities for each layer were computed similarly and the equations from Iqbal were modified by layer to include or exclude water vapor and ozone as appropriate. One might wonder why go to such trouble for a simple model. The answer lies in the combining of the atmospheric layers. The explanation is easiest if one studies the equations of the adding technique for combining atmospheric layers. One can see that the order of combining the atmospheric layers makes absolutely no difference to the total transmissivity calculated. However, the order will directly affect the atmospheric reflectivity for the combination of the layers. For this reason, it was very important to insure that the regions of dominant influence of water vapor and ozone were constructed in the proper layer. The adding technique of combining layers requires

both the total (direct and diffuse combined) transmittance and the total reflectance of each layer. At the surface, only the reflectivity is known.

To account for the multiple scattering effects of water vapor, the uniformly mixed gases, etc. in the layer containing the cloud, the transmission of the layer was calculated as if no clouds existed. The layer transmission was equated to an exponential and solved to obtain an extinction coefficient for the 'clear sky' in this layer. This extinction coefficient was added to the cloud droplet extinction coefficient to obtain the extinction coefficient for the entire layer. The layer extinction coefficient was used in the two stream solution which accounts for multiple scattering. In this way, the effects of multiple scattering were applied to all the constituents in the layer containing the clouds.

2.7.4.4 Combining The Atmospheric Layers And The Surface Reflectivity

Once the reflectivity and transmissivity of each layer (including the surface) have been determined, then the layers are combined using the adding technique, two layers at a time. The adding technique produces four equations for combining the layers. The equations reperesent:

1. The radiation reflected from the combination of the two layers (R).

2. The radiation transmitted by the combination of
   the two layers (T).

3. The radiation reflected upward onto the bottom
   of the top layer (U).

4. The radiation transmitted downward onto the top
   of the bottom layer (D).

Appendix B develops the equations for each situation. For
the incoming solar radiation, the layers are combined from
the top down, two layers at a time. By choosing the desired
equation from the adding technique at each step, the
radiation reflected from the atmosphere-surface combination
as well as the radiation incident on the surface can be
obtained.

These steps are accomplished for two different cases,
from the different equivalent path lengths through the side
and the top of the cloud. The solution to the radiative
transfer equation assumes a plane-parallel layer. The
radiation passing through the side of the cloud is treated
as if it was a plane-parallel layer with a thickness equal
to the equivalent path distance through the side of the
cloud. The radiation passing through the top of the cloud is
treated similarly. The model produces three sets of
reflectances and transmittances indicative of the entire
atmosphere. The three sets of reflectances and
transmittances represent:

1. the clear sky atmosphere

2. the combination of the clear layer above the cloud, the radiation passing through that top of the cloud, the clear layer below the cloud, and the surface reflectivity

3. the combination of the clear layer above the cloud, the radiation passing through the side of the cloud, and the clear layer below the cloud, and the surface reflectivity.

Using the irradiance falling on the top of the atmosphere, the radiation reaching the surface of the Earth can be computed for the three cases. The radiation reaching the surface of the Earth from the three cases is weighted by the relative area each represents on a horizontal surface. As suggested by Welch and Wielicki, performing this calculation enables one to compute the effects of broken cloud cover regardless of the cloud shape. For clear sky cases, the Bird model values will be obtained. For overcast sky cases, the cloud layer will be treated as plane-parallel with the radiation entering the top of the clouds.

2.7.4.5 Satellite Observation Of The Surface

For a satellite, the process described is repeated for a different set of equivalent path distances through the top and side of the cloud as well as a different air mass for the clear sky. These differences are the result of viewing geometry. All the layer transmissivities and reflectivities are computed again using the new atmospheric path distances.

Because the radiation is coming from the surface, the atmospheric layers are combined from the bottom (surface) to the top of the atmosphere. The exact opposite of the incoming radiation. Once the transmissions for the atmosphere have been recomputed, the radiation leaving the surface of the Earth is taken as the source irradiance and is used to compute the irradiance arriving at the top of the atmosphere. The radiation arriving at the top of the atmosphere is weighted according to the relative areas of the clear sky, top, and side of the cloud as viewed from the satellite to obtain the radiation reaching the satellite.

2.7.4.6 Direct And Diffuse Radiation Beneath The Cloud

The adding technique uses the total transmittance (direct plus diffuse) of the layers and computes a total transmittance for the combination of layers. At the surface, the values of direct and diffuse radiation are desired. To determine the direct radiation portion of the total combined transmittance including the cloud, a simple Beer's law approximation is used. The Beer's law solution is for the direct radiation (plus a small amount of forward scattered radiation). The Beer's law solution has the form:

$$\text{Transmittance} = e^{-\tau}$$

where

τ - optical depth

By subtracting the Beer's law solution from the total
solution of the equation of radiative transfer, the
proportion of direct and diffuse components can be
approximated. To summarize, the direct and diffuse radiation
components beneath the cloud are computed as follows:

$$\text{Total} = \frac{(1.0 - G^2)\, e^{-Kt}}{1.0 - G^2\, e^{-Kt}}$$

$$\text{Direct} = e^{-Kt}$$

$$\text{Diffuse} = \text{Total} \quad - \quad \text{Direct}$$

where

K - Absorption coefficient

t - Thickness of the cloud

G = (r-s) / (r+s)   (See Section 2.7.4.2)

This simple technique separates the direct and diffuse
components of the radiation underneath the cloud. This same
technique determines the amount of radiation from the target
at the surface which reaches the satellite observation point
directly.

2.8 Radiation Reaching The Surface

The radiation from the clear sky and cloud must be
weighted by their respective areas to get accurate results
using plane parallel solutions.

2.8.1 Weighting Each Component Of Radiation

My technique for weighting the three components of radiation is based on the projected area of each component onto the ground (See Figure 2.8.1.A). The projected area of clear sky between the clouds could vanish if the solar zenith angle and the dimensions of the clouds are such that shadowing occurs. However, there will always be lanes of clear sky in the array of rectangular clouds. There may not be projected areas of clear sky associated with a striated cloud field. For demonstration purposes, the following discussion will consider a rectangular array of clouds with radiation reaching the ground in the clear space between the clouds. The first step is to calculate the projected dimensions of the areas on the ground. (Refer to Figure 2.8.1.B). To determine the weights of each component of radiation, one only needs to compute the areas on the ground relative to the total area. For this particular case, the areas turn out to be:

$$FADR = \frac{FRACTIONAL\ AREA}{TOTAL\ AREA} = \frac{D\ (W+D) + W\ (D - H \tan \theta)}{(W+D)^2}$$
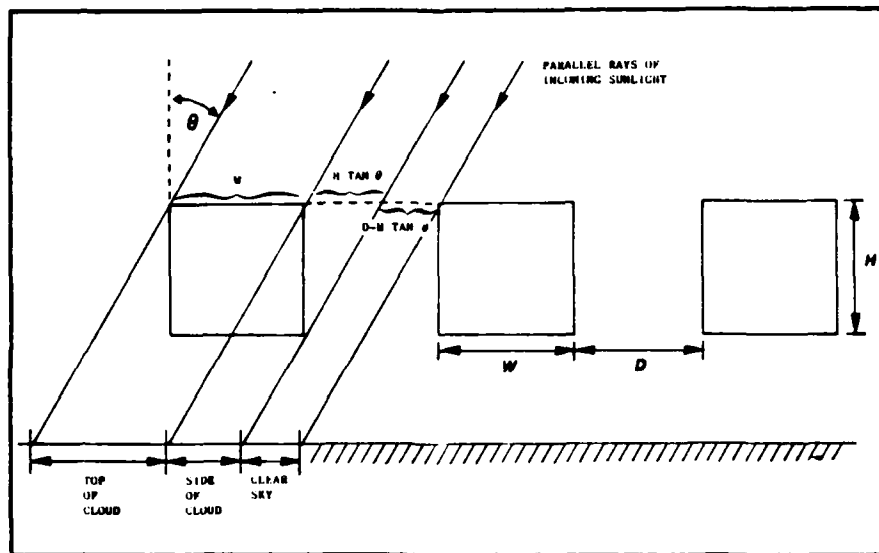
Figure 2.8.1.A

Side view projection of radiation reaching the surface through
the clear sky, the side of the cloud, and the top of the cloud.

D = Cloud separation
H = Cloud height
W = Cloud width
θ = Solar zenith angle
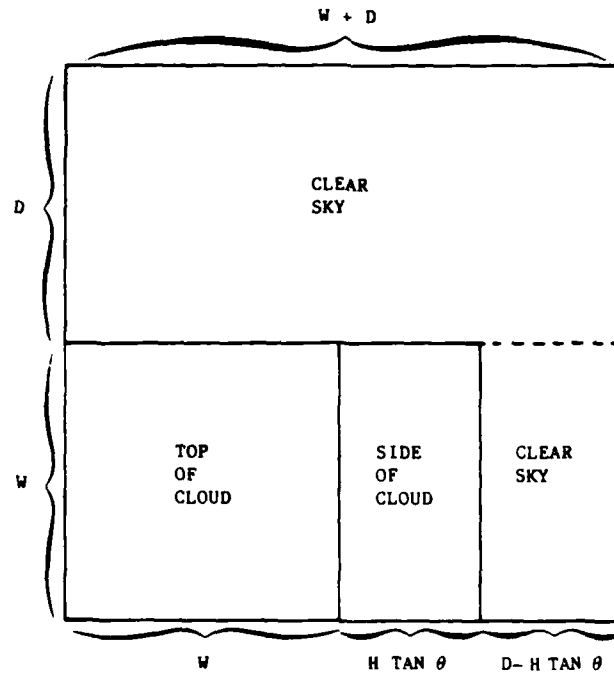
Figure 2.8.1.B

Fractional area weights for the components of radiation through
the clear sky (FADR), the side of the cloud (FASC), and the top of
the cloud (FATC)

$$FADR = \frac{D(W+D) + W(D- H\tan\theta)}{(W+D)^2}$$

$$FASC = \frac{W(H\tan\theta)}{(W+D)^2}$$

$$FATC = \frac{W^2}{(W+D)^2}$$

$$FASC = \frac{W \, (H \tan \theta)}{(W + D)^2}$$

$$FATC = \frac{W^2}{(W + D)^2}$$

FADR – Fractional area of direct (clear sky) radiation

FASC – Fractional area of radiation through the side of
the cloud

FATC – Fractional area of radiation through the top of the
cloud

W   – Width of the cloud

D   – Separation between the clouds

H   – Height of the clouds

θ – Solar zenith angle relative to a flat surface

Once the weighting for each component of radiation has been
determined, the radiation reaching the surface can be
computed.

2.8.2 Calculating The Radiation Reaching The Surface

Each of the components of the radiation (clear sky,
cloud side, and cloud top) can be broken into direct-normal

and diffuse horizontal radiation. This is accomplished for the areas underneath the clouds by the Beer's law technique described in Section 2.7.4.6. The average direct normal and diffuse horizontal radiation can be computed in the following way:

$$DN = (FADR * DNC) + (FASC * DNSC) + (FATC * DNTC)$$

$$DF = (FADR * DFC) + (FASC * DFSC) + (FATC * DFTC)$$

where

DF   – Total diffuse radiation

DFC – Diffuse radiation from the clear sky

DFSC – Diffuse radiation from the side of the cloud

DFTC – Diffuse radiation from the top of the cloud

DN   – Total direct-normal radiation

DNC – Direct-normal radiation from the clear sky

DNSC – Direct-normal radiation from the side of the cloud

DNTC – Direct-normal radiation from the top fo the cloud

Once the total direct-normal (DN) and the total diffuse (DF) radiation reaching the surface have been computed, then the amount of radiation reaching an inclined plane surface can be determined.

2.8.3 Radiation Arriving At An Inclined Plane

The diffuse radiation is assumed to be isotropically distributed throughout the sky. This is not true. Making this assumption simplifies the solution. Hooper and Brunger (1980) compared the results of several modelling assumptions. Among them were the isotropic assumption and the heliocentric assumption for the diffuse radiation. According to Hooper and Brunger, making the isotropic assumption will give conservative predictions (underestimates) for partially cloudy conditions, but it gives good approximations for overcast conditions. They indicate that the isotropic diffuse assumption will result in underestimates of the diffuse irradiance on sun-facing slopes, and overestimates of diffuse irradiance on slopes not facing the sun. Under varying sky conditions and a sloping surface, the error between calculated diffuse using the isotropic assumption and the measured diffuse can be as large as 56 percent (Hooper and Brunger, 1980).

To compute the radiation arriving at an inclined plane surface, the percentage of the sky visible to the plane must be computed. To compute the percentage of the sky visible to the plane, the ratio of the surface area of the lune-shaped portion of the sky visible to the inclined plane divided by the surface area of a hemisphere was calculated. To compute the percentage of sky and ground visible to the inclined plane, the surface areas of the two regions shown in Figure 2.8.3.A need to be determined.
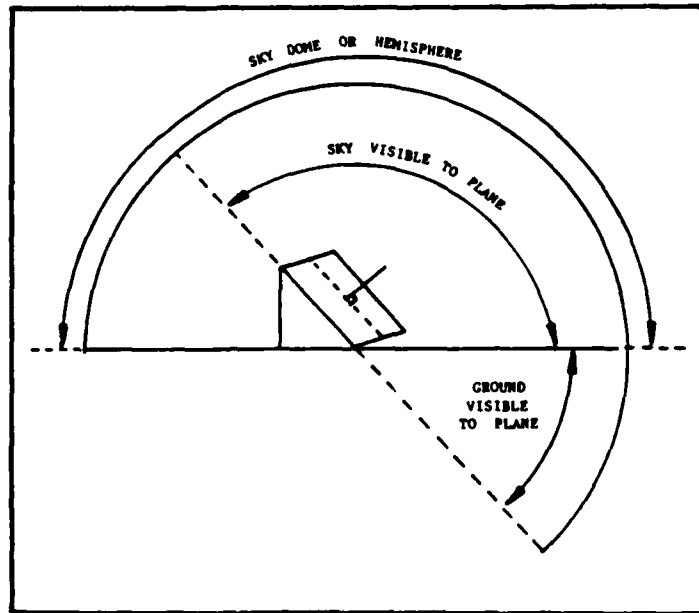
Figure 2.8.3.A

Regions of sky and ground visible to inclined plane

$$S_1 = 2\ R^2 \beta \qquad\qquad S_2 = 2\pi R^2 - 2\ R^2 \beta$$

where

S_1 — Surface area of the sky hemisphere not visible to the inclined plane

S_2 — Surface area of the sky hemisphere visible to the inclined plane

β — Zenith angle of the inclined plane measured relative to the normal of a flat surface

At this point, the two solid angles of interest can be computed. The solid angles representing the portions of the inclined plane's hemisphere visible to the sky and visible to the ground may be computed as follows:

$$SASKY = \frac{S_2}{R^2} = \frac{2\ R^2 - 2R^2 \beta}{R^2} = 2(\pi - \beta)$$

$$SAGND = \frac{S_1}{R^2} = \frac{2R^2 \beta}{R^2} = 2(\beta)$$

The direct radiation must be modified by the solar zenith angle relative to the inclined plane and the diffuse radiation must be modified by the percentage of the sky visible to the plane. The equations for the direct and

diffuse radiation reaching the surface are :

$$DR = DN * \cos(ZPLANE)$$

$$DFS = DF * PCTSKY$$

where

DFS — Diffuse radiation reaching the inclined plane from the sky

DR — Direct radiation reaching the inclined plane

ZPLANE — Solar zenith angle relative to the inclined plane

Because the plane is inclined, diffuse radiation is received from both the sky and the ground. The ground diffuse radiation is computed in the following manner:

$$GNDDIF = [DN * \cos (ZFLAT) * SFCRFL \qquad +$$
$$DF * GNDRFL]$$

where

GNDDIF — Diffuse radiation reflected by the ground

GNDRFL — Hemispheric or diffuse reflectance, not angle dependent

SFCRFL — Direct radiation surface reflectance, dependent on the solar zenith angle relative to a flat surface

The first term is the reflected portion of the radiation directly incident on the horizontal ground. The second term is the reflected portion of the diffuse radiation incident on the horizontal ground. To obtain the ground diffuse contribution to the radiation incident on the inclined

plane, the ground diffuse radiation must be divided by the solid angle subtended by a horizontal surface (Lambertian surface assumed) and multiplied by the solid angle of the ground as viewed from the inclined plane. The global radiation arriving at an inclined plane is:

$$GBL = DN * \cos(ZPLANE)$$
$$+ DF * PCTSKY$$
$$+ [DN * \cos(ZFLAT) * SFCRFL$$
$$+ DF * GNDRFL] * SAGND / \tau$$

where

GBL — Global radiation arriving at the inclined plane which includes direct, sky diffuse, and ground diffuse radiation

SAGND — Solid angle subtended by the ground as viewed from the inclined plane

ZPLANE — Solar zenith angle relative to the normal vector of the inclined plane

PCTSKY — Percentage of sky visible to inclined plane

To compute the radiation reaching the satellite observation point, the radiation leaving the surface of the inclined plane must be calculated. It is evaluated using the following equation:

$$\text{SHZERO} = (\ \text{DN} * \cos(\text{ZPLANE}) * \text{PLNRFL}$$

$$+ \text{DF} * \text{PCTSKY} * \text{GNDRFL}$$

$$+ [\ \text{DN} * \cos(\text{ZFLAT}) * \text{SFCRFL} * \text{PLNRFL}$$

$$+ \text{DF} * \text{GNDRFL} * \text{GNDRFL}\ ] * \text{SAGND} / \tau\ )\ /\tau$$

where

SHZERO — Radiation leaving the inclined plane located at the surface of the Earth

PLNRFL — Direct radiation surface reflectance of the inclined plane, dependent on the solar zenith angle relative to the normal vector of the inclined plane

2.9 Satellite Observation Of The Surface

The solar spectral model computes the irradiance reaching a satellite in orbit. To define the satellite viewing geometry, the satellite zenith angle relative to the horizontal surface at the inclined plane's location must be given. In order to determine the solid angles needed for the computation of the radiation reaching the satellite, the horizontal extent of the plane surface must be given. The model uses a fixed viewing geometry of the satellite. In other words the viewing geometry does not change relative to the inclined plane or target on an hourly basis. However, the model will sum the total radiation reaching the satellite position with the fixed viewing geometry throughout the day. While this is not representative of practical situations where the geometry of the satellite

relative to a fixed ground location changes with each orbit, it will give an estimate of the radiation which might be accumulated at satellite altitude through the course of a day. The user may get around this by computing several instantaneous or hourly cases with different viewing angles and summing them.

Since the geometry for the satellite will probably be different from the geometry of the sun relative to the inclined plane, all the calculations concerning the fractional areas of clear and cloudy skies, the equivalent path distances throughout the clouds, and the zenith angle relative to the inclined plane must be calculated for the path between the Earth and the satellite. Since the path distance through the atmosphere will be different, the atmospheric parameters affected by the atmospheric path distance must be computed again. Exactly the same procedures for computing the radiation reaching the surface from the sun have been followed in determining the radiation reaching the satellite. The only difference is that the source of radiation is the radiation leaving the inclined plane's surface (SHZERO) instead of the extraterrestrial solar spectrum (HZERO). The radiation leaving the inclined plane's surface is assumed to be a direct source of radiation. The direct-normal radiation reaching the satellite from the target plane (DNO) and the diffuse radiation reaching the satellite from the target plane (DFO) constitute the radiation from the target itself. Scattered radiation from

the atmosphere also reaches the satellite. Depending on the position of the sun relative to the satellite, this radiation may be mostly forward scattered or backscattered radiation (See Figures A.3 and A.4). The radiance of the atmosphere is calculated based on whether the geometry indicates forward or backward scattering of radiation. The radiance of the atmosphere includes any radiation scattered by the atmosphere before reaching the ground on the incoming path from the sun to the surface. Radiation scattered by clouds is included in the computation of the radiance of the atmosphere. Since the radiance of the atmosphere is computed from the adding technique as if it included all the radiation scattered over an entire hemisphere, it was necessary to multiply the atmospheric radiance by the solid angle of the plane. It is assumed the radiation reaching the satellite is determined by the instantaneous field-of-view of the satellite.

The satellite sensor is assumed to be pointing at the target so there is no equivalent term for the direct radiation (DR) for the satellite as with the surface radiation. One significant difference in the calculations of the incoming and outgoing radiation is the combination of the layers of the atmosphere. In one case, the layers are combined from the top of the atmosphere downward and in the other case the layers are combined from the bottom of the atmosphere upward. A second significant difference is the inclusion of a term to account for the radiance of the

atmosphere. The equations for the radiation reaching the satellite are:

$$DNO = (FADRO * DNCO) + (FASCO * DNSCO) + (FATCO * DNTCO)$$
$$+ LATM * SATGT$$
$$DFO = (FADRO * DFCO) + (FASCO * DFSCO) + (FATCO * DFTCO)$$

where

DFCO   – Diffuse radiation observed by the satellite in the clear sky

DFSCO – Diffuse radiation observed by the satellite through the side of the cloud

DFTCO – Diffuse radiation observed by the satellite through the top of the cloud

DFO   – Diffuse radiation observed by the satellite from the target

DNCO   – Direct-normal radiation observed by the satellite in the clear sky

DNTCO – Direct-normal radiation observed by the satellite through the top of the cloud

DNO   – Direct-normal radiation observed by the satellite from the target

FADRO – Fractional area of the clear sky radiation as observed from the satellite

FASCO - Fractional area of the radiation through the side of the
         cloud as observed from the satellite

FATCO - Fractional area of the radiation through the top of the
         cloud as observed from the satellite

LATM   - Radiance of the atmosphere

SATGT - Solid angle of the target

2.10 Obstructions And Mountain Modelling

Obstructions have been included in the model. These
obstructions allow the computation of daily radiation by
modifying the beginning and ending times that direct
radiation may fall on the inclined plane. The obstructions
do not modify the length or amount of diffuse radiation
time. From sunrise to sunset, diffuse radiation is received
even though direct radiation from the sun is blocked. These
obstructions were designed to estimate the radiation
reaching the surface in a mountainous area or an area with
buildings. These calculations will likely be underestimates
in every case. The model does not account for the effects of
multiple reflections due to nearby inclined surfaces which
contribute to the total radiation received at a particular
location. The following assumptions are made when including

the obstructions:

1. The obstructions are assumed to be far enough from the inclined plane that the radiation reflected from the obstructions can be considered negligible.

2. The obstructions exactly block sunrise and sunset until the desired elevation angle is reached.

3. The obstruction is assumed to block an insignificant portion of the diffuse sky radiation regardless of the elevation angle to the top of the obstruction.

4. The inclined plane is resting on a horizontal surface between either one or two obstructions and does not receive radiation reflected from any other nearby inclined object.

The obstructions are defined by the elevation angles to the top of the obstruction as measured from a horizontal surface at the location of the inclined plane. While the usefulness of this type of obstruction is very limited, it provides a starting point for some preliminary studies of how obstructions affect the radiation reaching an inclined plane surface.

CHAPTER III

ANALYSIS OF MODEL RESULTS

In this chapter, the discussion will focus on the model results. The analysis of the model will contain comparisons with data when available. The specific goals are to:

1. Compare the model results with observations

2. Assess the effects of spectral surface albedos

3. Assess the effects of cloud type, thickness, and amount

4. Assess the effects of solar zenith angle (which is directly affected by latitude, and hour angle)

The effects of turbidity, water vapor amount, air mass path, solar zenith angle, and ozone amount for clear skies have been published by others (Bird and Riordan 1984; Hatfield, Giorgis, Flocchini, 1981). Since the intent of this work is to concentrate on the effects of surface albedo, cloud type and amount, cloud thickness, solar zenith angle, and cloud albedo, the effect of the other parameters will be discussed only when directly pertinent to interpreting the results.

3.1 Comparison With Observation

The first step is to compare the model against data. The Bird simple clear sky model (Bird, 1984) is the basis for the overall model and was modified to contain spectral aerosol single scattering albedos, spectral aerosol forward to total scattering ratios, spectral ground albedos and tilted surfaces. To confirm that these changes have maintained the integrity of the original model, comparisons with observed clear sky data were completed.

3.1.1 Clear Sky Data

There are two sources of data for the clear sky comparisons. Broadband data was obtained from the Solar and Meteorological Research Program at the University of Michigan. Spectral data was obtained from the Solar Energy Research Institute (SERI) in Golden, Colorado.

The broadband data from the University of Michigan consists of data which covers several spectral bands. The instrumentation used to collect this data was the Eppley Precision Spectral Pyranometer (PSP), the Eppley Pyheliometer, and the Eppley Ultraviolet (UV) radiometer. The global and diffuse radiation on a horizontal surface was measured by the Eppley PSP's. The Eppley PSP measuring the diffuse radiation was shaded by an occulting disk mounted on a solar tracker. This method was preferred to the shadow

band technique because it was unnecessary to apply shadow band corrections and introduce uncertainties associated with those corrections. The alignment of the occulting disk is very important in correctly measuring the diffuse radiation and only those days with proper alignment were used for comparison. The occulting disk is 5 cm in diameter and 50 cm from the pyranometer. This produces a 5.7 degree field-of-view which is blocked by the occulting disk and was chosen so that the blocked field-of-view matched the angular field-of-view of the Eppley Pyrheliometer which measured the direct-normal radiation. Another Eppley PSP was mounted on a south-facing surface tilted at 42.3 degrees (the latitude of Ann Arbor, Michigan). This pyranometer measured the total solar radiation arriving at the tilted surface in the spectral band 0.28 to 2.8 micrometers. (Department of Atmospheric and Oceanic Science, University of Michigan, 1979).

Summary Of Data From The University Of Michigan

Global radiation	0.28	to 2.8	micrometers
Diffuse radiation	0.28	to 2.8	micrometers
Direct-normal	0.28	to 2.8	micrometers
Global Ultraviolet	0.290	to 0.385	micrometers
Global with red filter (RG-2)	0.63	to 2.8	micrometers
Total radiation with 42.3 Deg Tilt	0.28	to 2.8	micrometers

The spectral data was obtained from the Solar Energy Research Institute (SERI). "Spectral irradiance measurements were taken with SERI-modified LI-COR model LI-1800 portable spectroradiometers. These units were modified by

incorporating integrating spheres (used in measurements of global irradiance), direct beam modules (used to measure direct normal irradiance in a 5 degree field-of-view, and temperature controllers. The instruments are calibrated and operated at 40 degrees Celsius and are shielded (except aperture) from direct sunlight to prevent heating above the control temperature. The optical system of the LI-1800 consists of a filter wheel, holographic grating monochromator, and a silicon detector. The wavelength range is 300-1100 nm with a bandwidth of 6 nm and a step size of 1, 2, 5, or 10 nm, which is selected by the user. The total scan time for the 300 to 1100 nm at 2 nm steps is about 27 seconds. A portable terminal and an internal microprocessor are used to start the scans and to perform data storage, reduction, and retrieval functions." (Riordan, 1986).

Summary Of Data From SERI

Global spectral	300 to 1100 nanometers (0.3 to 1.1 micrometers)
Direct-normal spectral	300 to 1100 nanometers (0.3 to 1.1 micrometers)
Global spectral with 37.0 deg tilt	300 to 1100 nanometers (0.3 to 1.1 micrometers)

3.1.2 Comparison With Spectral Clear Sky Observations

The data obtained from Dr. Riordan at SERI consisted of observations made on August 7, 1985 (Day 219) at Golden, Colorado (latitude 39.75 N, longitude 105.16 W). Spectral

observations of the global total radiation on a surface
tilted at 37 degrees zenith angle were made. The tilted
surface was aligned so that it was sun-facing at the time
each measurement was taken. At the same time, the
corresponding direct-normal radiation was measured. Spectral
observations of the global radiation on a horizontal surface
and the corresponding direct-normal radiation were also
made. From the 10 sets of observations obtained from Dr.
Riordan, only one was for a horizontal surface. Three sets
of observations will be compared. They were chosen to span
the range of solar zenith angle covered by the observations.
Table 3.1.2 lists some of the pertinent atmospheric
characteristics at the time of the observations. The water
vapor value for this day was obtained from the National
Weather Service (NWS) and the atmospheric turbidity (aerosol
optical depth at 500 nm) was calculated using a sun
photometer (Riordan, 1986). The model requires a surface
albedo and the surface albedo thought to be most
representative of Colorado was the bare soil surface.
Colorado lacks heavy broadleaf foliage and has predominantly
pine, aspen, and evergreen trees. The vegetation is also
relatively sparse; even in the months of high growth. These
conclusions were drawn from the personal experience of the
author who spent four years in Colorado.

The spectral observation data for the horizontal
surface are plotted against the modelled spectral values and
are shown on Figure 3.1.2.A. The solid lines are the

Mode	Day No.	Collector Tilt Angle (deg)	Angle of Incidence (deg)	Solar Zenith Angle (deg)	Relative Air Mass	Surface Pressure (mb)	Atmospheric Turbidity (500 nm)	Precipitable Water Vapor (cm)	Cloud Cover (10ths) and Type
Global Total	219	37	24.36	61.36	2.078	818	0.069	1.32	.5 cumulus
Direct-Normal	219	-	-	61.36	2.078	818	0.069	1.32	1.5 cumulus
Global Total	219	0	59.26	59.26	1.949	818	0.078	1.32	1 cumulus
Direct-Normal	219	-	-	59.26	1.949	818	0.078	1.32	1 cumulus
Global Total	219	37	12.02	49.02	1.522	818	0.087	1.32	2 cumulus
Direct-Normal	219	-	-	49.02	1.522	818	0.087	1.32	2 cumulus

Table 3.1.2

Atmospheric Conditions At The Times Solar
Spectral Measurements Were Obtained
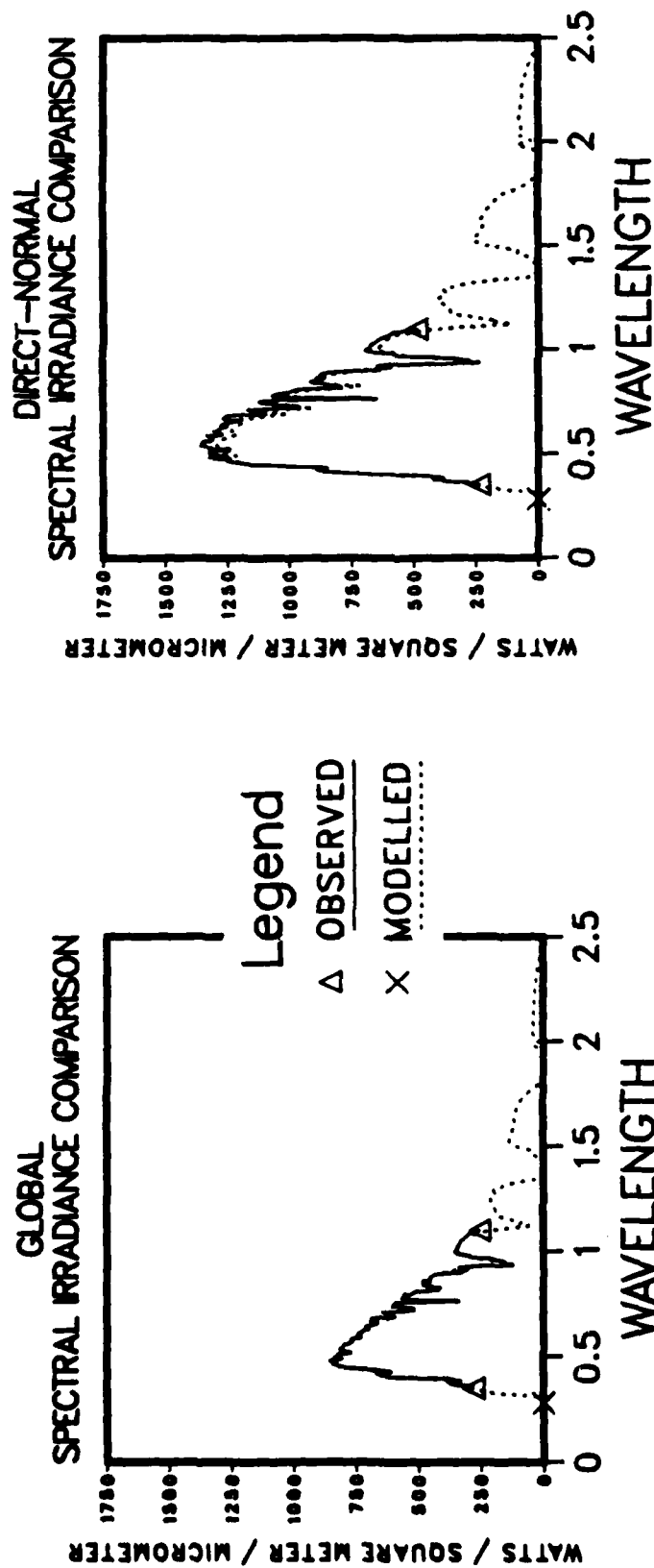
Figure 3.1.2.A

Comparison of Observed and Modelled Clear Sky Spectral Irradiances
For A Horizontal Surface

The global and direct-normal spectral irradiances are compared in the two plots.
The solid line represents the actual observation and the dashed line represents
the modelled irradiances. The solar zenith angle is 56.26 degrees. The wave-
length is in micrometers.
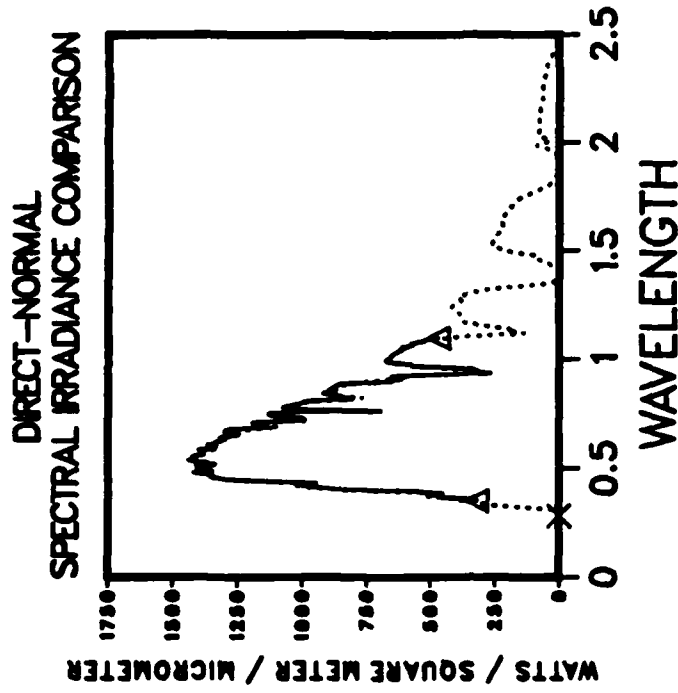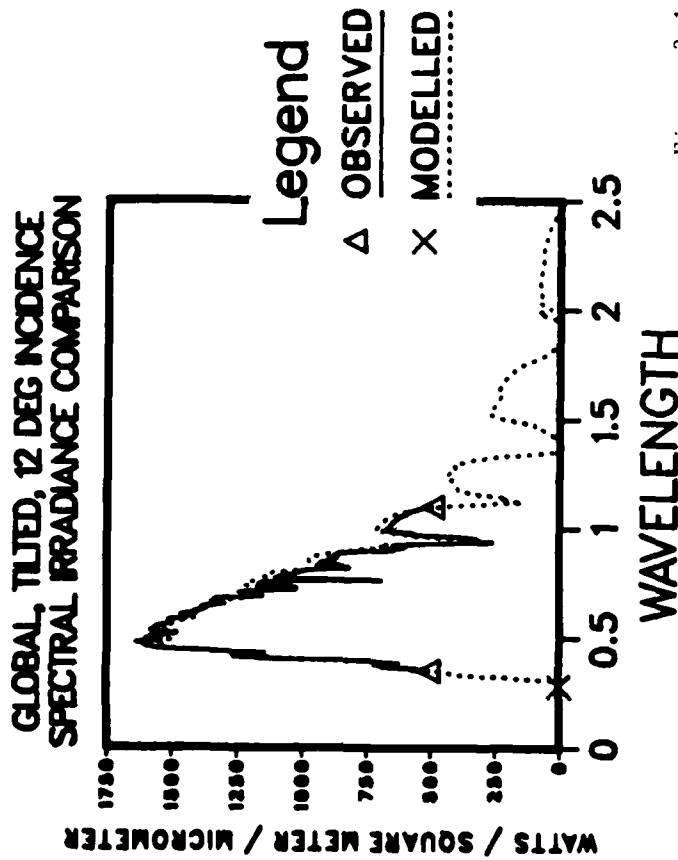
Figure 3.1.2.B

Comparison Of Observed And Modelled Clear Sky Spectral Irradiances
For A Sun-facing Tilted Surface (12 Degree Incidence)

The global and direct-normal spectral irradiances are compared in the two plots.
The solid line represents the actual observation and the dashed line represents the
modelled irradiances. The zenith angle of the tilted surface is 37 degrees and the
solar incidence angle relative to the tilted surface is 12.02 degrees. The wave-
length is in micrometers.
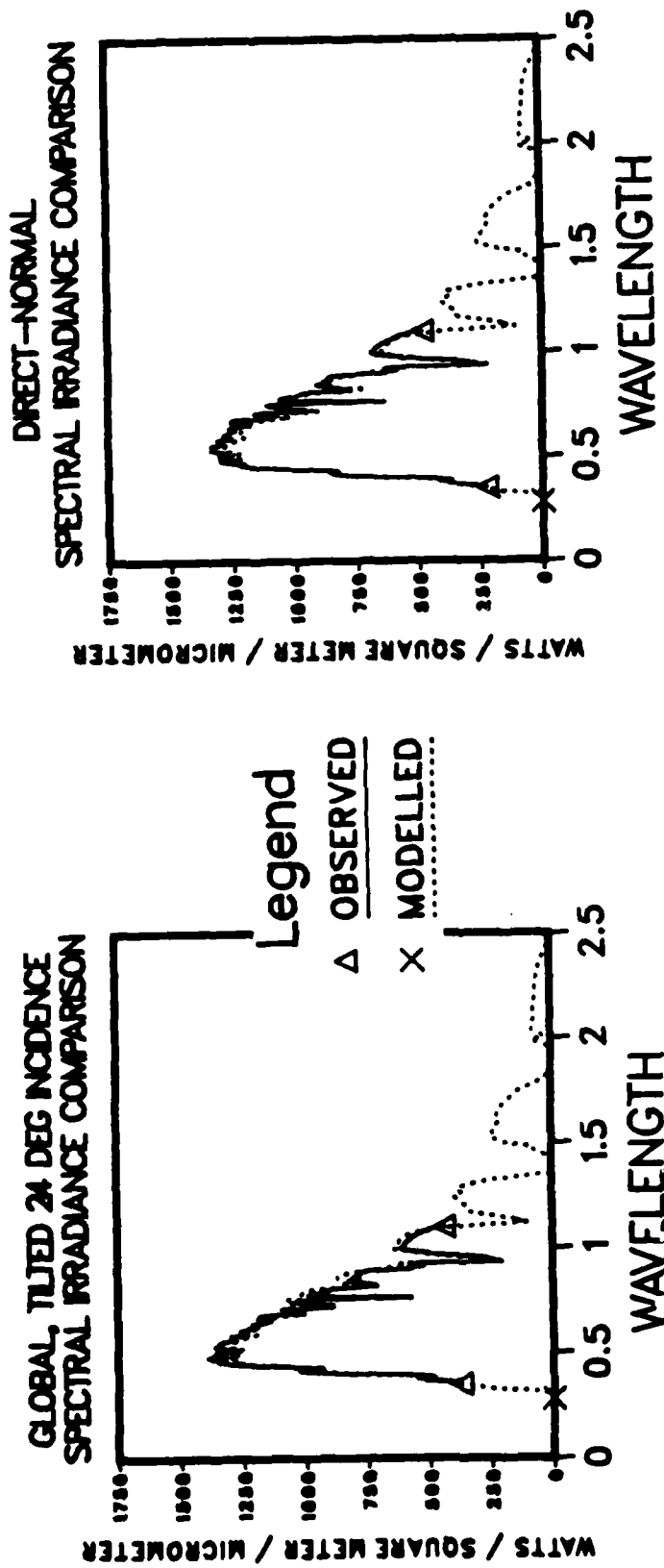
Figure 3.1.2.C

Comparison Of Observed And Modelled Clear Sky Spectral Irradiances
For A Sun-facing Tilted Surface (24 Degree Incidence)

The Global and direct-normal spectral irradiances are compared in the two plots.
The solid line represents the actual observation and the dashed line represents
the modelled irradiances. The zenith angle of the tilted surface is 37 degrees
and the solar incidence angle relative to the tilted surface is 24.36 degrees.
The wavelength is in micrometers.

observed values and the dotted lines are the modelled

values. The majority of the disagreement of the direct

normal radiation with observations is that the modelled

values are almost always lower than measurement. This is

expected since the model computes the direct radiation while

the measurement contains both direct and circumsolar diffuse

radiation. This also is in agreement with the assumptions

concerning the formulation of the transport equation used

for this model. The form of the transport equation selected

for use in this model tends to over-attenuate the radiation

reaching the surface of the Earth. After scanning the

modelled and observed values, the largest disagreement is

approximately 80 watts / sq m /μm out of a total observed of

nearly 1100 watts / sq m /μm at the peak. This corresponds

to a maximum error of 7.5%. The majority of the spectral

comparisons are much smaller than this maximum and fall

below the 5% error level. Based on the comparison plots of

the direct-normal and the global radiation with

measurements, it is reasonable to infer that the overall

accuracy is within 5 percent. While it's desirable to obtain

spectral diffuse observations to compare with the model

diffuse values, spectral diffuse observations are not

available at this time.

The spectral observations for a tilted surface are

plotted against the model values in Figures 3.1.2.B and

3.1.2.C. The close agreement between the modelled and

observed values indicate the model properly accounts for

tilted surfaces. Bird's original simple clear sky model
(Bird, 1984) did not account for tilted surfaces or spectral
albedos. Bird's latest model (Bird and Riordan, 1984)
handles tilted surfaces by using the technique of Justus and
Paris (1984). Figure 3.1.2.B compares the data for a
sun-facing 37 degree tilted surface where the solar zenith
angle relative to the tilted surface is 24.36 degrees.
Figure 3.1.2.C compares the data when the solar incidence
angle is 12.02 degrees. In both instances, the comparison is
good. Based on the comparisons, the overall accuracy is
likely within the desired 5% error for the majority of
tilted surface orientations. Note that the global radiation
reaching the tilted surface is greater than the
direct-normal radiation arriving at the same location. This
is attributable to the sky and ground diffuse radiation. The
ground diffuse radiation is defined as the radiation
reflected from the ground which reaches the collector
surface. The maximum direct radiation a surface could
receive is when the surface is direct-normal to the incoming
solar beam. Since the tilted surface is not oriented normal
to the incoming sunlight, the direct radiation must be less
than the direct-normal radiation. This means the addition of
the sky and ground diffuse radiation to the direct radiation
causes the global total radiation to be greater than the
direct-normal radiation. This contrasts with a horizontal
surface and clear sky conditions where the global radiation
(direct plus sky diffuse only) is usually less than the

tilted surfaces. Bird's original simple clear sky model (Bird, 1984) did not account for tilted surfaces or spectral albedos. Bird's latest model (Bird and Riordan, 1984) handles tilted surfaces by using the technique of Justus and Paris (1984). Figure 3.1.2.B compares the data for a sun-facing 37 degree tilted surface where the solar zenith angle relative to the tilted surface is 24.36 degrees. Figure 3.1.2.C compares the data when the solar incidence angle is 12.02 degrees. In both instances, the comparison is good. Based on the comparisons, the overall accuracy is likely within the desired 5% error for the majority of tilted surface orientations. Note that the global radiation reaching the tilted surface is greater than the direct-normal radiation arriving at the same location. This is attributable to the sky and ground diffuse radiation. The ground diffuse radiation is defined as the radiation reflected from the ground which reaches the collector surface. The maximum direct radiation a surface could receive is when the surface is direct-normal to the incoming solar beam. Since the tilted surface is not oriented normal to the incoming sunlight, the direct radiation must be less than the direct-normal radiation. This means the addition of the sky and ground diffuse radiation to the direct radiation causes the global total radiation to be greater than the direct-normal radiation. This contrasts with a horizontal surface and clear sky conditions where the global radiation (direct plus sky diffuse only) is usually less than the

direct-normal radiation.

3.1.3 Comparison With Broadband Clear Sky Data

The model can determine the radiation in any spectral
band between 0.28 and 4.0 micrometers. In addition, the
model can accumulate the amount of radiation over a time
interval of less than one hour or over the entire day. Daily
values of broadband radiation were tabulated from broadband
observations made at the University of Michigan for the
Solar and Meteorological Research Program. To test the model
against observed daily values, it was necessary to choose
days where the sky was clear and the variation in the
turbidity and water vapor was reasonably minimized. Ed
Ryznar, a researcher at the University of Michigan, had for
his own studies selected a set of clear days from the
observations (Ryznar, 1981). A clear day is defined as a
cloudless day. From this data set, one day each month was
selected as representative of a clear sky day. Days were
selected where all (or all but one) of the instruments were
aligned, calibrated, and working. The values of turbidity
(at 500 nm) and water vapor amount were made using a sun
photometer. The sun photometer measurements were made
irregularly during the day. Some days had more measurements
than others. Based on the measurements available for each
day, a typical value of turbidity and a typical value of the
water vapor amount was chosen as representative of that day.

The largest variation in the water vapor amount over a day
was 0.27 cm and the largest variation in the turbidity (at
500 nm) over a day was 0.045. Table 3.1.3.A contains the
atmospheric parameters observed for clear sky days. The
model calculated the daily amount of radiation based on
these typical atmospheric values which were assumed constant
throughout the day.

The spectral surface albedo representing bare soil was
used in the model computations. The bare soil albedo was
chosen for comparison purposes because it was thought to
best represent Ann Arbor throughout the year. Using the same
spectral albedo throughout the year provides a baseline for
comparison purposes. It may be possible to obtain closer
agreement between the observed and modelled values by
changing the surface albedo on a monthly or seasonal basis.
However, performing such an analysis would perhaps create
the impression of having selectively chosen the surface
albedo to obtain the best results. From the author's point
of view, this is not desirable.

In late 1982, a volcano (El Chichon) erupted in Mexico
and spewed ash and other constituents into the atmosphere.
The volcanic cloud associated with this eruption reached Ann
Arbor, Michigan during October 1982. For comparison with the
clear sky days chosen previously, a set of clear sky days
during the year following the volcanic eruption was also
selected. These days were chosen using the same criteria as
the previous set of clear sky days. While there is no

absolute guarantee, it is hoped that the primary difference between the two data sets will be the aerosol distribution. As before, one clear sky day each month was chosen. Table 3.1.3.B contains the atmospheric parameters used for the El Chichon clear sky days. The modelled daily values were based on these typical atmospheric values which were assumed constant throughout the day.

The observed versus the modelled values of the global, direct-normal, direct, diffuse, UV, RG2, and tilted surface (42.3 degrees) have been plotted for the normal clear sky days and the El Chichon clear sky days. Figures 3.1.3.C and D show the normal clear sky comparison plots. Figures 3.1.3.E and F show the El Chichon clear sky comparison plots. Note that the scales have been varied from plot to plot to highlight the differences between the observed and modelled values. Tables 3.1.3.G and 3.1.3.H contain a simple error analysis of the normal clear sky and the El Chichon clear sky cases respectively.

For the typical clear sky cases, the broadband global and total measurements (global, RG2, and tilted) agree with the modelled daily values. The other measurements (direct-normal, direct, diffuse, and UV) do not agree as well. The direct-normal and direct modelled values appear to consistently underestimate the observed values; while the modelled diffuse values appear to consistently overestimate the observed diffuse. In the worst case, this overestimate is nearly 100 percent of the observed daily values. However,

MONTH	YEAR	DAY OF THE YEAR	DAY OF THE MONTH	TURBIDITY (500 nm)	WATER VAPOR (cm)
JAN	81	18	18	0.1	1.0
FEB	82	34	4	0.16	0.19
MAR	82	72	13	0.2	0.3
APR	81	105	15	0.13	0.38
MAY	81	140	20	0.305	0.80
JUN	81	168	17	0.25	1.0
JUL	80	188	6	0.3	2.20
AUG	81	231	19	0.2	1.0
SEP	80	262	18	0.2	2.20
OCT	80	284	10	0.14	1.3
NOV	81	315	11	0.14	0.79
DEC	81	344	10	0.12	0.3

Table 3.1.3.A

Atmospheric Parameters For The Clear Sky Days
At Ann Arbor, Michigan

MONTH	YEAR	DAY OF THE YEAR	DAY OF THE MONTH	TURBIDITY (500 nm)	WATER VAPOR (cm)
OCT	82	299	26	0.31	1.14
NOV	82	319	15	0.17	0.55
JAN	83	1	1	0.28	0.51
JAN	83	18	18	0.22	0.14
FEB	83	44	14	0.41	0.97
MAR	83	71	12	0.18	0.56
APR	83	110	20	0.30	0.50
MAY	83	129	9	0.23	0.40
JUN	83	173	22	0.263	2.31
JUL	83	194	13	0.168	1.38
AUG	83	236	24	0.241	2.73
OCT	83	282	9	0.125	0.88

Table 3.1.3.B

Atmospheric Parameters For The Clear Sky Days With
The El Chicon Volcanic Cloud At Ann Arbor, Michigan

GLOBAL

DIFFUSE

DIRECT—NORMAL

DIRECT

Legend

× MODELLED
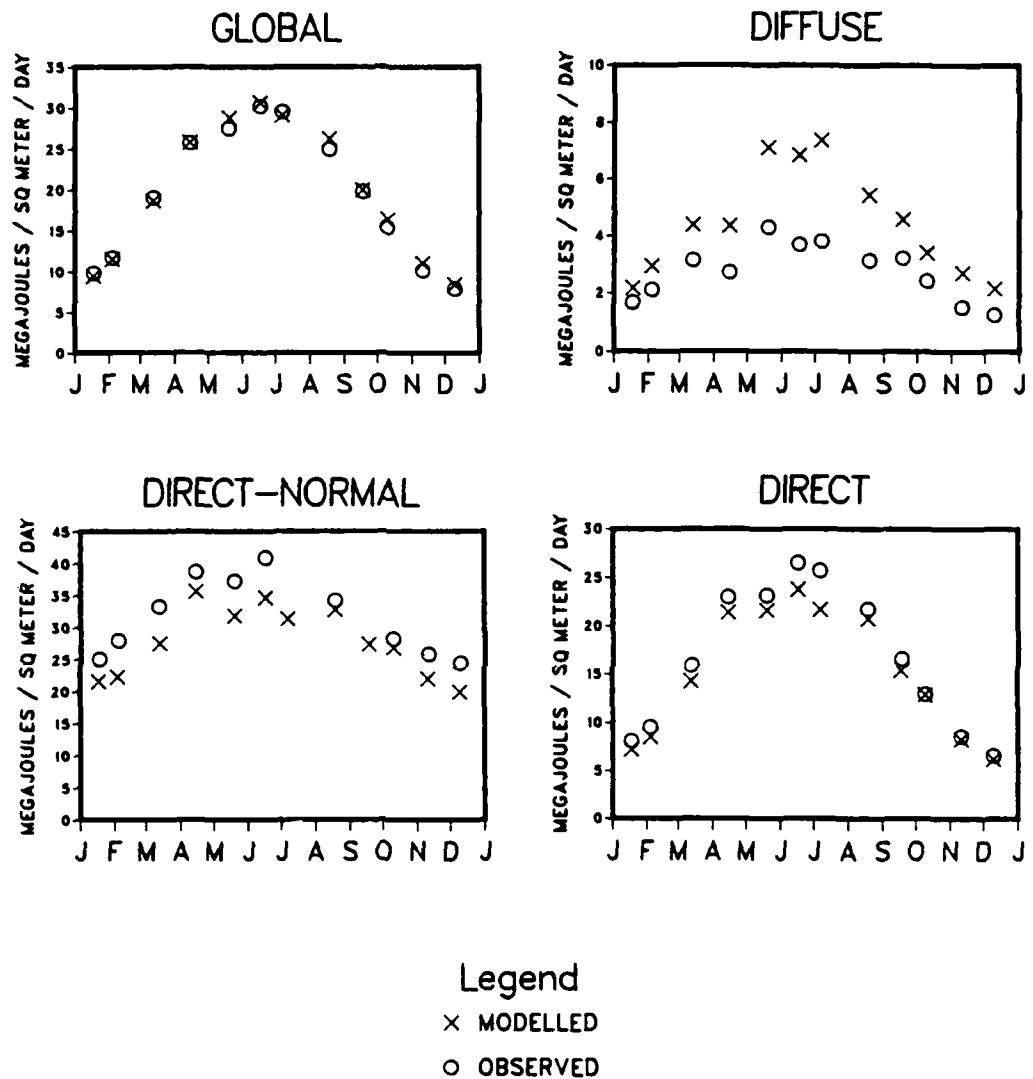
O OBSERVED

Figure 3.1.3.C

Daily Irradiance Comparison

The daily observed irradiance is compared with the daily modelled
irradiance. The spectral band is 0.28 to 2.8 micrometers.
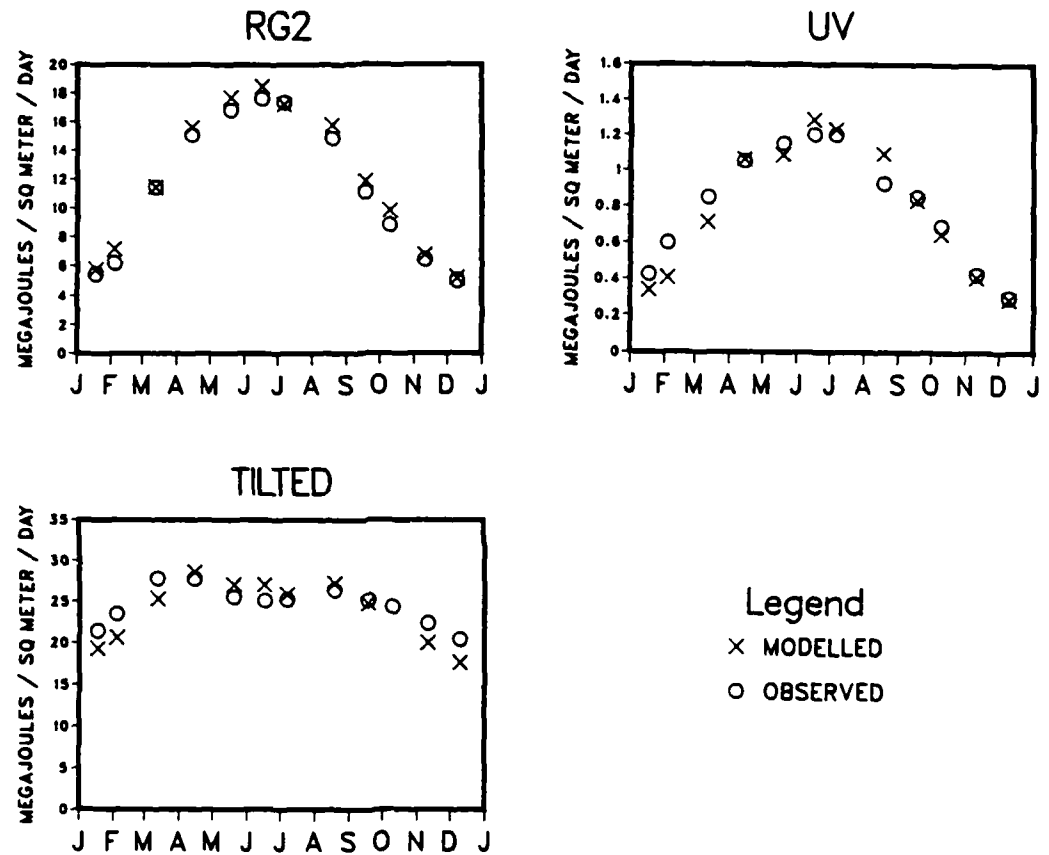
Figure 3.1.3.D

Daily Irradiance Comparison

The daily observed irradiance is compared with the daily modelled
irradiance. The spectral band is 0.28 to 2.8 micormeters.
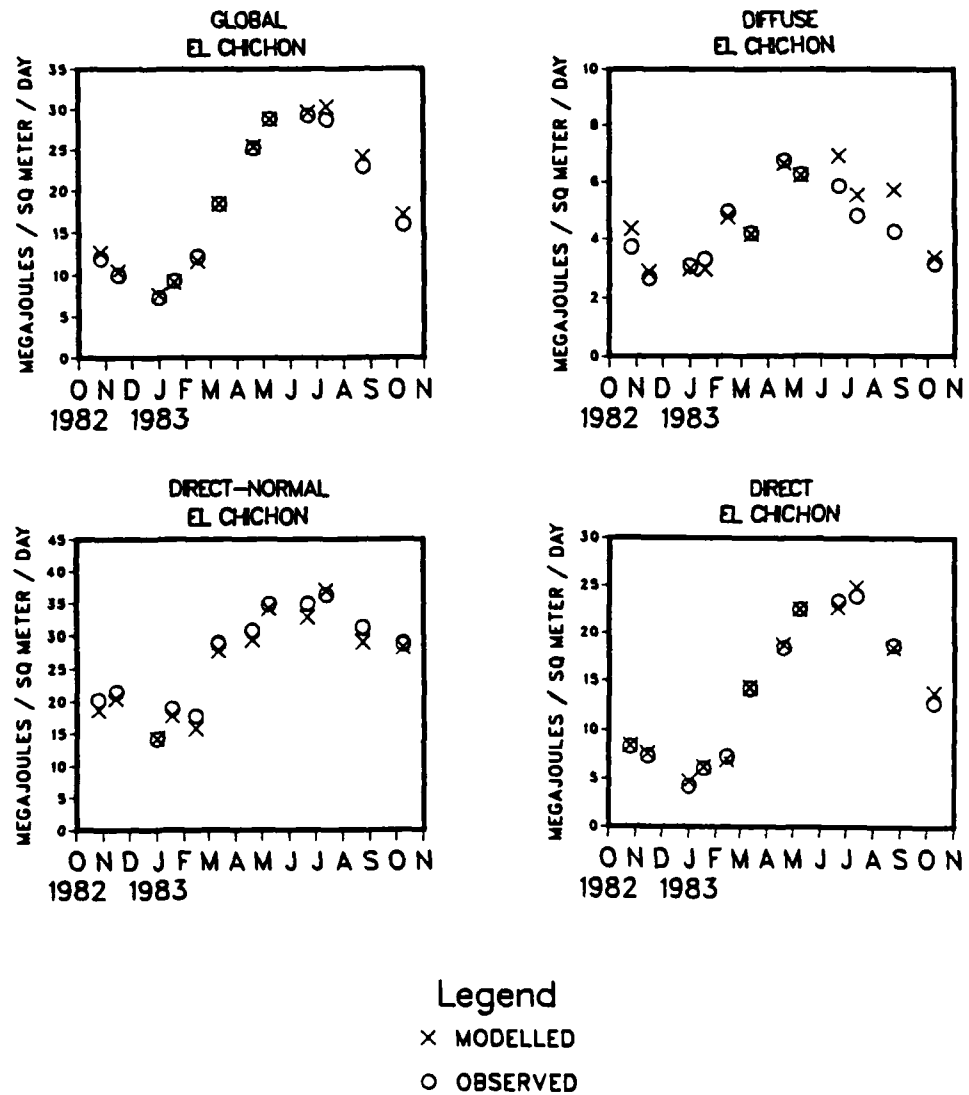
Figure 3.1.3.E

Daily Irradiance Comparison
With The El Chichon Volcanic Cloud

The daily observed irradiance is compared with the daily modelled
irradiance. The spectral band is 0.28 to 2.8 micrometers.
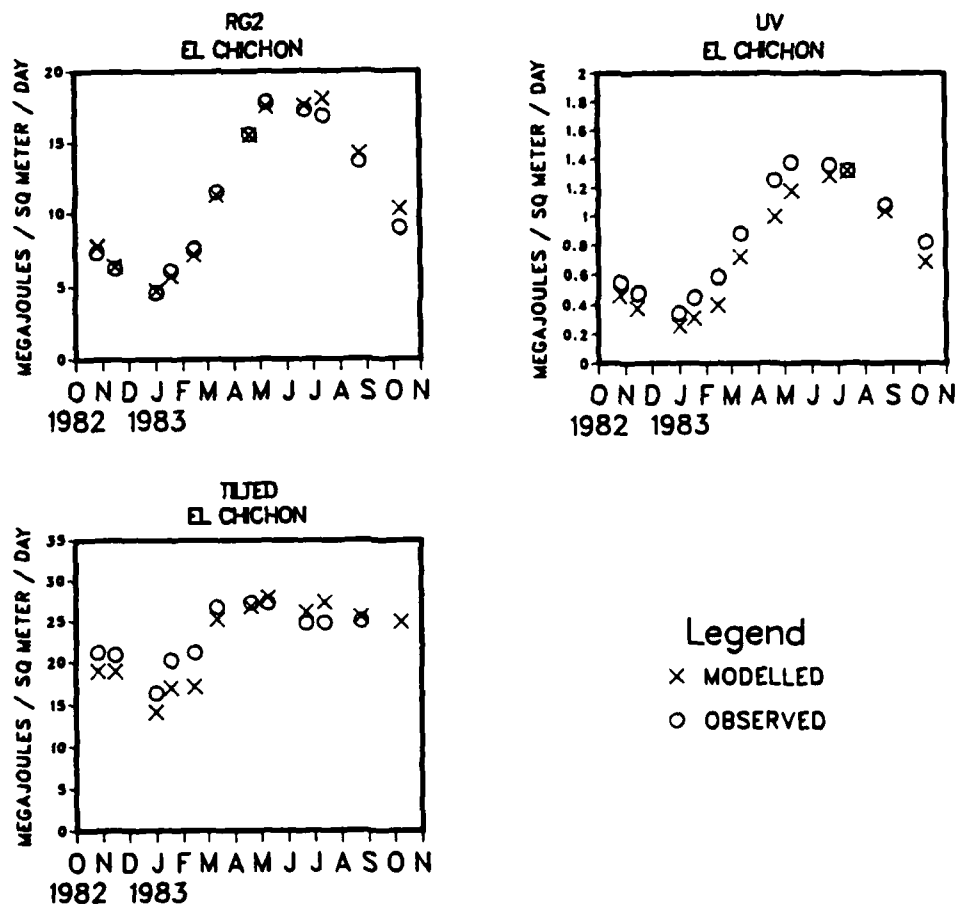
Figure 3.1.3.F

Daily Irradiance Comparison
With The El Chichon Volcanic Cloud

The daily observed irradiance is compared with the daily modelled
irradiance. The spectral band is 0.28 to 2.8 micrometers.

RADIATION TYPE	SMALLEST DIFFERENCE (MJ / DAY)	ERROR (%)	LARGEST DIFFERENCE (MJ / DAY)	ERROR (%)
Global	0.044	0.17	1.287	5.10
Direct-Normal	1.37	4.86	6.253	15.30
Direct	0.38	5.7	4.0	15.5
Diffuse	0.5	29.9	3.55	93.2
Ultraviolet	0.011	1.04	0.1	33.22
RG2 (Red Filter)	0.0	0.0	0.97	15.67
Tilted	0.4	1.58	2.845	13.29

Table 3.1.3.G

Model Errors Associated With The Clear Sky Days

RADIATION TYPE	SMALLEST DIFFERENCE (MJ / DAY)	ERROR (%)	LARGEST DIFFERENCE (MJ / DAY)	ERROR (%)
Global	0.24	0.8	1.608	5.61
Direct-Normal	0.03	0.21	2.193	7.022
Direct	0.022	0.097	0.886	3.709
Diffuse	0.042	0.67	1.465	34.641
Ultraviolet	0.003	0.22	0.255	20.383
RG2 (Red Filter)	0.051	0.32	1.188	7.048
Tilted	0.476	1.7	4.012	18.945

Table 3.1.3.H

Model Errors Associated With The El Chichon Clear Sky Days

RADIATION TYPE	ESTIMATED PERCENTAGE ERROR (RURAL AEROSOL) DISTRIBUTION	ESTIMATED PERCENTAGE ERROR (UNKNOWN AEROSOL) DISTRIBUTION
Global	$\pm$ 0 – 7	$\pm$ 15
Direct-Normal	$\pm$ 5 – 10	$\pm$ 25
Direct	$\pm$ 5 – 10	$\pm$ 25
Diffuse	$\pm$ 15 – 20	$\pm$ 100
Ultraviolet	$\pm$ 15 – 20	$\pm$ 50
RG2 (Red Filter)	$\pm$ 5 – 10	$\pm$ 50
Tilted	$\pm$ 10 – 20	$\pm$ 50

Table 3.1.3.I

Qualitative Estimates of Model Error

the overestimate in the modelled diffuse values and the underestimate in the direct and direct-normal radiation values nearly compensate for each other. The result is consistently more accurate broadband global and total radiation values. This is expected, due to the formulation of the transport equation, where the direct radiation is dependent on the aerosol and Rayleigh transmittances and the diffuse radiation is dependent on the complement of those transmittances.

The most influential factor in the clear sky model is the aerosol distribution. In this model, the aerosol distribution was assumed to resemble the rural aerosol distribution. The clear sky days probably have an aerosol distribution different from the rural aerosol distribution. Since both the direct-normal, direct, and diffuse values depend on the aerosol transmittance, an inappropriate aerosol distribution will affect the three quantities. The clear days probably have an aerosol distribution which has fewer particles at every radius than the rural aerosol distribution. This will mean a higher transmittance through the atmosphere and less scattering. This is observed in the plots; reduced direct-normal and direct values and increased diffuse values. Fortunately, the amount of underestimate in the direct case and the overestimate in the diffuse case tend to offset each other so that the global and total radiation values show consistently less error when compared with observation. The aerosol distribution should be

significantly different for the El Chichon clear sky cases and one should see a definite change in the comparison of observed and modelled values.

Reviewing the plots of the modelled versus observed values for the El Chichon clear sky cases and the typical clear sky cases, one can see the El Chichon comparisons indicate closer agreement especially in the direct-normal, direct, and diffuse quantities. This indicates the effects of the volcanic cloud over Ann Arbor tends to more closely resemble the model calculations using the rural aerosol distribution than the distribution from the clear sky days without the volcanic cloud. One obvious conclusion that can be drawn is that the aerosol distribution is very important. This model should only be used with those cases which closely approximate the rural aerosol distribution. One turbidity value at 500 nm is not sufficient to determine whether the rural aerosol distribution should be used. Three to five turbidity measurements should be obtained at different wavelengths and compared with the turbidities generated using the rural aerosol model to be more certain whether the aerosol distribution resembles the modelled rural aerosol distribution. Since the model has only one aerosol distribution, it is limited in application to those situations which closely approximate a rural aerosol distribution (particularly if numeric accuracy is required). The model's usefulness could be expanded by having more than one aerosol distribution available.

Because there is not sufficient data available to determine how close either the clear sky or the El Chichon clear sky aerosol distributions are to the rural aerosol distribution used in the model, it is impossible to quantitatively assign error to the model. However, Tables 3.1.3.G and 3.1.3.H show the maximum and minimum absolute error for the days used in the plots. The smallest and largest differences in megajoules per day were divided by the observed daily values to obtain the percentage error. The tables indicate the errors between the observed values and the modelled values. Realizing a difference in the aerosol distributions affected the errors, one can infer what the range of error for the model might be based on whether the aerosol distribution resembles the rural aerosol distribution. Table 3.1.3.I consists of inferred estimates of how good the model might typically be for both a rural aerosol distribution and an unknown aerosol distribution. The error estimates are subjective but reflect the error one could expect when using the model. The observed versus modelled comparisons only cover a few of the possible situations. The inferred error estimates are an attempt to give a typical error for the model and not an upper bound for the model error.

3.1.4 Cloudy Sky Data

There are no good cloudy sky data against which to compare this model against. A good data set will be defined as one where enough information is available to completely describe a particular set of circumstances. There are many problems inherent in comparing this model with observations. To begin with, there are no rectangular clouds in the real atmosphere. Based on the study by Welch and Zdunkowski (1980), suitable dimensions for rectangular clouds could be used to obtain realistic calculations provided data regarding the size and separation distances between the clouds were available. The model assumes a particular geometry for the clouds (rectangular array of clouds, striated array of clouds or an overcast). Very few observations of cloud cover describe the cloud pattern in the sky. The model calculates the spatial average of the radiation reaching the ground in the clear sky and under the cloud. The instrumentation measuring the radiation is basically a point collector. The instrumentation is either in the sunlight or in the shadow of a cloud (not both at the same time). This presents a problem in comparing the observations to the modelled values. If one assumes that over an hour the instruments will pass in and out of the cloud shadows, the integration of the instrument measurements into hourly totals may provide a data set for comparison. However, the variability in such data would probably be large since the accuracy of such measurements would depend on the size of the clouds and their velocity.

Overcast skies present fewer problems than partially cloudy skies. In overcast situations, the instrumentation is always in the 'shadow' of the clouds and the spatial average under the clouds is the same value the instrumentation will measure. The problem with the overcast situation is determining the cloud thickness. While rawinsondes can give information about the cloud bases and tops it is not highly accurate. A rawinsonde passing out of the top of a cloud at saturation will continue to show high dewpoints until the sensor dries sufficiently. By the time this occurs, the rawinsonde could have travelled several tens of meters or more. The cloud amounts reported in observations are highly subjective and not necessarily numerically accurate assessments of the amount of cloud cover. The combination of all these problems casts doubt on whether the model can be checked for accuracy. The accuracy of the model will not be decided by the data currently available. More complete observations must be taken in order to test this and future models of this sort. However, in the interests of verifying trends shown by the model, several days of cloudy sky data will be evaluated. There are many unknown quantities which must be estimated and given to the model in lieu of observation. The ability of any model to reproduce observation under these less than ideal conditions is very low.

The data was obtained from the Solar and Meteorological Research Program at the University of Michigan. The

instrumentation and measurements were exactly the same as those described in Section 3.1.1 for clear sky data. The nearest complete National Weather Service surface observation site (Detroit Metropolitan Airport) is approximately 15 miles east. The nearest rawinsonde station is located in Flint, Michigan approximately 50 miles north. Some observations are kept at the University of Michigan, but the only cloud parameters kept are the cloud type and amount. The cloud amount is recorded in terms of scattered, broken and overcast. There is no estimate of cloud tops. As with most observations, no information is kept on the size or structure of the observed cloud formations. There is also no information on where the clouds may be located in the sky relative to the observation site. The estimates of cloud amount and cloud thickness are very important in getting model results. The variation between 0.1 to 0.4 for scattered clouds and 0.5 to 0.9 for broken clouds can cause large differences in the model results.

The cloudy observations were developed from composite information from limited observations taken in Ann Arbor (NWS), observations from Detroit Metro (NWS), and rawinsonde data from Flint, Michigan (NWS). All the cloudy observations were during the hour of 1400 to 1500 (2 p.m. to 3 p.m.) local time. The cloud amounts were matched between the Detroit (Metro) and Ann Arbor observations in terms of the categories scattered, broken, and overcast. When they matched, the Detroit observation was used to obtain the

cloud amount in tenths. The Detroit observation was also
used to determine the cloud type and cloud bases. The Flint
rawinsonde was used to determine the cloud bases, cloud
tops, cloud thickness and to determine if more than one
cloud layer existed. Only those cases where the Detroit
observation and rawinsonde data gave the same cloud base was
used. Since this model is for a single layer of cloud, those
days on which the rawinsonde indicated more than one
possible layer of cloud were discarded. Air Weather Service
Manual 105-124 on the use of the Skew T, Log P thermodynamic
diagram in analysis and forecasting indicates that clouds
are usually present when the dewpoint depression is less
than 6 degrees Celsius. While there are several methods for
determining cloud tops, bases, and thicknesses, this method
is simple and just as reliable as the other techniques. The
cloud tops and thicknesses were determined from the Flint
rawinsonde using this technique. No information is available
about the dimensions or the location of the clouds. A cloud
size was chosen that represents a typical cloud (500 m). The
spacing between the clouds was varied to obtain the correct
cloud amounts. The precipitable water was obtained from the
National Climatic Center for Detroit, Michigan for the
desired days. The surface pressure was obtained from the
Detroit observation. Table 3.1.4.A lists the observed
parameters for the cloudy observations.

Turbidity measurements were taken on the days where the
mornings were clear and the aftermoons were cloudy or vice

DAY	TURBIDITY (500 nm)	WATER VAPOR (CM)	SURFACE PRESSURE (MB)	CLOUD BASE (M)	CLOUD TOP (M)	CLOUD TYPE	CLOUD AMOUNT (TENTHS)	CLOUD THICKNESS (M)
05/12/84	0.14	0.96	982.6	1520	1824	CU	2	304
06/03/84	0.16	1.57	982.2	1520	2128	CU	1	608
07/29/84	0.12	1.24	992.9	1216	1672	CU	2	456
03/09/85	0.18	0.71	989.5	912	1976	CU	1	1064
06/28/85	(0.10)	1.80	988.6	1368	2432	CU	1	1064
06/28/84	0.15	2.00	979.0	1520	3040	CU	6	1520
11/20/84	0.074	0.48	1000.3	1064	1672	SC	7	608
03/06/85	0.12	0.48	1004.3	760	1520	CU	5	760
02/03/84	(0.10)	0.78	970.6	760	3344	SC	10	2584
03/16/84	(0.10)	0.23	994.4	517	1216	SC	10	699

Table 3.1.4.A

Atmospheric Parameters of Cloudy Observations

versa. Choosing an appropriate turbidity value for the model
was accomplished by picking days where the clear sky
turbidity measurements were made in the morning and the sky
became cloudy in the afternoon. A water vapor amount was
inferred for the afternoon from the results of the morning
sun photometer measurements. These water vapor amounts
agreed with the precipitable water amounts obtained from the
National Climatic Center. The largest difference between the
National Climatic Center values and the sun photometer was
0.2 cm. For consistency, the National Climatic Center values
of precipitable water were used. On days where the turbidity
measurements could not be obtained (overcast days), a
turbidity value of 0.1 at 500 nm was used. These values are
enclosed in parentheses in Table 3.1.4.A.

3.1.5 Comparison With Broadband Cloudy Sky Observations

The observed versus modelled results are listed in
Table 3.1.5.A. The agreement between observation and model
is poor. This was expected. Conventional observations do not
provide the detail necessary to accurately compare the model
with observations. The model was designed for very specific
geometric cases (an array of clouds, striated clouds or
overcast clouds). In the scattered and broken cases, there
is no information about the geometry of the cloud formation.
There is also no information about the length of time the
sensor was in the cloud shadow or in the direct sunlight.

DAY	OBS OR MOD	GLOBAL (MJ/M^2)	DIFFUSE (MJ/M^2)	DIRECT-NORMAL (MJ/M^2)	RG2 (MJ/M^2)	UV (MJ/M^2)
05/12/84	OBS	3.509	2.071	3.110	2.024	0.157
	MOD	2.673	0.522	2.425	1.579	0.115
06/03/84	OBS	3.544	1.371	2.972	2.023	0.153
	MOD	2.942	0.484	2.702	1.735	0.128
07/29/84	OBS	3.253	0.805	2.596	1.868	0.145
	MOD	2.545	0.461	2.330	1.492	0.111
03/09/85	OBS	2.597	0.678	2.836	1.582	0.113
	MOD	1.515	0.364	1.976	0.921	0.056
06/28/85	OBS	3.355	0.767	2.660	1.972	0.144
	MOD	2.851	0.394	2.662	1.667	0.127
06/28/84	OBS	2.803	1.404	1.535	1.900	0.125
	MOD	1.177	0.519	0.714	0.673	0.056
11/20/84	OBS	0.905	0.584	-	0.477	0.037
	MOD	0.277	0.179	0.475	0.165	0.010
03/06/85	OBS	2.162	1.078	1.413	1.277	0.096
	MOD	0.766	0.253	0.903	0.459	0.029
02/03/84	OBS	0.740	0.453	-	0.334	0.032
	MOD	0.004	0.004	0.000	0.0006	0.0003
03/16/84	OBS	1.042	0.738	-	0.577	0.049
	MOD	0.071	0.071	0.000	0.032	0.004

Table 3.1.5.A

Comparison Of Cloudy Observations And Cloudy Model Calculations

This information is very important when comparing with observation. The time the sensor is in the direct sunlight versus the cloud shadow has a large impact on the measured irradiance. A significant portion of the difference between the observations and the model calculations is probably attributable to this factor. Coupled with the fact that the cloud geometries were probably not the same as those used in the model, there is reason to expect substantial differences between the observations and the modelled values.

To accurately compare a model with measurements, very specialized and detailed observations must be kept. Information on both the time and spatial characteristics of the cloud pattern as well as the location of the clouds, the cloud geometry, and the cloud dimensions will be needed. Even though the model comparison with observation is poor, there is sufficient reason to expect it to be and this indicates that present observations do not sufficiently characterize each situation to allow accurate comparison.

One piece of information can be derived from the comparison with observation, however. While all of the modelled values are too low in comparison to actual observation, the modelled values for the overcast cases are much too low. The observed cases are for very thick clouds (699 and 2584 meters). This indicates a problem in the modelling of the clouds. The simple solution to the radiative transfer equation used to represent the cloud is not indicative of actual cloud characteristics. Based on the

comparison, the results indicate that the extinction of radiation through the cloud is probably too large as the cloud becomes thick. Since both the cloud reflection and transmission properties are determined from the solution to the same radiative transfer equation, the solution to the cloud albedo should exhibit differences from measurement.

3.1.6 Cloud Reflectance Data

A limited amount of cloud albedo data is available for comparison; Kondratev presents cloud albedo measurements made from aircraft by Chel'tsov (Kondratev, 1969, translation, 1973). The data is based on measureme.. s taken above an overcast. Kondratev indicates cloud albedo varies with cloud thickness, cloud type, water content of the cloud, solar altitude, and the underlying surface albedo. The underlying surface albedo can produce a variation of 30 to 40 percent in the cloud albedo (Kondratev,1969). Kondratev indicates the higher the surface albedo, the higher the cloud albedo; and the lower the surface albedo, the lower the cloud albedo. The model confirms the basic trends indicated by Kondratev. This model computes the reflectance of the cloud-atmosphere-ground combination as well as the cloud albedo (based on the characteristics of the cloud alone). The modelled cloud albedo will be smaller than the modelled cloud-atmosphere-ground albedo. The thickness of the cloud will determine the degree of

influence of the surface albedo. This suggests a strong
connection between the underlying surface albedo and the
cloud-atmosphere-ground albedo (total albedo). Since no
specific data sets against which to test the model in this
respect are available, it will only be noted here that the
trends produced by the model are in agreement with observed
trends. Table 3.1.6.A from Kondratev (1969) indicates
changes in cloud albedo with different underlying surfaces.
For comparison, the cloud albedo as a function of cloud
thickness was computed for three different underlying
surfaces for Archangel, Soviet Union. The model produced
cloud-atmosphere-ground albedos for Archangel, Soviet Union
with the following parameters set:

Latitude	64.66 N
Longitude	41.00 E
Hour Angle	0.00
Cloud Type	Stratocumulus
Cloud Amount	Overcast
Cloud Height	1000.00 m
Turbidity (500 nm)	0.1
Water Vapor	2.0 cm

Both Kondratev's data in Table 3.1.6.A and the modelled
albedos in Table 3.1.6.B exhibit similar qualities. The
largest differences associated with cloud albedos occurred
when the underlying surface had a low albedo. When the
underlying surface has a high albedo, the distinction
between the cloud albedos virtually disappears regardless of
the thickness of the cloud. The thickness of the cloud has a
larger effect on the cloud albedo for lower surface

**Albedo (%) of clouds of lower stratum with different
density for various types of underlying surface**

Underlying surface	Breaking of snow, tenths	Clouds			Clear sky
		dense	inter-mediate	translucent	
Snow, 9-10 tenths	0	86	83	79	79
	1	82	76	70	70
	1-2	73	67	58	57
	2-3	71	61	51	45
Tundra	—	61	46	30	17
Water	—	58	45	25	8

Table 3.1.6.A

Albedo of Clouds With Various Underlying Surfaces

(From Kondratev, 1969)

CLOUD THICKNESS (M)	KONDRATEV	TURBID WATER	BARE SOIL	FRESH SNOW
50	0.29	0.53	0.55	0.63
100	0.37	0.62	0.63	0.67
200	0.50	0.68	0.68	0.70
300	0.62	0.70	0.70	0.71
400	0.71	0.71	0.71	0.72
500	0.79	0.72	0.72	0.72

Table 3.1.6.B

Comparison Of Changes In Cloud Albedo With Cloud Thickness
For Different Underlying Surfaces

reflectivities. It is the combination of the cloud thickness and the surface albedo which regulates the cloud albedo until the cloud becomes very thick. When the cloud becomes very thick the effect of the underlying surface on the cloud albedo is very small. Figure 3.1.6.C shows the cloud albedo computed by the model based on the cloud characteristics alone. Since the cloud is absorptive, the albedo approaches some limit but does not reach 100% regardless of how thick the cloud becomes. Of the four low cloud types modelled, the clouds shown in the figure represent the least absorbing cloud type (stratus) and the most absorbing cloud type (nimbostratus) as determined from the absorption coefficients. Figures 3.1.6.D gives an indication of the changes cloud type can make in affecting the cloud-atmosphere-ground albedo when the underlying surface is changed. While the changes are on the order of a few percent, a higher cloud-atmosphere-ground albedo is obtained for the most reflective cloud type when compared to a less reflective cloud type over the same surface albedo.

Chel'tsov's measurements of cloud albedo and cloud thickness provide a benchmark for comparing the model produced albedos. Chel'tsov's measurements were taken over Archangel (latitude 64.66 N, longitude 41.99 E), Soviet Union for several types of clouds. Of the categories of clouds used by Chel'tsov, the overcast stratocumulus category was the only one which contained a single cloud type directly analogous to one used in this model. For this

reason, only the stratocumulus category will be compared. Chel'tsov's values of cloud albedo versus cloud thickness are shown in Figure 3.1.6.E as reproduced from Kondratev (1969). The data indicates quite a bit of scatter. Since Chel'tsov's measurements were probably made on different days, the effects of solar zenith angle (solar altitude) are more than likely exhibited in the data. Kondratev does not state when Chel'tsov's measurements were taken. Differences in cloud conditions on distinct days also affect the measurements. These two facts may explain the scatter in the data. Because of Archangel's latitude, the solar zenith angle can get quite large for several months of the year.

The model calculated the cloud-atmosphere-ground albedos at Archangel, Soviet Union with the following parameters set:

Latitude:	64.66 N
Longitude:	41.00 E
Hour Angle:	0.00
Cloud Type:	Stratocumulus
Cloud Amount:	Overcast
Cloud Height:	1000.0 m
Turbidity (500 nm):	0.1
Water Vapor:	2.0 cm
Surface Albedo Type:	Bare Soil

The cloud albedo is dependent on the solar zenith angle since it determines the path distance a light ray must travel through the cloud. Day 166 was chosen as a representative summer day and is plotted against Chel'tsov's measurements in Figure 3.1.6.F. The curve plotted and labelled Kondratev in Figure 3.1.6.F is the curve Kondratev
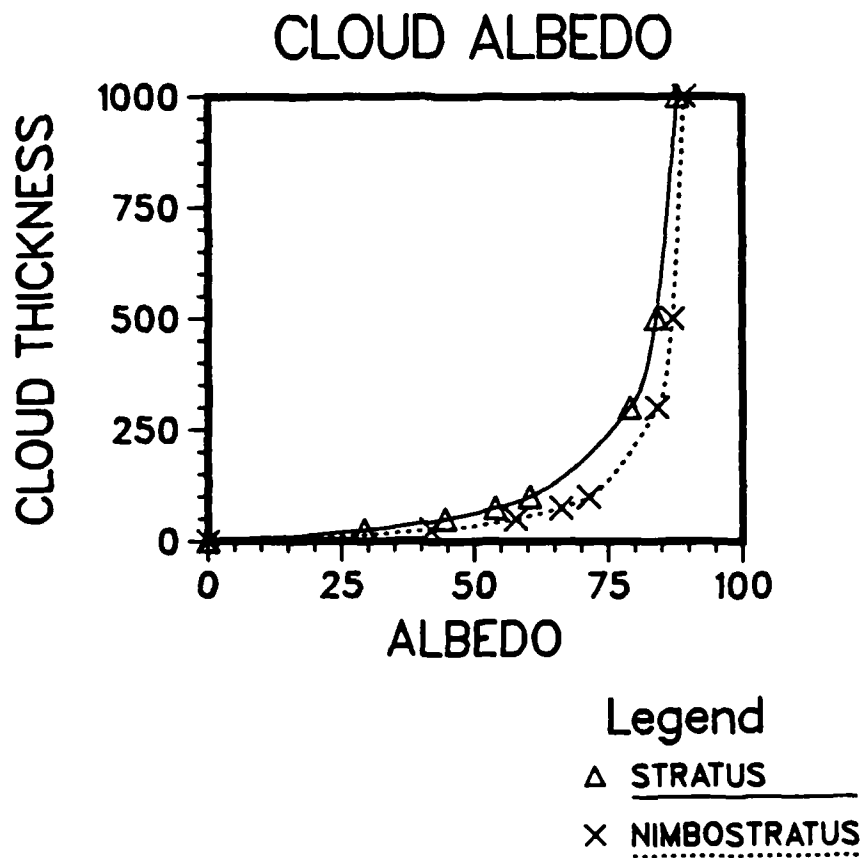
Figure 3.1.6.C

Model Calculation Of Cloud Albedo Based On Cloud Thickness
And Cloud Type

The cloud albedo is based on cloud characteristics alone
and the cloud albedo goes to zero as the cloud thickness
approaches zero.

CLOUD—ATMOSPHERE—GROUND ALBEDO
NIMBOSTRATUS CLOUD

CLOUD THICKNESS
(Meters)

ALBEDO

CLOUD—ATMOSPHERE—GROUND ALBEDO
STRATUS CLOUD

CLOUD THICKNESS
(Meters)

ALBEDO

Legend

△ snow surface

✕ wet sand surface
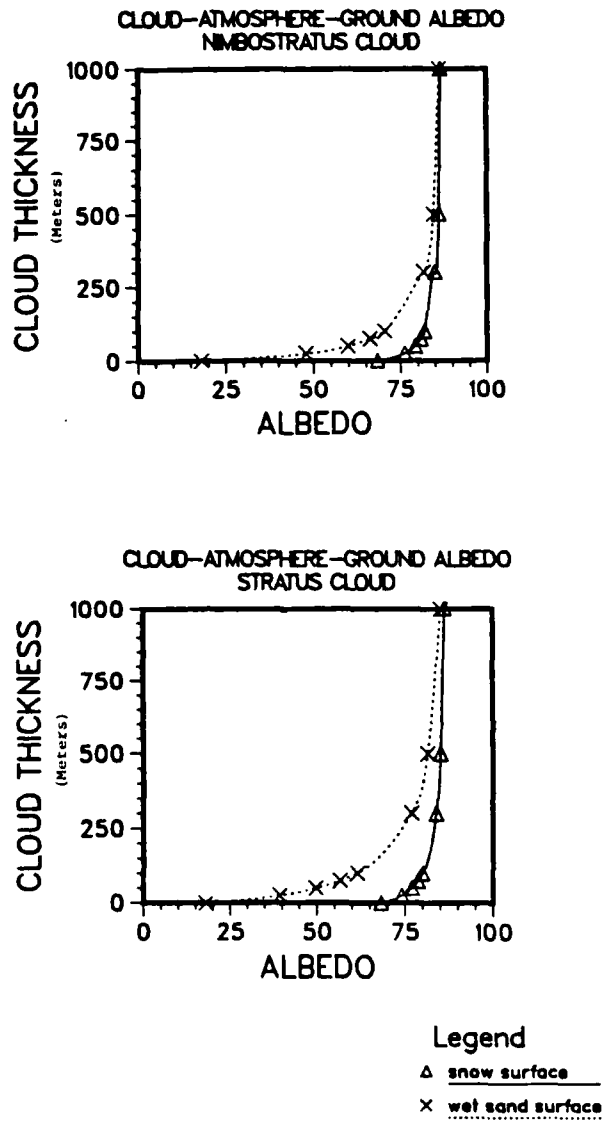
Figure 3.1.6.D

Combined Cloud-Atmosphere-Ground Albedo As A Function
Of Cloud Thickness

Day 174 was used for these calculations.

Dependence of albedo of clouds on thickness, from data obtained during flights. Arkhangelsk 1949-1950 [57].

1) Sc, 10 tenths, transilluminating; 2) Sc, Cu, 10 tenths; 3) Sc, 10 tenths; 4) Ac, 10 tenths.
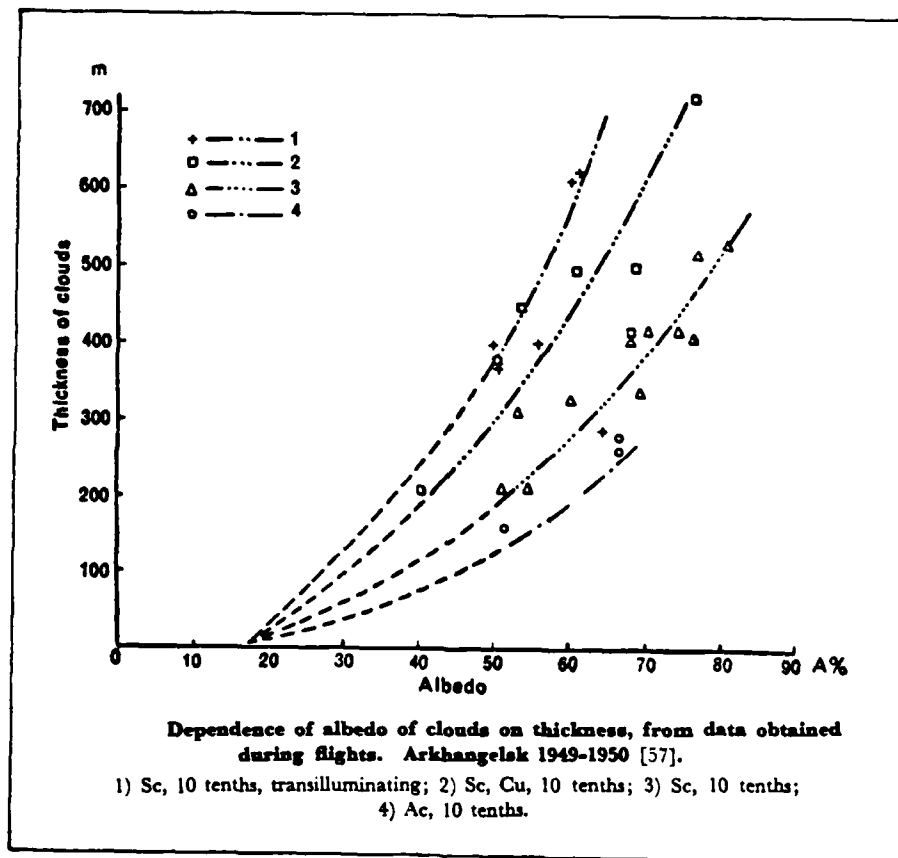
Figure 3.1.6.E

Cloud Thickness And Cloud Albedo

This figure represents data taken from aircraft above an overcast deck of clouds over Archangel, Russia (lat 64.66 N, lon 41.00 E). The curves fitted through the data highlight the change in albedo with thickness. (Kondratev, 1969).

CLOUD REFLECTANCE
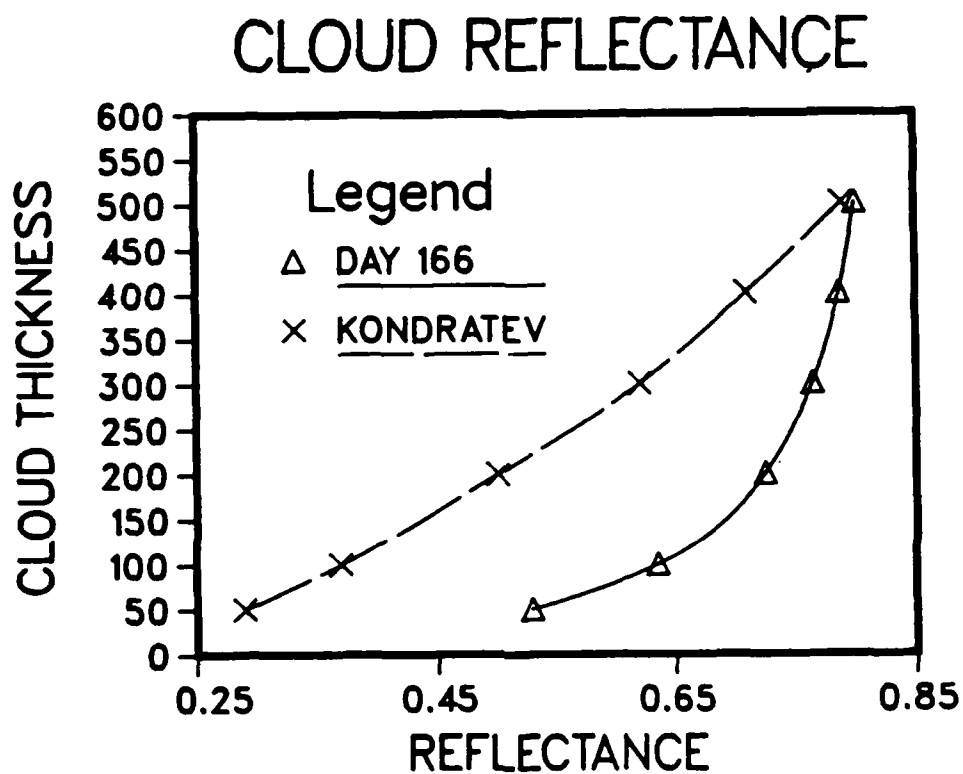
Figure 3.1.6.F

Comparison Of The Observed And Modelled Relationship Between
Cloud Thickness And Cloud Albedo

This figure contains the Kondratev curve for stratocumulus type
cloud and the modelled curve for stratocumulus type cloud. The
distinction between the curves indicates how the simplified solu-
tion for an abbreviated equation of radiative transfer differs
from observation.

CLOUD REFLECTANCE
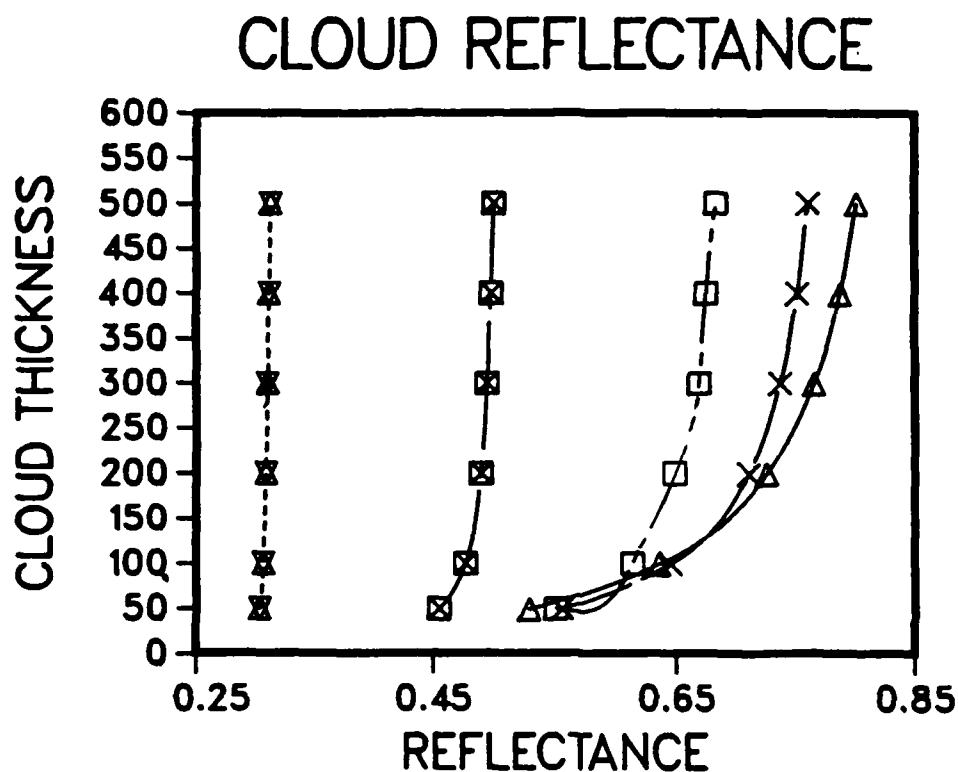
Legend

△	DAY 166	⊠	DAY 319
✕	DAY 258	⊠	DAY 349
□	DAY 288		

Figure 3.1.6.G

The Effects Of Solar Zenith Angle And Cloud Thickness
On Cloud Albedo

Five curves are plotted for cloud thickness versus cloud albedo
for different days of the year. Each day represents a different
solar zenith angle. The curves are representative of noon local
solar time.

fitted to Chel'tsov's data for stratocumulus cloud. The
difference in the shape of the modelled and observed cloud
albedo curves indicates that the calculated albedos can be
improved.

The effects of solar zenith angle on cloud albedo can
be demonstrated. The exact same scenario was modelled except
the day of the year was varied. During approximately 9
months of the year at Archangel, the effect of the solar
zenith angle is small. Figure 3.1.6.G demonstrates the
effects of solar zenith angle between days 166 and 349.
However, the solar zenith angle changes most rapidly during
the 3 winter months and the results of its effect on cloud
albedo is shown.

Several conclusions can be drawn from the above
comparison. The solution used by the model to compute the
cloud transmittances and reflectances exhibits more
exponential quality than the observations. Even so, the
basic effects caused by variations in cloud thickness, solar
zenith angle, cloud type, and surface albedo seem to
preserved.

3.2 The Effects Of Surface Albedo With A Clear Sky

The effects of surface albedo on the radiation received
by a plane at the Earth's surface can be evaluated with this
model. The effects of changing the spectral surface albedo
will vary in each part of the spectrum and it becomes nearly

impossible to quantify the error. For analysis purposes, the two spectral albedos available in the model which tend to represent the extremes were compared. For this and the following sections, the degree of change will be stated in terms of the largest differences noted.

3.2.1 Daily Effects Of Surface Albedo With A Clear Sky

The effects of surface albedo are expected to be the smallest for a horizontal surface and larger for tilted surfaces. The changes should also be the smallest for a clear sky. In a clear sky, there is no multiple scattering between the clouds and the ground. While there is some multiple scattering between the ground and the atmosphere, the magnitude of it does not compare with the changes in multiple scattering between cloud and ground. To verify these common sense deductions, the set of clear sky days for Ann Arbor without the volcanic cloud was modelled using the exact same parameters except for the surface albedo. Instead of using the bare soil surface albedo, the snow and the wet sand albedos were used. These two surfaces were chosen because they represent the largest difference between the seven surface albedo types in the model. The turbid water surface is the lowest surface albedo of all the albedo types in the model. However, the water surface was not used because it violates the assumption that the surface is Lambertian. The differences observed should represent large

variations due to surface albedo effects. Figure 3.2.1.A
shows the comparison plots of the modelled daily values of
the global, diffuse, UV, RG2, and tilted surface radiation.

The largest variation with surface albedo occurs during
the summer months and the smallest during the winter months.
As the solar zenith angle becomes large, the surface albedo
increases. Paltridge and Platt's formulation for this change
is nearly exponential as the solar zenith angle increases
and the differences between surface types will begin to
disappear as the solar zenith angle becomes large. This
means the differences in surface albedo will be most
pronounced at low solar zenith angles and least pronounced
at high solar zenith angles; an effect demonstrated in every
comparison plot.

The maximum amount of variation due to changing surface
albedo has been estimated by taking the largest difference
between the snow albedo case and the wet sand case and
dividing it by the wet sand value. The variation due to a
change in surface albedo for a horizontal surface at
mid-latitude (Ann Arbor) is approximately:

Global	6.13%
Diffuse	23.63%
UV	19.14%
RG2	2.17%

For a surface tilted at 42.3 degrees, the variation in the
global total radiation is 23.21%. While the percentage for a
tilted surface is nearly the same as for a diffuse
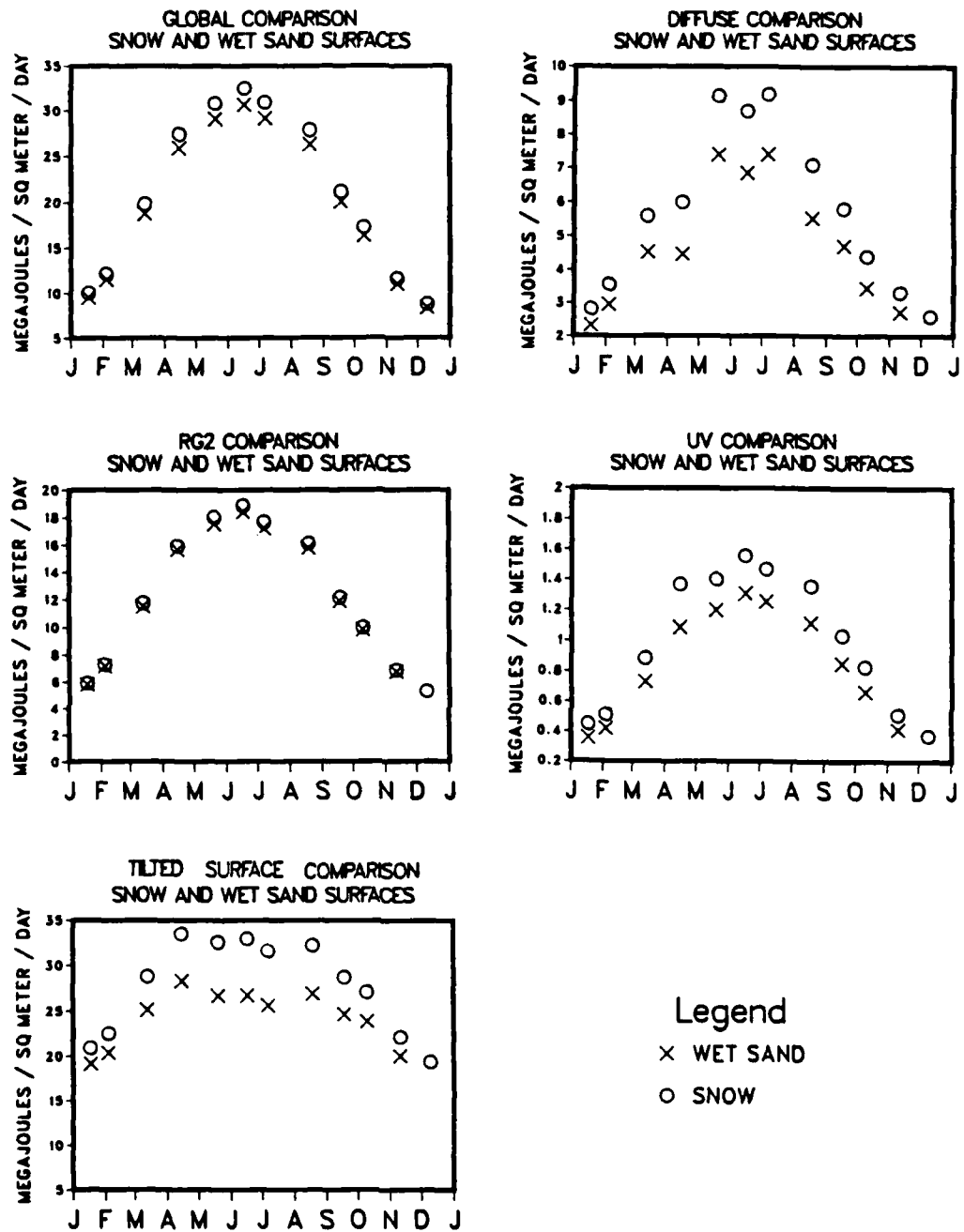
Figure 3.2.1.A

Comparison Of Daily Irradiance Under Clear Skies
With Snow And Wet Sand Surfaces

horizontal surface, the amount of radiation accumulated by the tilted surface is much greater. The direct radiation arriving at the south-facing tilted surface is greater than that arriving at a horizontal surface due to the plane orientation. However, the differences observed are due to the changes in the sky and ground diffuse radiation. The effects of low solar zenith angle can be seen on the tilted surface just as for the horizontal surface. The differences are greatest in Ann Arbor's summer when the solar zenith angle is smallest. The double peak in the tilted surface plot is due to the orientation of the surface relative to the solar position during the year. The shape of the curve can be changed by adjusting the orientation of the plane surface. The effects of different surface orientations have been presented by Kondratev (1977) and Robinson (1966).

3.2.2 Spectral Effects Of Surface Albedo With A Clear Sky

While the broadband variations of surface albedo are interesting, they do not provide the detail that a spectral example can show. For the sake of simplicity, a day near the equinox (day 74) was chosen for this analysis; a day when the solar zenith angle is not particularly high or low. To compare the cases, the following parameters were held constant:
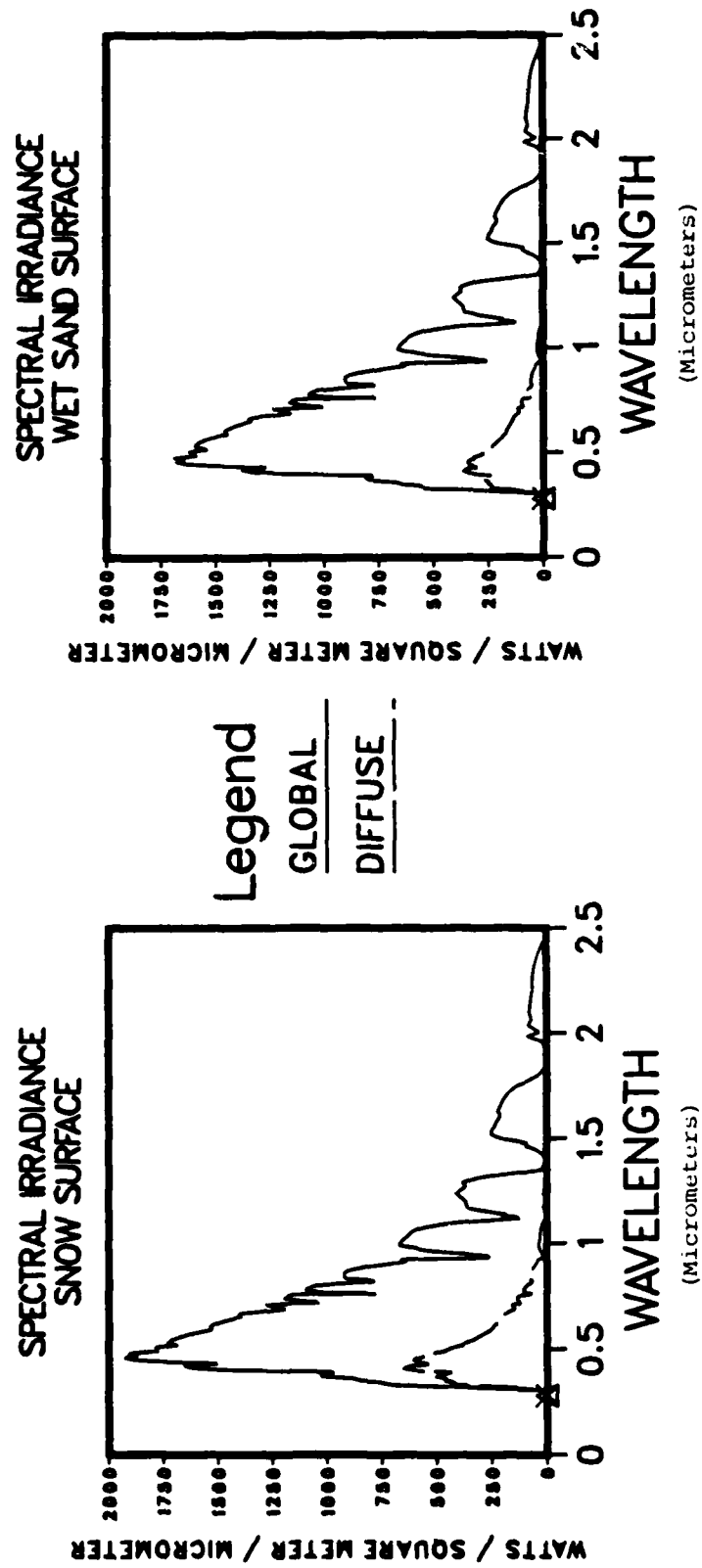
Figure 3.2.2.A

Comparison Of The Global And Diffuse Spectral Irradiances
Under Clear Skies With Snow and Wet Sand Surfaces

Turbidity (500 nm)	0.100
Water Vapor	2.000 cm
Surface pressure	1013.000 mb
Hour angle	0.000 (noon)
Ozone amount	0.364 cm

The cases were for Ann Arbor, Michigan (latitude 42.2833 N, longitude 83.7333 W). Figure 3.2.2.A highlights the differences for horizontal snow and wet sand surfaces. The variation in the diffuse radiation has caused the differences in the figures. The direct radiation reaching the horizontal surface is the same in each case. The broadband difference (0.28 to 4.0 micrometers) represented by these plots is 47.094 watts per square meter. This represents a difference of 6.37% in the global radiation and a change of 45.77% in the diffuse radiation. In this case (and typically in most other cases), the largest changes tend to occur between 0.4 and 0.7 micrometers, an atmospheric window where absorption by the atmosphere is small. Throughout the spectrum, atmospheric absorption causes the effects of multiple scattering to be enhanced more in some regions than others.

3.3 Broadband Effects Of Clouds And Surface Albedo

The modelling of clouds and surface albedo present many problems. One of which is trying to account for the many parameters which influence the results. To analyze the effects of one or two parameters, the other parameters need to be held constant so the effect of varying one variable can be determined. For this reason, the cases in this section have the following variables fixed:

Latitude	42.2833 N	Deg
Longitude	83.7333 W	Deg
Turbidity (500nm)	0.1	
Water Vapor	2.0	cm
Ozone	0.3620	cm
Day	174	
Hour Angle	0.0	Noon
Sky Condition	Overcast	

The intent of the following sections is to demonstrate the effects of cloud cover on the radiation reaching a plane at the Earth's surface. The solar zenith angle will be the same in each case.

3.3.1 Cloud Thickness, Cloud Type, and Surface Albedo

The purpose of this section is to demonstrate the qualitative effects of cloud thickness, cloud type, and surface albedo on the radiation reaching a plane at the surface of the Earth. The cloud types and surface albedos have been chosen so as to obtain the maximum variation. Of the cloud types available in this model, stratus is the

least absorptive and nimbostratus is the most absorptive. Of the surface albedo types, snow is the most reflective and wet sand the least reflective . Combinations of these cloud and surface albedo types will span the range of variation due to each factor. Figure 3.3.1.A shows the same situation with a snow surface. Figure 3.3.1.B shows the effect of varying the cloud thickness over a snow surface for both a stratus and nimbostratus overcast.

The change in cloud type can reduce the radiation for a given thickness by up to 50 percent. For global radiation, a change in cloud thickness can reduce the radiation by up to 100 percent for thick clouds. The diffuse radiation is shown to first increase for thin clouds and later decrease for thicker clouds. The effect is caused by the combination of the scattering and absorbing properties of the cloud. As the cloud becomes thicker, the absorption becomes large enough to compensate for the increase in scattering and the diffuse radiation decreases. When the cloud is thin, the absorption does not compensate for the increase in scattering by the cloud and the diffuse radiation increases. The maxima in the diffuse radiation occur when the clouds are between 25 and 50 meters thick. The direct radiation plotted as a function of thickness is identical in both figures. The global and diffuse radiation are affected by varying the cloud type, cloud thickness, and surface albedo. The snow or high surface albedo causes more radiation to be received at the surface than the wet sand or low albedo surface regardless
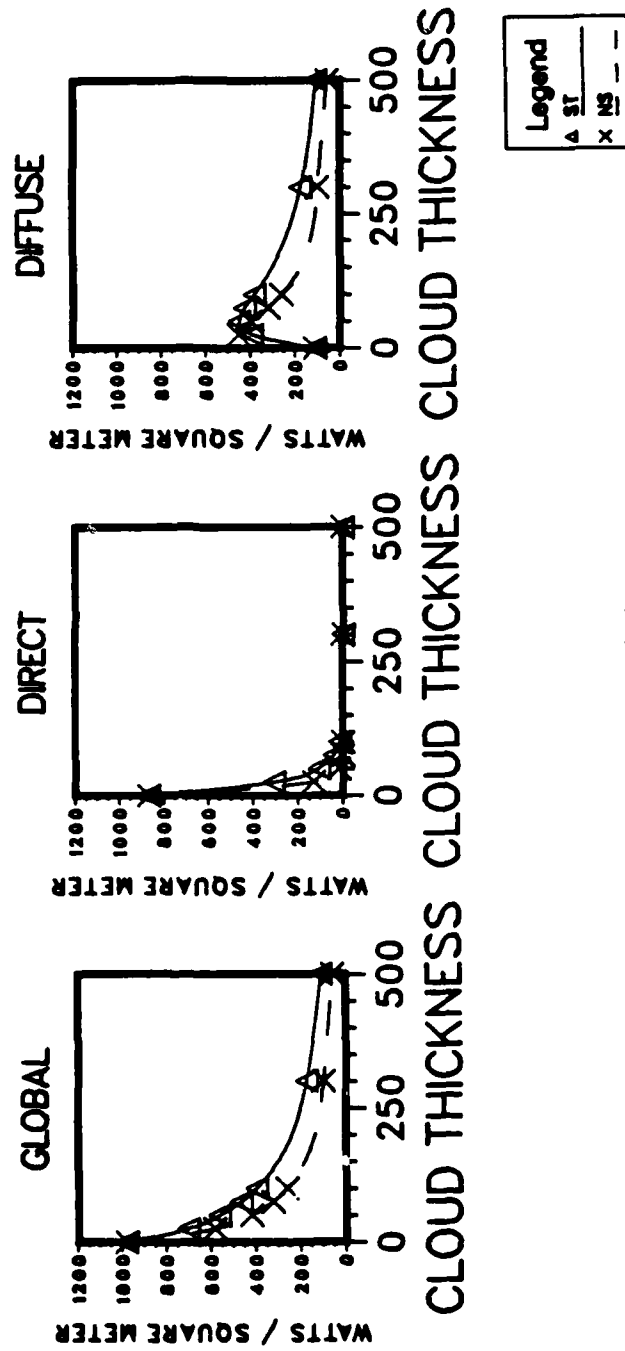
Figure 3.3.1.A

Comparison Of The Effects Of Cloud Thickness And Cloud Type
For Overcast Skies With A Wet Sand Surface

The cloud thickness is in meters.
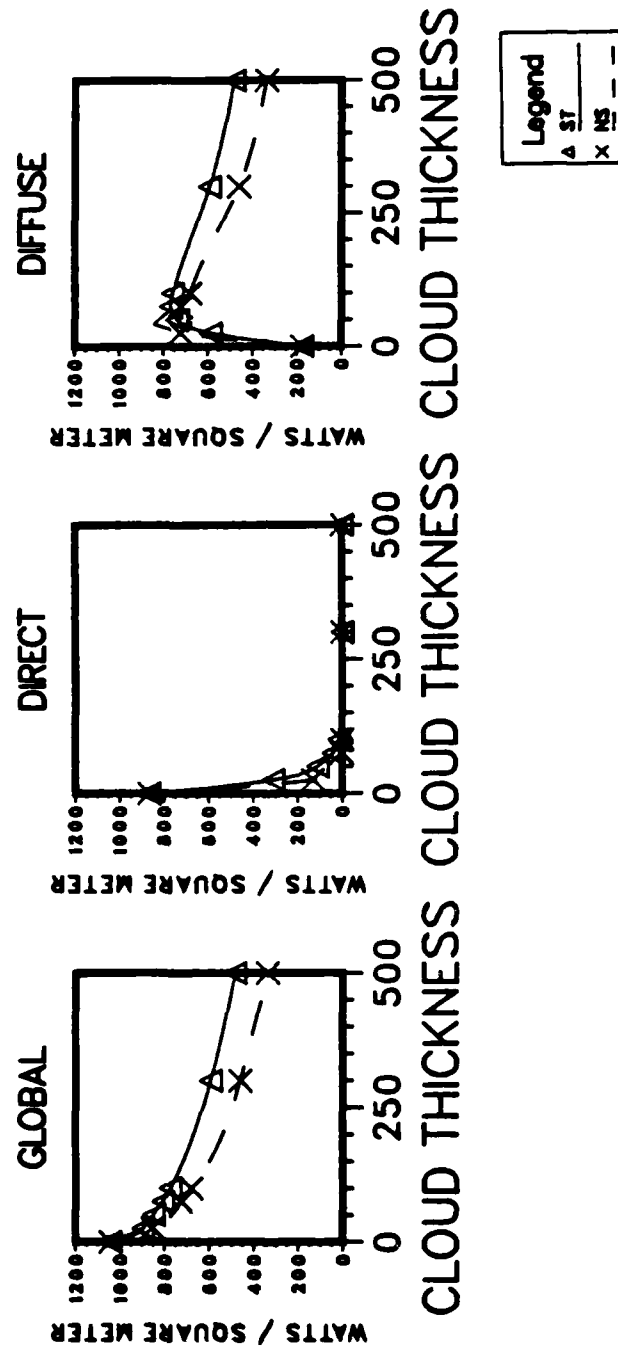
Figure 3.3.1.B

Comparison Of The Effects Of Cloud Thickness And Cloud Type
For Overcast Skies With A Snow Surface

The cloud thickness is in meters.

of cloud type or cloud thickness.

Based on Figures 3.3.1.A and B, the following conclusions can be drawn. Of the three parameters (cloud thickness, cloud type, and surface albedo), the cloud thickness has the greatest effect on the radiation reaching the surface of the Earth. Surface albedo produces the second largest effect and cloud type produces the smallest effect of the three parameters.

3.3.2. Cloud Amount, Cloud Type, And Surface Albedo

For the comparisons in this section, the same parameter values were used as in the last section. To quantify the variation in cloud amount, the cloud thickness was constant at 100 meters. The clouds were assumed to be in a rectangular array similar to a typical field of cumulus clouds. The cloud bases were chosen to be 100 meters on each side. The distances between the clouds a were adjusted to produce the cloud coverage. The radiation reaching the surface is the average amount of radiation from the clear sky, through the side of the rectangular cloud, and through the top of the rectangular cloud. In other words, it represents the spatial average of radiation reaching the surface. Figures 3.3.2.A and B represent the variation in radiation reaching the surface of the Earth due to changing cloud amount, cloud type, and surface albedo.
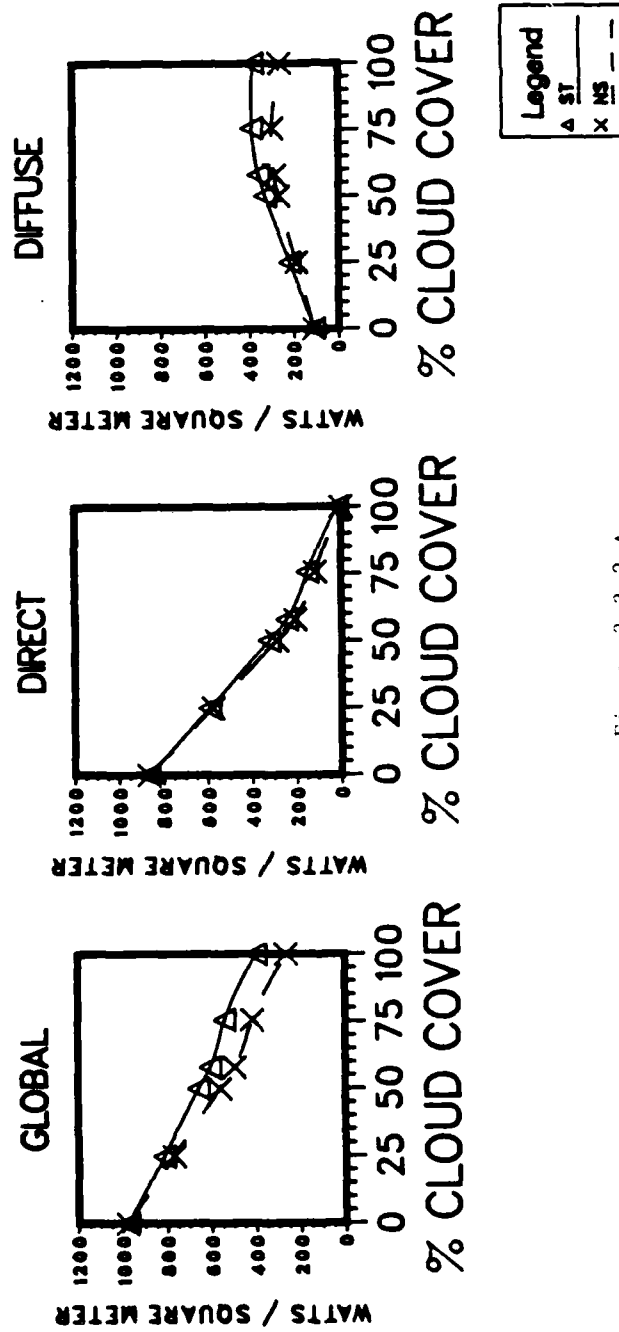
Figure 3.3.2.A

Comparison Of The Effects Of Cloud Amount And Cloud Type
For Partially Cloudy Skies With A Wet Sand Surface

163
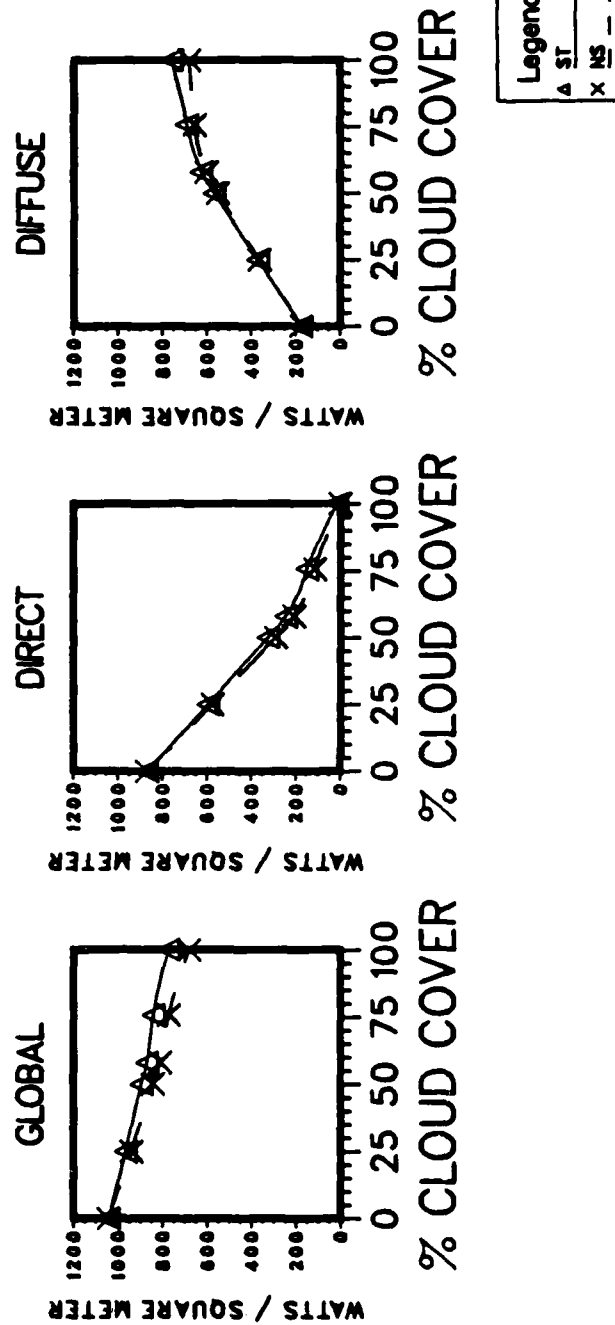
Figure 3.3.2.B

Comparison Of The Effects Of Cloud Amount And Cloud Type
For Partially Cloudy Skies With A Snow Surface

By comparing Figures 3.3.2.A and B, one can determine that cloud amount has the largest influence on the radiation reaching the surface of the Earth. In comparison, surface albedo has the second largest effect; while cloud type has the smallest effect.

3.3.3 Cloud Thickness, Cloud Amount, Surface Albedo, and Cloud Type

By comparing the figures in sections 3.3.1 and 3.3.2, one can quantify which of the four parameters has the largest effect on the radiation reaching the surface of the Earth. Qualitatively, it is straight-forward to determine from the figures that cloud amount plays the dominant role. The other parameters in descending order of importance are cloud thickness, surface albedo, and cloud type. These conclusions were drawn based on the reduction in the radiation reaching the surface of the Earth. It is possible to generate cases where the cloud thickness will be the dominant factor instead of the cloud amount. However, in most instances the order of influence of the parameters will be as listed.

3.4 Spectral Effects Of Clouds And Surface Albedo

The spectral effects of varying cloud thickness, cloud amount, surface albedo, and cloud type will be discussed.

Many parameters have been held constant so that the effects of cloud thickness, cloud amount, surface albedo, and cloud type can be demostrated. For these cases, the following variables were constant:

Latitude	42.2833 N	Deg
Longitude	83.7333 W	Deg
Turbidity (500 nm)	0.1	
Water Vapor	2.0	cm
Ozone	0.3639	cm
Day	74	
Hour Angle	0.0	Noon

In each of the following sections, a different parameter will be evaluated in combination with the surface albedo. This will give some insight into the interrelationship between cloud parameters and the surface albedo.

3.4.1 Spectral Effects Of Cloud Thickness And Surface Albedo

Figures 3.4.1.A through D illustrate the effects of varying the cloud thickness and changing the surface albedo. Figures 3.4.1.A and B show the effects of varying the thickness of overcast nimbostratus cloud with a snow surface. Figures 3.4.1.C and D demonstrate the same situation with a wet sand surface. Figures 3.4.1.B and D indicate that once the cloud thickness becomes large, the differences observed are due to changes in the diffuse radiation alone. This is because there is so little direct radiation coming through a 'thick' cloud. Figures 3.4.1.A and C illustrate two effects; the effect of cloud thickness

166

Figure 3.4.1.A

Comparison Of The Effects Of Cloud Thickness On The Global And Diffuse
Spectral Irradiances For A Nimbostratus Overcast With A Snow Surface

The global radiation decreases with each increase in thickness (clear sky: top line; 25 m
thickness: middle line; 100 m thickness: bottom line). The diffuse radiation increases
then decreases with changes in thickness. The wavelength is in micrometers.

Figure 3.4.1.B

Comparison Of The Effects Of Cloud Thickness On The Global And Diffuse
Spectral Irradiances For A Nimbostratus Overcast With A Snow Surface

The global and diffuse radiation are decreasing with each increase in thickness (100 m thickness:
top line; 500 m thickness: bottom line). The wavelength is in micrometers.

DIFFUSE SPECTRAL IRRADIANCE
OVC NS WET SAND

WATTS / SQUARE METER / MICROMETER

WAVELENGTH

Legend

CLEAR

25 M

100 M

GLOBAL SPECTRAL IRRADIANCE
OVC NS WET SAND

WATTS / SQUARE METER / MICROMETER

WAVELENGTH

Figure 3.4.1.C

Comparison Of The Effects Of Cloud Thickness On The Global And Diffuse Spectral
Irradiances For A Nimbostratus Overcast With A Wet Sand Surface

The global radiation decreases with each increase in thickness (clear sky: top line; 25 m
thickness: middle line; 100 m thickness: bottom line). The diffuse radiation increases then
decrease with a change in thickness (clear sky: bottom line; 25 m thickness: top line; 100 m
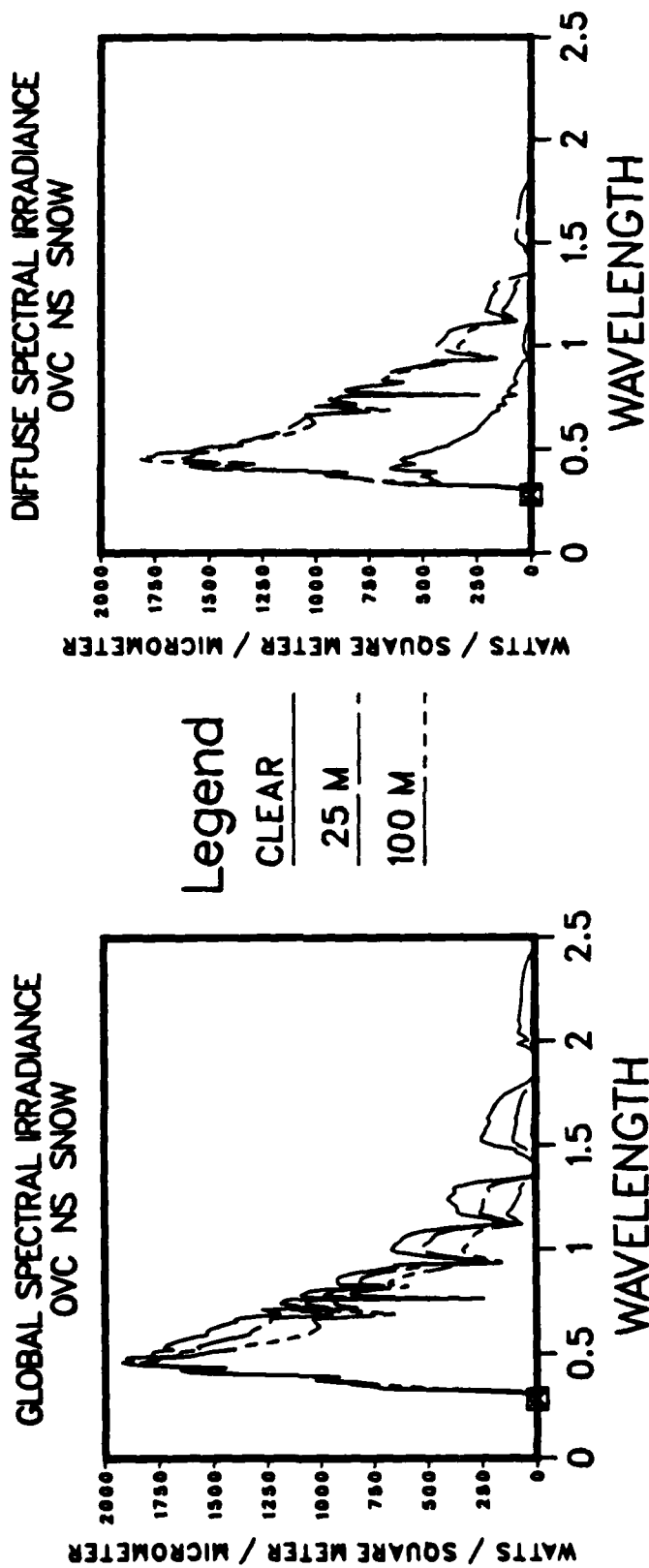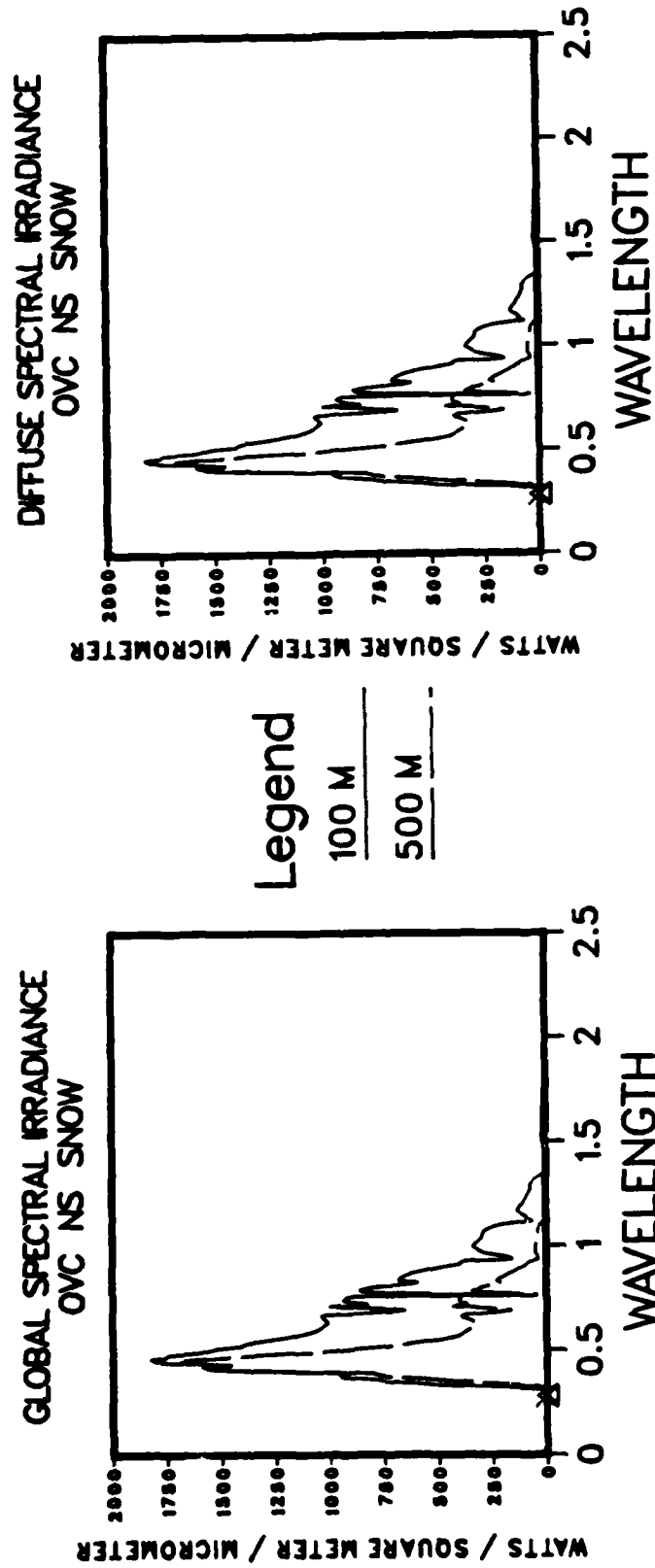thickness: middle line). The wavelength is in micrometers.

Figure 3.4.1.D

Comparison Of The Effects Of Cloud Thickness On The Global And Diffuse Spectral
Irradiances For A Nimbostratus Overcast With A Wet Sand Surface

The global radiation and diffuse radiation decrease with the change in the cloud thickness
(100 m thickness: top line; 500 m thickness: bottom line). The wavelength is in micro-
meters.

and the effect of changing the surface albedo. As shown
previously with the broadband cases, the effect of cloud
thickness is to continually reduce the global radiation and
to first increase and then decrease the diffuse radiation.
These same trends are observed in the spectral plots. The
largest changes in the spectral cases occur in the region of
the atmospheric window; although changes occur throughout
the spectrum.

Comparing the global and diffuse radiation plots for
cloud thicknesses less than 100 meters (Figures 3.4.1.A and
D), one can determine that the effect of high surface albedo
is to produce minimal change in the global and diffuse
radiation reaching the surface. The decline in the global
and diffuse radiation with thickness of the cloud occurs
slowly with a high albedo surface. In comparison, a low
albedo surface shows more pronounced variations with
thickness changes in both the global and diffuse radition.
High surface albedos tend to slow the reduction in both
global and diffuse radiation due to thickness changes.

3.4.2 Spectral Effects Of Cloud Amount And Surface Albedo

Figures 3.4.2.A and B demonstrate the spectral effects
of varying the cloud amount. In the cases presented, the
cloud thickness was a constant 100 meters, the cloud base
was 100 meters square, and the distance between the clouds
was varied to obtain the desired cloud amount. For the cases

DIFFUSE SPECTRAL IRRADIANCE
SNOW SURFACE

GLOBAL SPECTRAL IRRADIANCE
SNOW SURFACE

Legend
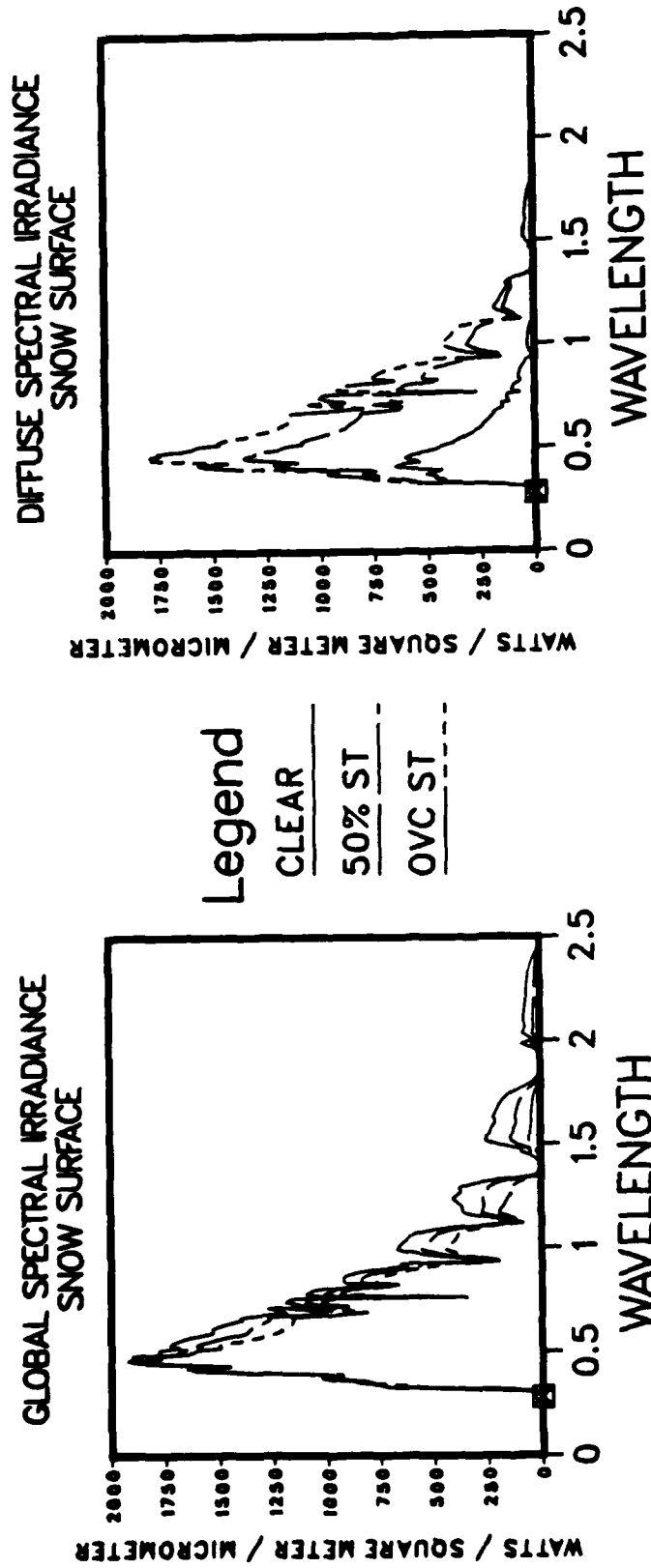
CLEAR _____
50% ST _ _ _
OVC ST _ _ _ _

Figure 3.4.2.A

Comparison of The Effects Of Cloud Amount On The Global And Diffuse Spectral
Irradiances For Stratus Cloud With A Snow Surface

The global radiation decreases with each increase in cloud amount (clear sky: top line;
50% stratus: middle line; overcast: bottom line). The diffuse radiation becomes larger
with each increase in cloud amount (clear sky: bottom line; 50% stratus: middle line;
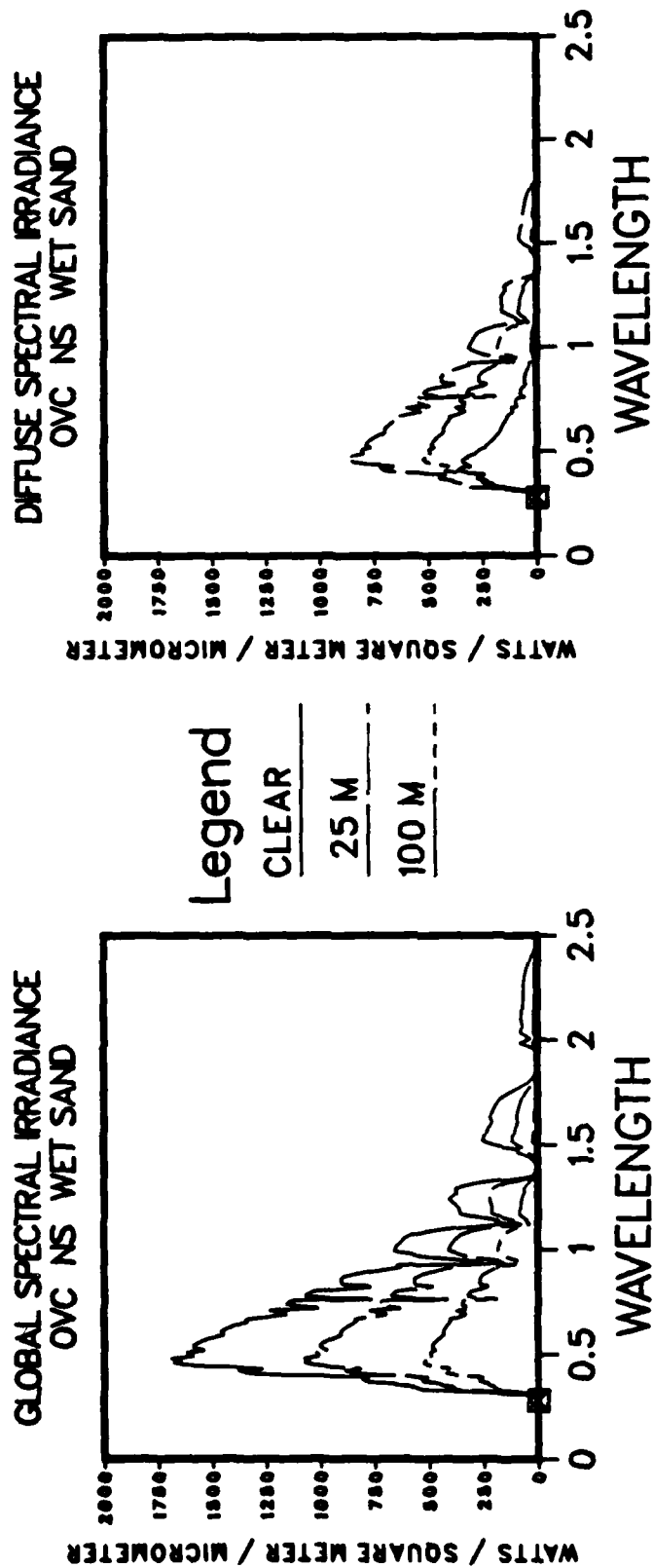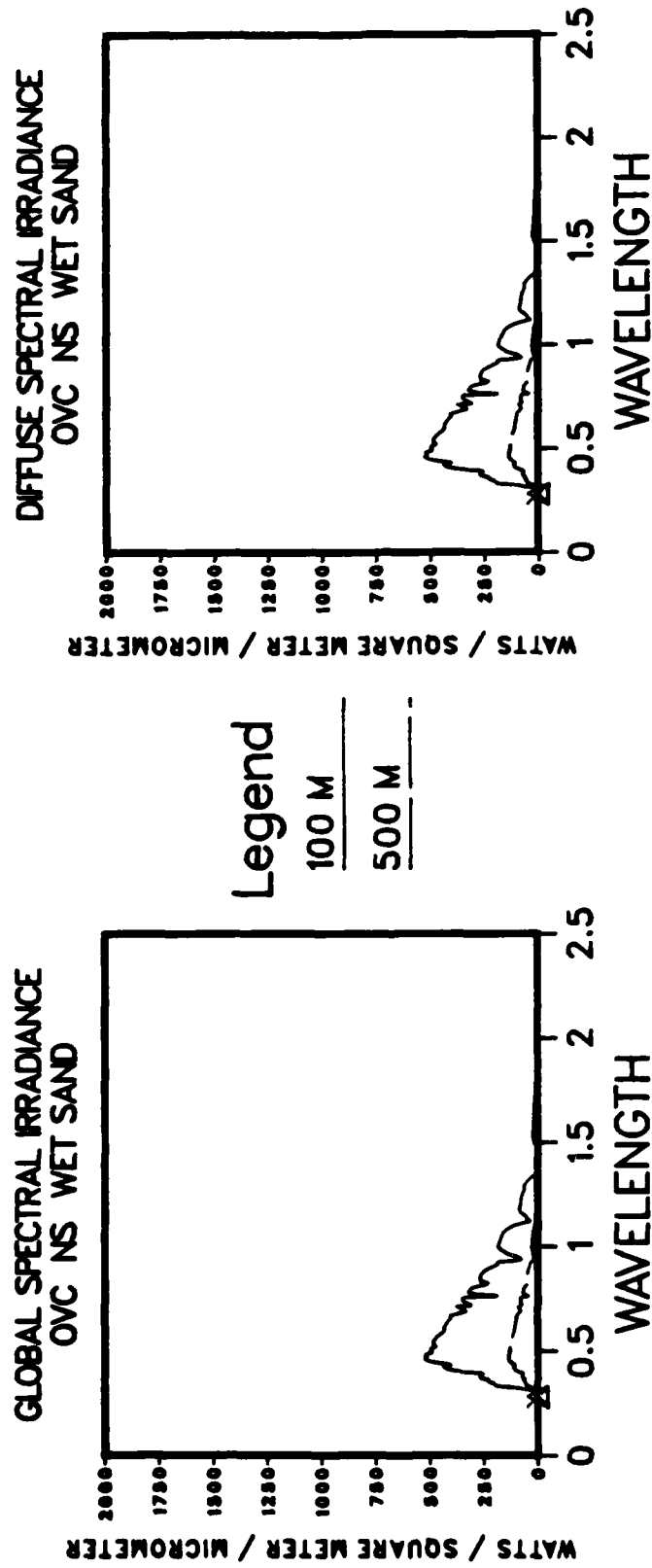overcast: top line). The wavelength is in micrometers.
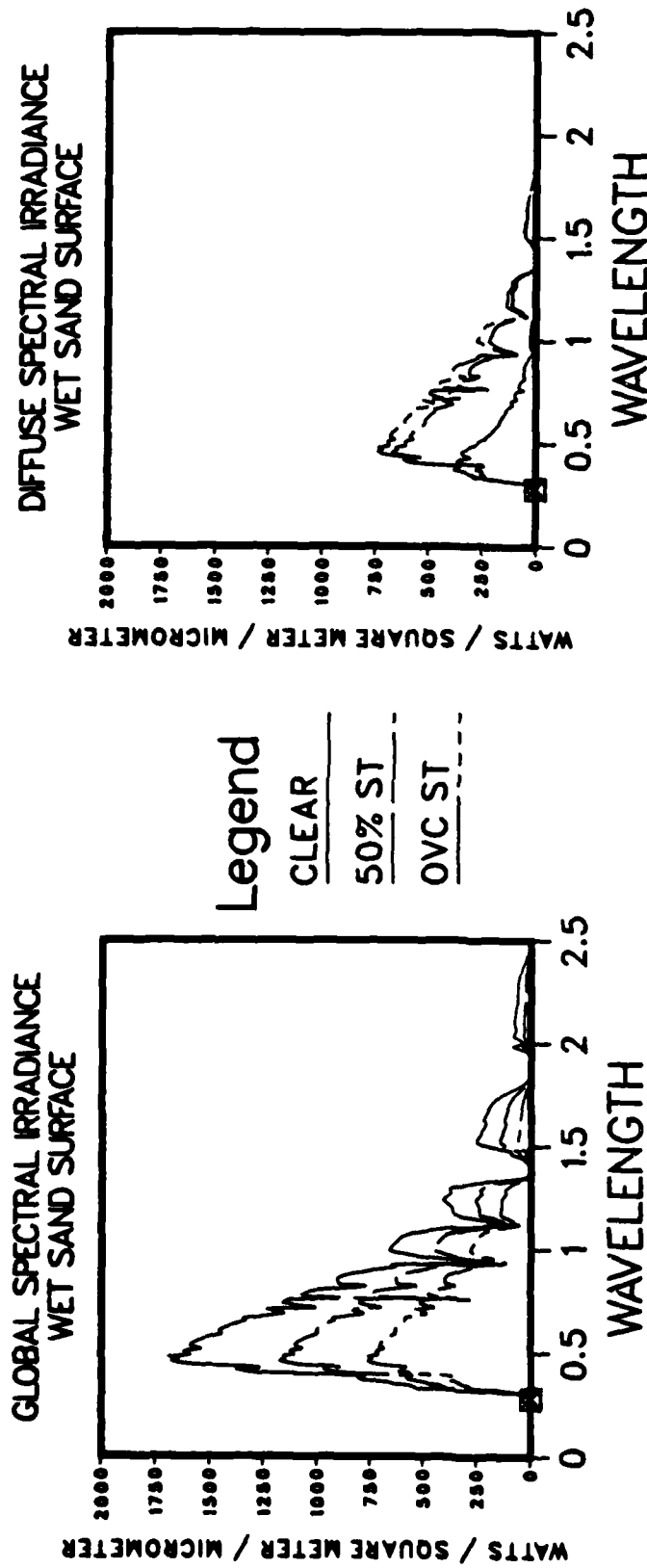
Figure 3.4.2.B

Comparison Of The Effects Of Cloud Amount On The Global And Diffuse Spectral
Irradiances For Stratus Cloud With a Wet Sand Surface

The global radiation decreases with each increase in cloud amount (clear sky: top line;
50% stratus: middle line; overcast: bottom line). The diffuse radiation becomes larger
with each increase in cloud amount (clear sky: bottom line; 50% stratus: middle line;
overcast: top line). The wavelength is in micrometers.

shown, a stratus cloud was used. The degree of variation is most pronounced for a low albedo (wet sand) surface. Varying the cloud amount over a snow surface produces larger variations in the diffuse radiation than by varying the thickness. The reason is the sky is not completely filled with cloud. The diffuse radiation increases in proportion to the amount of cloud cover. By the same token, the direct radiation decreases proportionately. The result is a larger variation in the diffuse component for a change in cloud amount when compared to a change in cloud thickness.

The surface albedo exhibits similar effects with the change in cloud amount as it did with the change in thickness. The global radiation tends to decline more slowly with increasing cloud amount over a high albedo surface than over a low albedo surface. The diffuse radiation increases more rapidly over a high albedo surface with changes in cloud amount than when over a low albedo surface. The low albedo surface tends to cause significant differences in the global radiation for a change in cloud amount while causing relatively small changes in the diffuse component. A high albedo surface tends to cause relatively small changes in the global radiation and relatively large changes in the diffuse radiation for a change in cloud amount.

3.4.3 Spectral Effects Of Cloud Types

The effects of cloud type and surface albedo can be
seen in some of the previous figures. For comparison
purposes, the global radiation for a stratus overcast and a
nimbostratus overcast for a wet sand surface are shown in
Figure 3.4.3.A. A wet sand surface was chosen for this
section because the lower albedo surface causes the most
differentiation between the cases. The cloud thicknesses are
25 meters and 100 meters respectively. The changes due to
the cloud type become larger as the cloud thickness
increases. The difference in the global radiation at the
peak in each curve is approximately 20 percent of the
stratus value for a cloud thickness of 25 meters. For a
cloud thickness of 100 meters, the difference is
approximately 25 percent. Depending on the spectral
interval, the percentage may be higher or lower. However,
the most significant effects take place in the region
between 0.4 and 0.7 micrometers.

Figure 3.4.3.B highlights the significance of cloud
type as it relates to cloud amount. The plots demonstrate
about a 15 percent difference in the global radiation
between the peaks of each curve for 50 percent cloud
coverage. For an overcast, the difference at the peak when
compared to the value of the stratus curve at the peak is
approximately 33 percent. The degree of influence of cloud
type is obviously interrelated with the other parameters.
However, a reasonable estimate of the change caused by cloud
type through either cloud thickness or cloud amount may

175
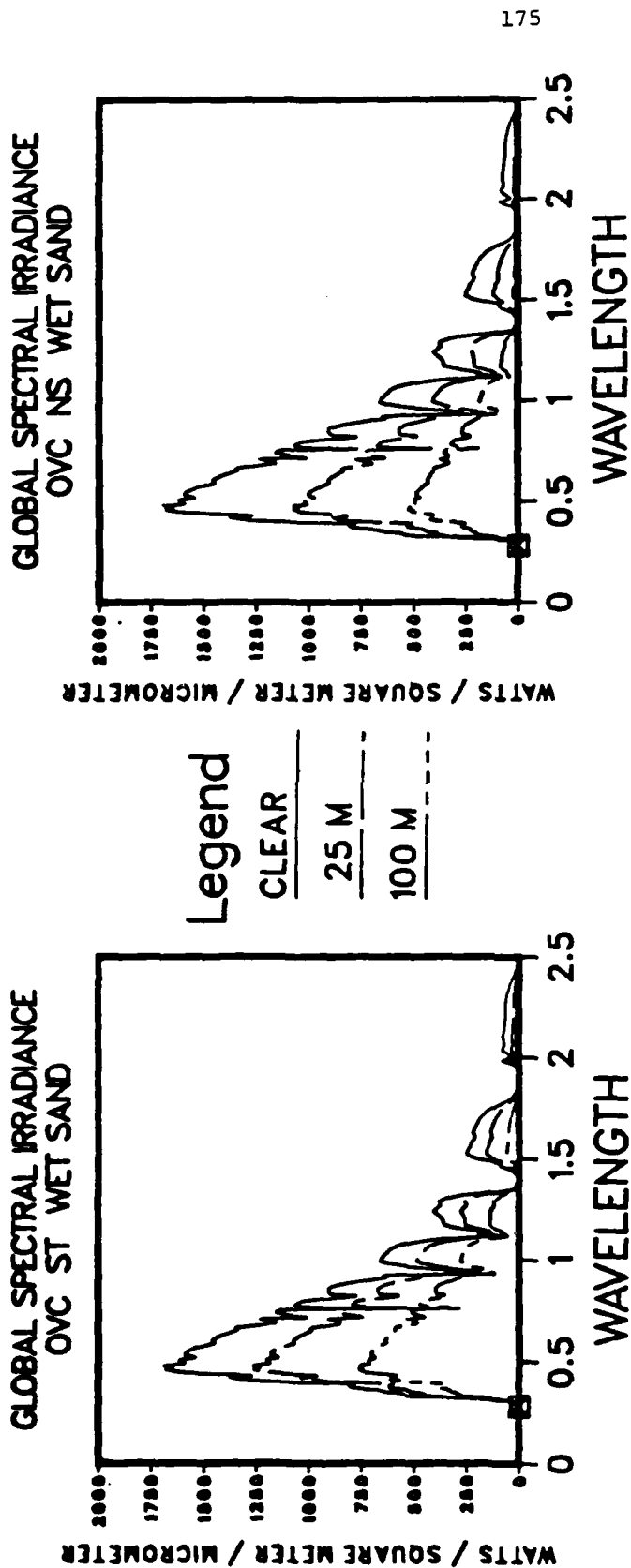
Figure 3.4.3.A

Comparison Of The Effects Of Cloud Type And Cloud Thickness
Changes Over A Wet Sand Surface

The wavelength is in micrometers.

176
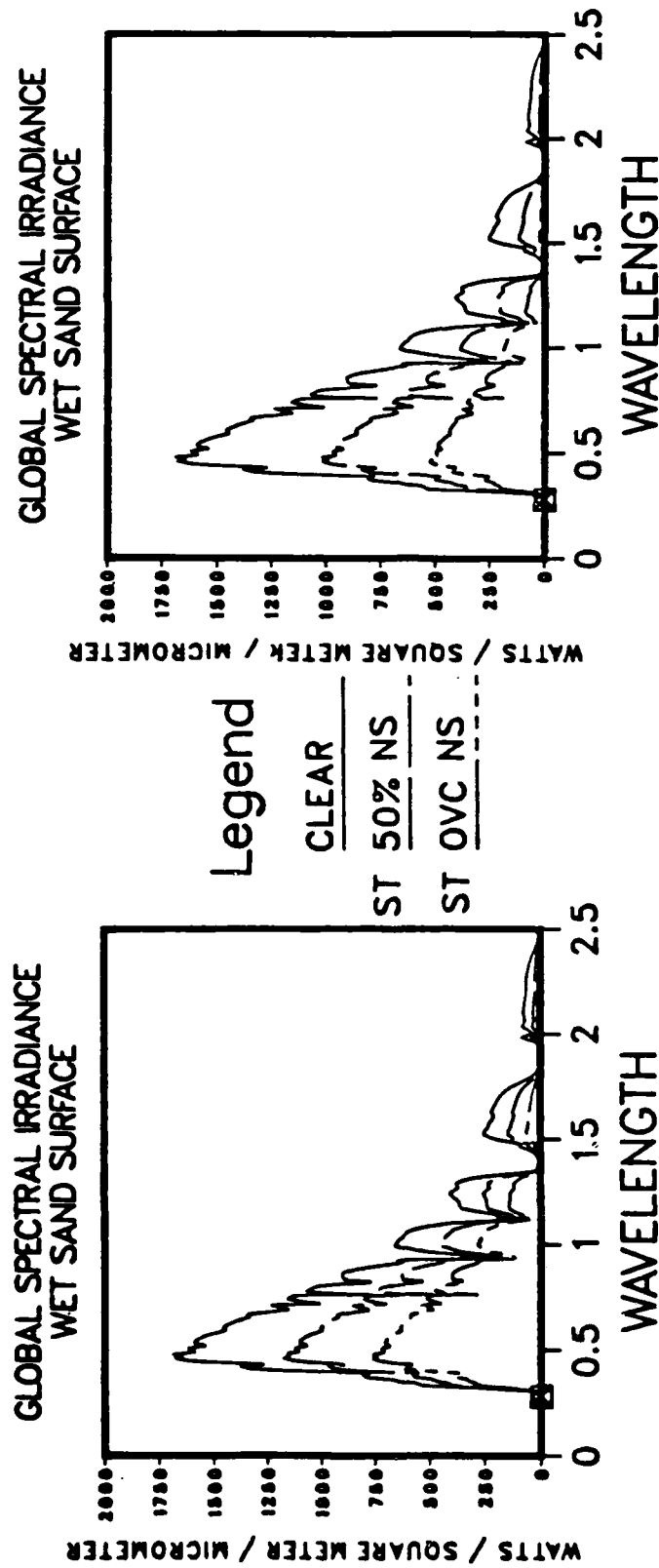
Figure 3.4.3.B

Comparison Of The Effects Of Cloud Type And Cloud Amount Changes
Over A Wet Sand Surface

The wavelength is in micrometers.

AD-A171 284   A SIMPLE SOLAR SPECTRAL MODEL FOR STUDYING THE EFFECTS   3/3
               OF CLOUD COVER AND...(U) AIR FORCE INST OF TECH
               WRIGHT-PATTERSON AFB OH   A M POWELL 1986
UNCLASSIFIED   AFIT/CI/NR-86-123D   F/G 4/1   NL

END
DATE
FILMED
10-86
DTIC

1.0

4.5
5.0
5.6
6.3
7.1
8.0

2.8

3.2

3.6

4.0

2.5

2.2

2.0

1.1

1.8

1.25

1.4

1.6
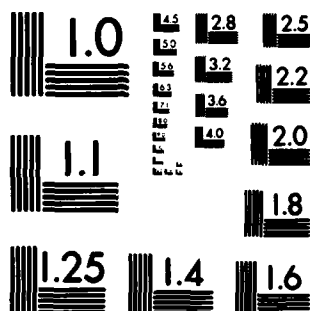
'CROCOPY RESOLUTION TEST CHART
NATIONAL BUREAU OF STANDARDS-1963-A

range from 15 to 50 percent depending on the precise
circumstances.

3.5 Comparison With An Empirical Model

The Air Resources Laboratory (ARL) developed an
empirical model for hourly solar radiation based on solar
zenith angle, cloud amount, and preciptation. This model
does not include many of the parameters in the solar
radiation model developed for this dissertation. Factors of
importance which are left out of the ARL model are cloud
thickness, cloud type, water vapor amount, and turbidity.
The ARL model calculates the clear sky and cloudy sky hourly
irradiances in kilojoules per square meter. The empirical
equation for the clear sky model is:

$$SRC = A_o + A_1 \cos(ZA) + A_2 \cos^2(ZA) + A_3 \cos^3(ZA)$$

The empirical equation for cloudy skies is:

$$SR = SRC (C_o + C_2 OPQ + C_3 OPQ^2 + C_4 OPQ^3 + C_5 RN)$$

where

SRC = Solar radiation for clear skies (kilo-joules per square
meter)

SR = Solar radiation for cloudy skies (kilo-joules per square
meter)

ZA = Solar zenith angle

OPQ = Number of tenths of opaque cloudiness divided by 10

RN = Precipitation, 0 when no precipitation is reported and 1
when some form of precipitation is reported

The equation for cloudy skies is for opaque clouds and is
the form of the equation used when the number of minutes of
sunshine is not available. When the number of minutes of
sunshine is available, another empircal equation is used
which contains the constant C_1. The number of minutes of
sunshine was not included in this model, so the above
equation was used for comparison. The empirical constants in
the equation were determined for specific sites around the
United States. There are two sets of coefficients; one for
the morning and one for the afternoon. Ann Arbor, Michigan
was not one of the sites for which coefficients were
determined. This comparison will be completed for Madison,
Wisconsin. The empirical constants for the equations can be
obtained for a number of locations for each month of the
year from the National Climatic Center, Air Resources
Laboratory, or the Solar Energy Measurements and
Instrumentation Training Course from the Department of
Atmospheric and Oceanic Science at The University of
Michigan.

There are a number of parameters which must be applied
to the solar model that cannot be used in the empirical
model. A list of the parameters used for a horizontal
surface follow:

Latitude	43.083 degrees N
Longitude	89.416 degrees W
Day	166
Solar Zenith Angle	31.677 degrees
Surface Type	Bare soil
Cloud width	500.0 meters
Cloud separation	Varies depending on cloud amount

CLOUD AMOUNT (TENTHS)	REGRESSION MODEL (MJ/M^2)	SOLAR MODEL (MJ/M^2)	CLOUD THICKNESS (M)	WATER VAPOR (CM)	TURBIDITY (500 nm)
CLEAR	3.038	3.243	–	0.5	0.1
		3.196	–	1.0	0.1
		3.122	–	2.0	0.1
2	3.010	2.838	50.0	2.0	0.1
		2.642	150.0	2.0	0.1
		2.473	300.0	2.0	0.1
5	2.977	2.413	50.0	2.0	0.1
		1.924	150.0	2.0	0.1
		1.499	300.0	2.0	0.1
6	2.967	2.270	50.0	2.0	0.1
		1.683	150.0	2.0	0.1
		1.252	300.0	2.0	0.1
7	2.957	2.127	50.0	2.0	0.1
		1.442	150.0	2.0	0.1
		1.084	300.0	2.0	0.1
10	2.930	1.742	50.0	2.0	0.1
		0.947	150.0	2.0	0.1
		0.536	300.0	2.0	0.1

Table 3.5.A

Regression Model Versus Solar Spectral Model Calculations

Table 3.5.A shows the comparison of the regression or empirical model versus the solar spectral model. The comparison demonstrates differences due to the water vapor amount for a clear sky and differences due to cloud thickness for cloudy skies. The results in Table 3.5.A are in megajoules per square meter. The empirical model gives reasonable results based on the few parameters used in calculating the solar radiation. The solar spectral model demonstrates similar results and shows the variation due to cloud thickness and cloud amount as well. While an empirical model may be used for very rough estimates of the amount of solar radiation, they do not represent the variation in the solar radiation which would be of interest to someone building a solar collector or other solar oriented device. Solar models which have more physical parameters allow one to better evaluate the changes due to a variety of factors.

3.6 Radiance At The Top Of The Atmosphere

This model calculates the solar radiance at the top of the atmosphere as might be received by a satellite sensor. There are no known sets of observed spectral data of the type needed to compare with these calculations. However, there are calculations of the radiance at the top of the atmosphere. Bowker, Davis, Myrick, Stacy, and Jones (1985) presented a plot of such calculations (See Figure 3.6.A). It is impossible to reproduce the plot with the solar spectral

model due to many unknown factors and differences. The solar
zenith angle directly influences the amount of illumination
of a target at the surface. While the solar zenith angle is
known, the starting extraterrestrial solar irradiance is not
and there are several possible data sets in use. The amount
of surface illumination is critical in determining the
radiance at the top of the atmosphere. Other factors of
importance are the aerosol distribution, turbidity, water
vapor amount, etc. To illustate that the solar spectral
model computes radiances in the correct range of values, two
cases were calculated. One had a constant spectral albedo of
0.7 and the other case had a value of 0.1. The location was
at 20 degrees north latitude and assumed to be at an hour
angle of 0.0 degrees (local solar noon). The two cases are
plotted in Figure 3.6.B. When one compares the solar
spectral model results with Figure 3.6.A, one can see that
the model radiances are higher in one portion of the
spectrum and lower in another. Figure 3.6.A had the
absorption features 'removed for clarity'. This accounts for
some of the differences between the plots. In Figure 3.6.A,
beam radiance is the radiation which comes directly from the
target and total radiance is all the radiation which reaches
the top of the atmosphere. In Figure 3.6.B, global radiance
is equivalent to total radiance and direct radiance is
equivalent to beam radiance. The diffuse radiance is due to
radiation scattered by the atmosphere.

Figure 3.6.A
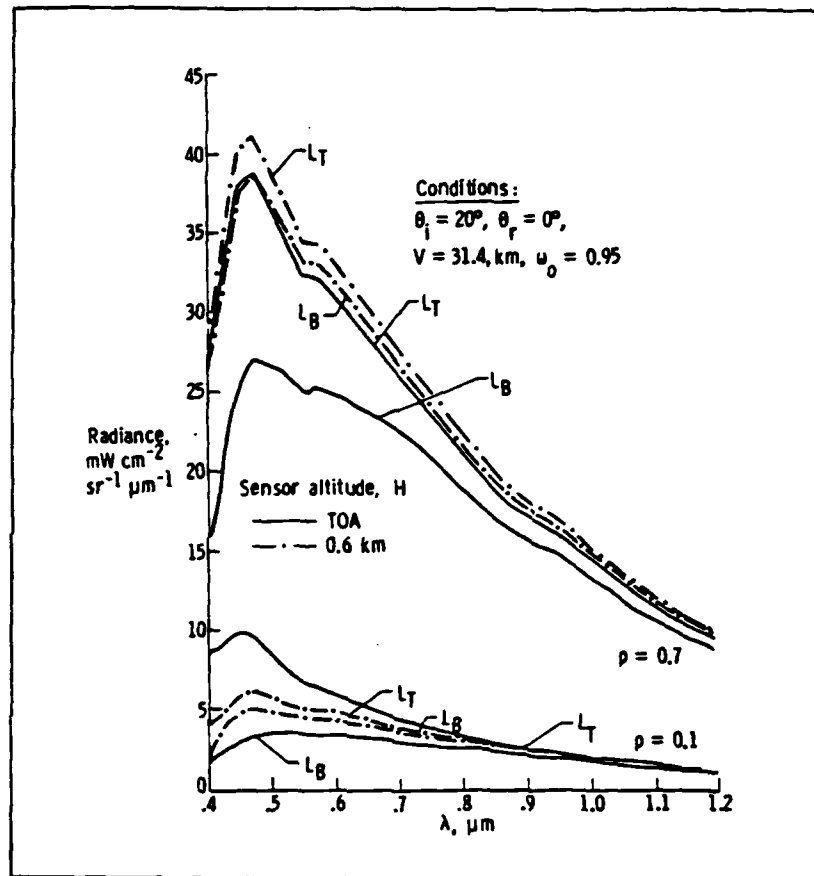
Radiance At The Top Of The Atmosphere

L_B – Beam radiance

L_T – Total radiance

ρ – Surface albedo

θ_r – Observation zenith angle

θ_i – Solar zenith angle

ω_0 – Single scattering albedo

V – Visual range

TOA – Top of atmosphere

The beam radiance is the radiation received directly from the target. The total radiance is the radiation received directly from the target plus any radiation scattered to the sensor by the atmosphere. (Bowker, Davis, Myrick, Stacy, and Jones, 1985)

RADIANCE — TOP OF ATMOSPHERE
CONSTANT REFLECTANCE 0.7

RADIANCE — TOP OF ATMOSPHERE
CONSTANT REFLECTANCE 0.1

MILLIWATTS / SQ CM / SR / MICROMETER

WAVELENGTH

WAVELENGTH

Legend

△ GLOBAL

✕ DIRECT

□ DIFFUSE
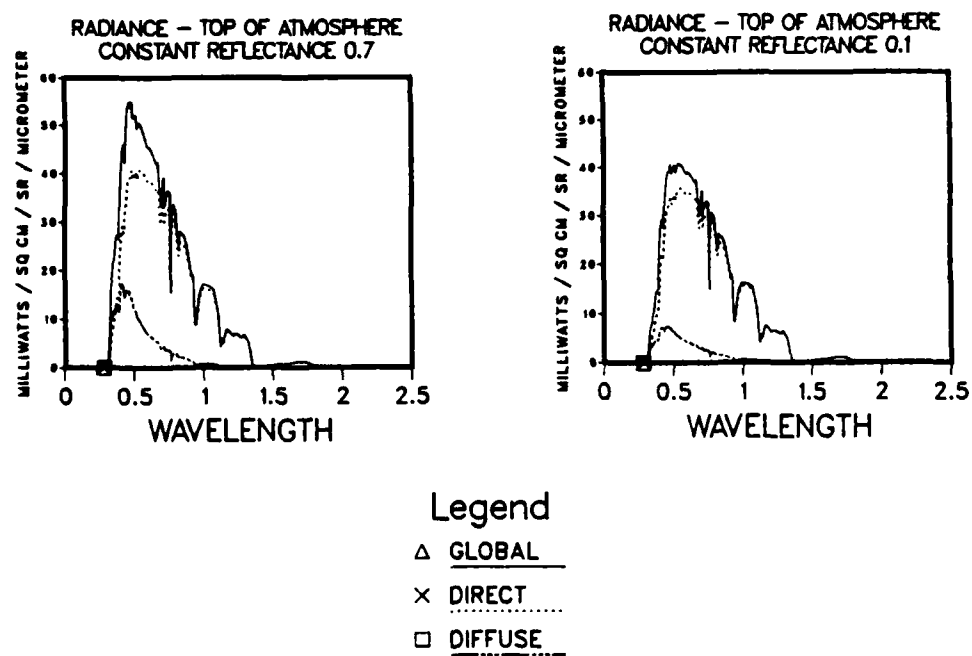
Figure 3.6.B

Radiance At The Top Of The Atmosphere For Surfaces
With Constant Spectral Reflectance

The wavelength is in micrometers.

In general, it appears the solar spectral model does a reasonable job of estimating the radiance at the top of the atmosphere for a clear sky. It is impossible to determine the accuracy of the model in computing radiances for the top of the atmosphere until observations have been obtained. However, it appears the model does generate answers within an order of magnitude based on the very loose comparison with the Bowker, Davis, Myrick, Stacy, and Jones plot.

3.7 Progation Of Error In The Model

The amount of error propagated by the model based on the uncertainties of the independent variables is a legimate concern. An analysis was performed to quantify the degree of error one might expect if one of the independent variables is not known accurately. This analysis will demonstrate which variables need to be measured most accurately to minimize model error. Because portions of this model are based on numerical techniques, it is not practical to obtain an analytic expression for the errors due to each independent variable. However, an estimate of error can be obtained by choosing a particular set of parameters and calculating the value of global radiation at the surface. The global radiation values compared with the original case will determine the error caused by uncertainties in the independent variables.

The particular case used as the basis for this analysis used the following parameter values:

Latitude	42.2833	deg
Longitude	-83.7333	deg
Surface Type	Bare Soil	
Hour Angle	0.0	deg (noon)
Ozone	0.3639	cm
Precipitable Water	2.0	cm
Turbidity	0.15	
Cloud Thickness	300.00	m
CLoud Width	500.00	m
Cloud Amount	0.50	percent
Cloud Height	1000.00	m

Table 3.7.A lists the independent quantities which were varied. With the exception of the surface pressure, all the variables were deviated by 10 percent from their original value. The surface pressure was assumed to be known within 15 millibars. Table 3.7.A gives the original, high, and low values for each variable.

Table 3.7.B shows the results of this analysis in terms of global radiation. The percentage error is the difference between the new global value minus the original global value divided by the original global value. By scanning the percentage error column, it is quite easy to determine which variables it is important to know accurately. Cloud amount and cloud thickness should be measured as precisely as possible if one expects to obtain accurate answers from the model. The variables which most influence the model calculations by uncertainty in observation are (most influence to least influence): cloud amount, cloud thickness, cloud width, precipitable water, turbidity,

VARIABLE	ORIGINAL CASE VALUES	LOW VALUE	HIGH VALUE	PERCENTAGE OF ORIGINAL VALUE
Ozone (cm)	0.3639	0.3275	0.4003	$\pm$ 10
Precipitable Water (cm)	2.0000	1.8000	2.2000	$\pm$ 10
Turbidity	0.1500	0.1350	0.1650	$\pm$ 10
Surface Pressure (mb)	1013.0	998.0	1028.0	$\pm$ 1.5
Cloud Thickness (m)	300.0	270.0	330.0	$\pm$ 10
Cloud Width (m)	500.0	450.0	550.0	$\pm$ 10
Cloud Amount	0.50	0.40	0.60	$\pm$ 10
Cloud Height (m)	1000.0	900.0	1100.0	$\pm$ 10

Figure 3.7.A

Assumed Uncertainties In Model Variables

VARIABLE	ORIGINAL GLOBAL VALUE	LOW GLOBAL VALUE	PERCENTAGE ERROR OF ORIGINAL	HIGH GLOBAL VALUE	PERCENTAGE ERROR OF ORIGINAL
Ozone	316.799	316.219	0.1831	317.393	0.1875
Precipitable Water	316.799	315.536	0.3986	318.117	0.4160
Turbidity	316.799	315.555	0.3927	318.057	0.3971
Surface Pressure	316.799	316.455	0.1086	317.146	0.1095
Cloud Thickness	316.799	309.944	2.1638	325.507	2.7487
Cloud Width	316.799	315.936	0.2724	318.522	0.5438
Cloud Amount	316.799	273.892	13.5439	368.295	16.2551
Cloud Height	316.799	316.792	0.0022	316.817	0.0057

Table 3.7.B

Propagation Of Error In The Model

The global radiation values are watts per square meter.

surface pressure, ozone amount, and cloud height. The cloud
amount and cloud thickness are by far the two most important
parameters to know accurately.

CHAPTER IV

CONCLUSIONS AND RECOMMENDATIONS

A spectral insolation model was designed which includes clear skies, cloudy skies, and inclined surfaces. Several typical spectral surface albedos are available in the model as well as several different cloud types. Only one aerosol distribution (rural) is included in the model. Interesting features of the model include the ability to sum the radiation over any desired wavelength band between 0.28 and 4.0 micrometers, and the ability to average the radiation over time. The flexibility designed into this interactive model is one of its strongest attributes.

The solar spectral model was compared against actual observations for clear skies. The observations were both spectral and broadband. The modelled values were within the accuracy goals of ± 5% for the global radiation and ± 15% for the diffuse radiation. The aerosol distribution was the most important factor in the clear sky. If the aerosol distribution of the atmosphere is not compatible with the rural aerosol distribution, then the model error will increase substantially depending on the amount of disparity between the observed and modelled aerosol distributions. A recommendation for further study is to include more than one

aerosol distribution in the model. A second recommendation is to use more than one turbidity value to determine the aerosol distribution. Turbidity measurements at several different wavelengths should be used to more accurately determine the observed aerosol distribution and to determine which model aerosol distribution to use.

The solar spectral model was compared against cloudy sky observations. The disagreement between modelled and observed values was large. Most of the differences are thought to be due to the inability of conventional surface observations to adequately describe the cloud situation. Specialized observations are required in order to compare the calculations from a model of this detail with observations. The observations should include the dimensions of the clouds, the geometry of the clouds relative to the instruments taking the measurements, and the time the instruments are in the cloud shadow versus the direct sunlight. The model should be modified to compute a time as well as spatial average and should include the use of the number of minutes of direct sunshine.

The cloudy sky comparison and the cloud albedo comparison indicated the solution for the cloud radiative transfer is not adequate. This was exhibited by the sharply reduced radiation transmitted through the cloud with increasing cloud thickness and the distinctly different shape of the cloud albedo curve when compared with Chel'tsov's measurements. While Paltridge and Platt

recommended the solution because of its simplicity, it has shortcomings. This solution is primarily useful when the absorption is small and when the optical depth of the layer is large (greater than 5). While the absorption is small in the visible portion of the spectrum and most water droplet clouds in the low atmosphere have large optical depths, the simple, two stream solution appears inadequate. The solution results in too rapid attenuation through the cloud and too rapid a change in cloud albedo with a change in cloud thickness. For future work, I would recommend another solution to the radiative transfer equation be used. It was not possible to establish the degree of inaccuracy due to the lack of suitable observations.

Even though the cloud modelling is in error, the effects of varying the cloud parameters and surface types could still be evaluated. The solar zenith angle has the greatest effect of all the parameters. The solar zenith angle affects the surface albedo, the path distance through the cloud, and the amount of direct radiation received on an inclined plane. The effect of solar zenith angle is demonstrated in the modelled albedos of overcast clouds at Archangel, Soviet Union where the day of the year determined the solar zenith angle which was largely responsible for the changes in the calculated albedos. The effect of solar zenith angle is particularly strong as the zenith angle becomes large, especially in cloudy skies.

While it is possible to choose a situation in which any particular parameter can be demonstrated to have a large effect, cloud amount has the largest influence of any of the cloud or surface parameters. The other factors in decreasing order of influence are cloud thickness, surface albedo, and cloud type. In typical situations, the cloud amount will dominate the scenario in terms of the radiation reaching the surface of the Earth. There are a number of situations where the cloud thickness can be the dominant parameter. These situations are usually when the cloud amount is large and most of the radiation is reaching the surface through the clouds. Cloud type is the least influential of the cloud parameters and was used to determine the cloud droplet distribution. As long as the cloud drop size distribution is broad the effects of clouds are generally characterized fairly well. It is the tail of the drop size distribution for the large drop sizes which is important. Relatively small changes in the number of large drops produce the greatest changes. As a consequence, future cloud modelling should concentrate on understanding how the distribution of the largest drops change with cloud type and cloud lifecycle. These same thoughts concerning drop size are also stated by Welch, Cox, and Davis (1980) and Ulaby, Fung and Moore (1981).

The effects of surface albedo have been particularly interesting. The surface albedo is influenced by solar zenith angle. For large solar zenith angles, changing the

surface type results in small changes of the solar radiation reaching the surface. High surface albedos insure the decrease in radiation which reaches the surface is minimized. Low surface albedos exhibit larger changes in the radiation reaching the surface.

While this model has shortcomings, it is a high resolution spectral model which includes clouds. Although this model is deficient in several areas due to the solutions used in the modelling, it provides a means of assessing the influence of a variety of parameters. When compared to empirical models the detail and variation one can obtain in the answers provides more information for users. Since this model is based on physical principles, it provides insight into problems where empirical models fail short.

In summary, this model provides a high degree of spectral resolution for both clear and cloudy skies. While the two stream solution for clouds is inadequate, the general results of the calculations can be used to infer amounts of radiation as well as general trends. Analysis via changing parameters can be of particular help to designers of solar and remote sensing equipment. Future research should attempt to better model the cloud radiative transfer properties. This model did not include the radiation reflected from the sidewalls of the clouds. The reflection from the cloud sidewalls should be included in future work. The technique of using simple geometry clouds and weighting

the respective areas of the clouds by the radiation entering
those areas seems to have merit. A more definitive
assessment of the technique cannot be made until more
detailed observations are taken.

APPENDIX A

CALCULATION OF THE IRRADIANCE ARRIVING AT THE SATELLITE OBSERVATION POINT

QUANTITIES:

A	– Area of (object)	(m^2)
E	– Irradiance on (object)	(W/m^2)
H_o	– Irradiance on top of atmosphere	(W/m^2)
I	– Intensity	(W/Sr)
L	– Radiance of (object)	(W/m^2-Sr)
M	– Reflected irradiance from (object)	(W/m^2)
R_s	– Distance from satellite to target	(m)
θ_1	– Solar zenith angle relative to a flat surface	
θ_2	– Solar zenith angle relative to the normal of a tilted plane	
θ_3	– Satellite zenith angle relative to the normal of a tilted plane	
θ_4	– Satellite zenith angle relative to a flat surface	
ρ	– Albedo or reflectance of (object)	
π	– Pi (3.14159)	
Φ	– Flux	(Watts)
τ_{atm1}	– Total atmospheric transmittance along the path from the sun to the target location	
τ_{atm2}	– total atmospheric transmittance along the path from the target location to the satellite	
Ω	– Solid angle of (object)	

DERIVATION:

(1)   Calculate flux caught by plane:

$$\Phi(\text{caught by plane}) = H_o \, A(\text{plane}) \cos(\theta_2) \, \tau_{atm2}$$

(2)   Irradiance on plane:

$$E(\text{on plane}) = \Phi(\text{caught by plane}) / A(\text{plane})$$

(3)   Irradiance reflected from plane:

$$M(\text{from plane}) = \rho(\text{plane}) \, E(\text{on plane})$$

ASSUMING Lambertian type scatter:

$$L(\text{plane}) = M(\text{from plane}) / \pi$$

(4)   Intensity in the direction of view:

$$I(\text{in the direction of view}) = L(\text{plane}) \, A(\text{plane}) \cos(\theta_3)$$

(5)   Flux at the satellite observation point:

$$\Phi(\text{satellite}) = I(\text{in the direction of view}) \, \tau_{atm2} \cdot A(\text{sensor}) / R_s^2$$

(6)   Irradiance at the satellite observation point:

$$E(\text{satellite}) = \Phi(\text{satellite}) / A(\text{sensor})$$

(7)   Solve for E(satellite) by backward substitution from step (6):

$$E(\text{satellite}) = \frac{1}{A(\text{sensor})} \; \frac{A(\text{sensor})}{R_s^2} \; \frac{A(\text{plane})}{A(\text{plane})} \; \tau_{ATM2} \cdot \cos(\theta_3) \cdot$$

$$\frac{\rho(\text{plane})}{\pi} \cdot H_o \cdot A(\text{plane}) \cdot \cos(\theta_2) \cdot \tau_{ATM1}$$

(8)   Reduce Equation:

$$E(\text{satellite}) = \frac{A(\text{Plane})}{R_s^2} \cdot \tau_{ATM1} \cdot \tau_{ATM2} \cdot \cos(\theta_2) \cdot \cos(\theta_3) \cdot \quad \frac{\rho(\text{plane})}{\tau} \cdot H_o$$

Note: Solid angle of plane $= \Omega(\text{plane}) = A(\text{plane}) / R_s^2$

L(of plane) $= \rho(\text{plane}) \, H_o / \tau$

$$E(\text{satellite}) = \Omega(\text{plane}) \cdot \tau_{atm1} \cdot \tau_{atm2} \; \cos(\theta_2) \; \cos(\theta_3) \; L(\text{plane})$$

(9) Determining the irradiance from the atmosphere :

The irradiance arriving at the satellite consists of two components

1. Radiation from the target plane
2. Radiation from the atmosphere

The viewing geometry will determine the radiance of the atmosphere. To simplify calculations, two assumptions have been made.

Assumption 1: If the angle formed by connecting the sun, target plane location, and the satellite is less than or equal to 90 degrees, then the atmospheric radiance is calculated from the radiation backscattered by the atmosphere.

Otherwise, if the angle formed is greater than 90 degrees, then the atmospheric radiance is derived from the radiation forward scattered by the atmosphere.

Assumption 2: Once the amount of atmospheric radiation backscattered (forward scattered) is computed, the atmospheric radiance is calculated by assuming the radiation uniformly scattered over the backscattering (forward scattered) hemisphere (π steradians).

Summary: If the (Sun-target-satellite) angle is less than or equal to 90 degrees then the atmospheric radiance is:

$$L(atmosphere) = E(backscattered) / \tau$$

Otherwise:

$$L(atmosphere) - E(forward\ scattered) / \tau$$

(10) Total irradiance arriving at the satellite observation point:

$$E(satellite) = \Omega(Plane) \cdot \tau_{ATM1} \cdot \tau_{ATM2} \cdot \cos(\theta_2) \cdot \cos(\theta_3) \cdot \frac{(plane)}{\tau} \cdot H_o$$

$$+ L(atmosphere)\,\Omega(sensor)$$

where

$$\Omega(sensor) = A(sensor) / R_s^2$$
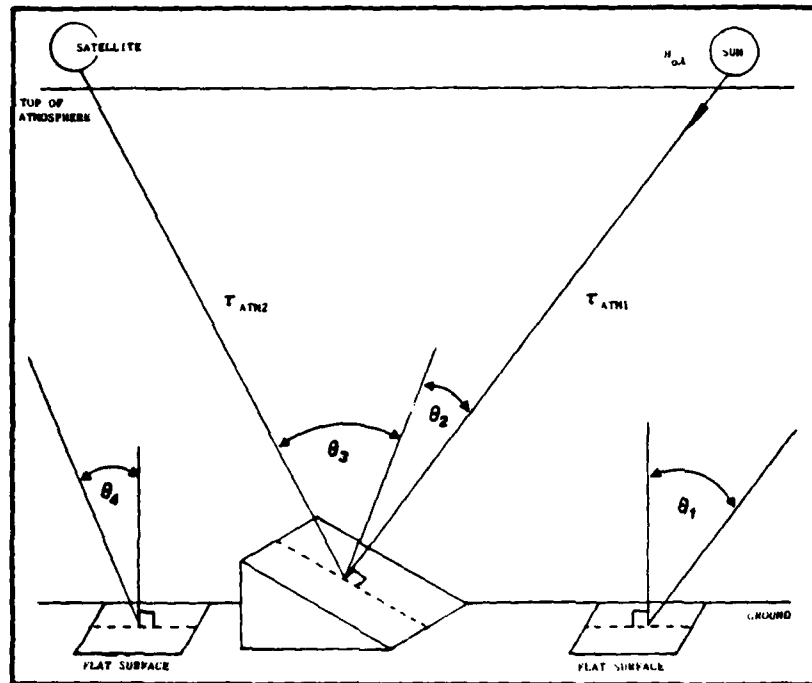
Figure A.1

Solar Zenith Angles Relative To Flat And Tilted Surfaces

$H_{o\lambda}$ = Extraterrestrial solar irradiance

θ_1 = Solar zenith angle relative to flat surface

θ_2 = Solar zenith angle relative to tilted surface

θ_3 = Satellite zenith angle relative to tilted surface

θ_4 = Satellite zenith angle relative to flat surface

τ_{ATM_1} = Transmission for the atmospheric path between the sun and target plane

τ_{ATM_2} = Transmission for the atmospheric path between the satellite and the target plane
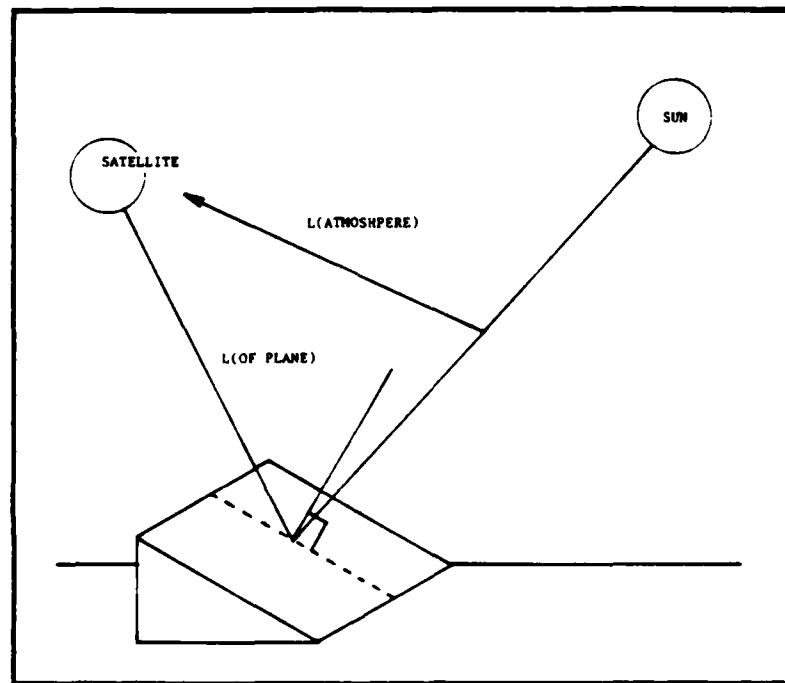
Figure A.2

Sources of radiance reaching the satellite
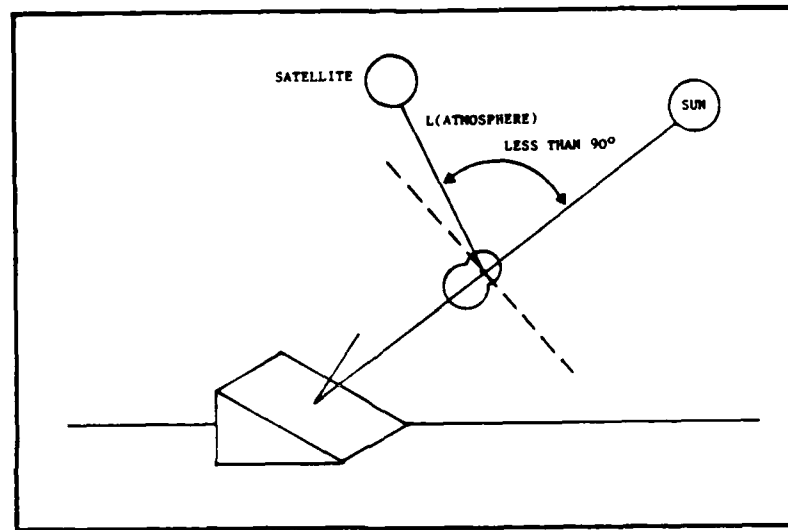
L(Atmosphere) = L(Backscattered) = E(Backscattered) / τ

Figure A.3

When the radiance of the atmosphere is derived from backscattered radiation
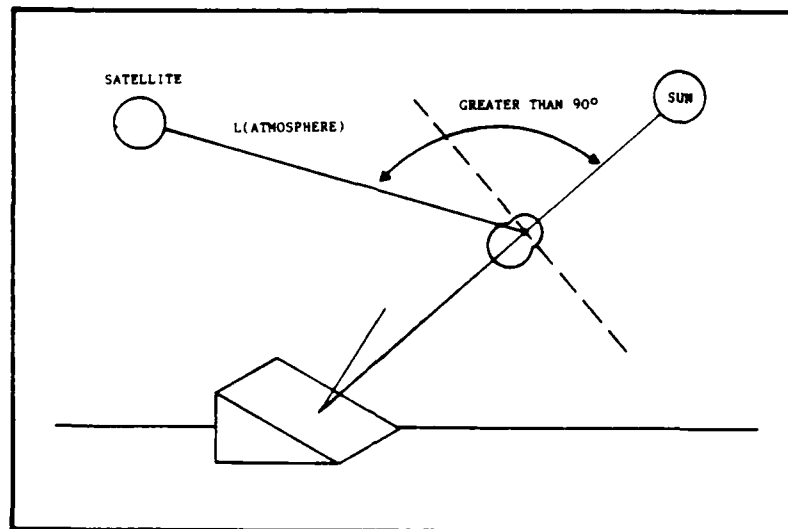
L(Atmosphere) = L(Forward Scattered) = E(Forward Scattered) $/\tau$

Figure A.4

When the radiance of the atmosphere is derived from forward scattered radiation

APPENDIX B

THE ADDING TECHNIQUE FOR COMBINING LAYERS

TERMS AND SYMBOLS:
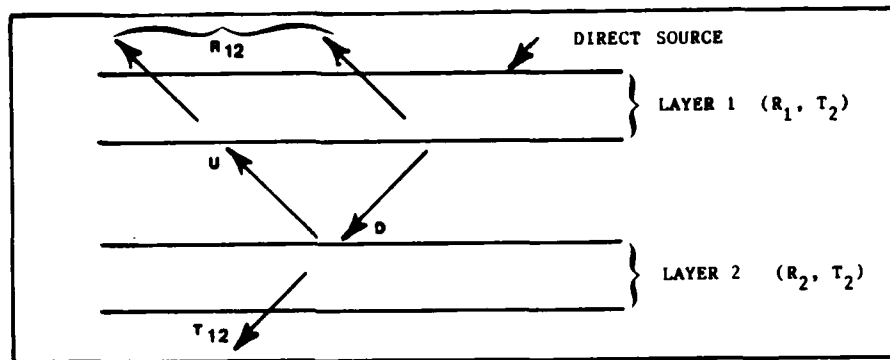
Figure B.1

General diagram of the components of radiation for the layers

TERMS:

D   = Downward transmission incident on top of bottom layer

R_1 = Reflectivity of top layer

R_2 = Reflectivity of bottom layer

R_{12} = Combined reflectivity of the two layers

T_1 = Transmissivity of top layer

T_2 = Transmissivity of bottom layer

T_{12} = Combined transmission of the two layers

U   = Upward transmission incident on bottom of top layer

ADDING TECHNIQUE WITH SOURCE ABOVE THE LAYERS

Figure B.2

Diagram of the components of radiation using the Adding
technique for combining two layers with known transmissivities
and reflectivities with the source above the layers.

EQUATIONS:

$$R_{12} = R_1 + T_1^2 R_2 + T_1^2 R_2 R_1 R_2 + T_1^2 R_2 R_1 R_2 R_1 R_2 + \ldots$$

$$= R_1 + T_1^2 R_2 (1 + R_1 R_2 + (R_1 R_2)^2 + \ldots)$$

$$= R_1 + T_1^2 R_2 / (1 - R_1 R_2)$$

$$U = T_1 R_2 + T_1 R_2 R_2 R_2 + T_1 R_2 R_1 R_2 R_1 R_2 + \ldots$$

$$= T_1 R_2 (1 + R_2 R_1 + (R_2 R_1)^2 + \ldots$$

$$= T_1 R_2 / (1 - R_1 R_2)$$

$$D = T_1 + T_1 R_2 R_1 + T_1 R_2 R_1 R_2 R_1 + \ldots$$

$$= T_1 (1 + R_2 R_1 + (R_2 R_1)^2 + \ldots)$$

$$= T_1 / (1 - R_1 R_2)$$

$$T_{12} = T_1 T_2 + T_1 T_2 R_2 R_1 + T_1 T_2 R_2 R_1 R_2 R_1 + \ldots$$

$$= T_1 T_2 (1 + R_2 R_1 + (R_2 R_1)^2 + \ldots)$$

$$= T_1 T_2 / (1 - R_1 R_2)$$

ADDING TECHNIQUE WITH THE SOURCE BELOW THE LAYERS
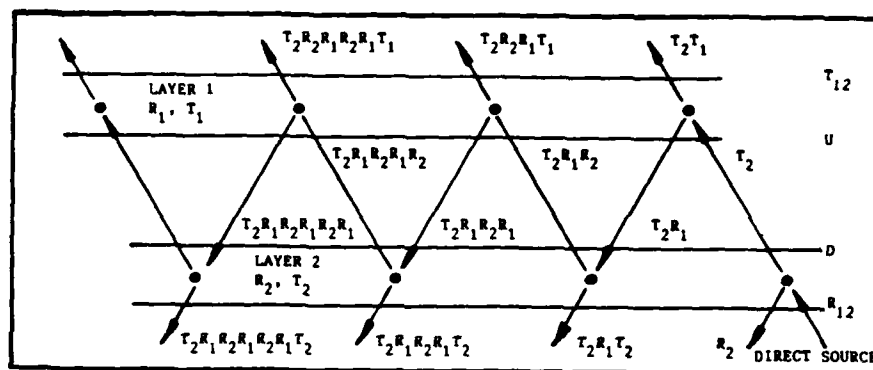
Figure B.3

Diagram of the components of radiation using the Adding technique for combining two layers with known transmissivities and reflectivities with the source below the layers.

EQUATIONS:

$$R_{12} = R_2 + T_2^2 R_1 + T_2^2 R_1 R_2 R_1 + T_2^2 R_1 R_2 R_2 + \cdots$$

$$= R_2 + T_2^2 R_1 (1 + R_1 R_2 + (R_1 R_2)^2 + \cdots)$$

$$= R_2 + T_2^2 R_1 / (1 - R_1 R_2)$$

$$U = T_2 + T_2 R_1 R_2 + T_2 R_1 R_2 R_1 R_2 + \cdots$$

$$= T_2 (1 + R_1 R_2 + (R_1 R_2)^2 + \cdots)$$

$$= T_2 / (1 - R_1 R_2)$$

$$D = T_2 R_1 + T_2 R_1 R_2 R_1 + T_2 R_1 R_2 R_1 R_2 R_1 + \cdots$$

$$= T_2 R_1 (1 + R_1 R_2 + (R_1 R_2)^2 + \cdots)$$

$$= T_2 R_1 / (1 - R_1 R_2)$$

$$T_{12} = T_2 T_1 + T_2 T_1 R_2 R_1 + T_2 T_1 R_2 R_1 R_2 R_1$$

$$= T_2 T_1 (1 + R_2 R_1 + (R_2 R_1)^2 + \cdots)$$

$$= T_2 T_1 / (1 - R_1 R_2)$$

ADDING TECHNIQUE WITH THE SOURCE BETWEEN THE LAYERS
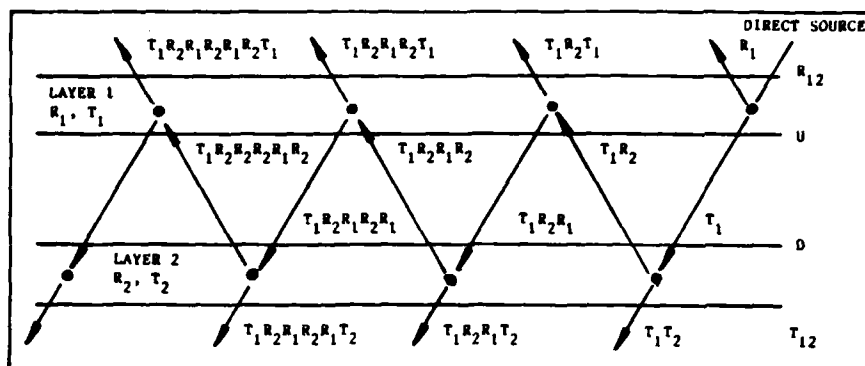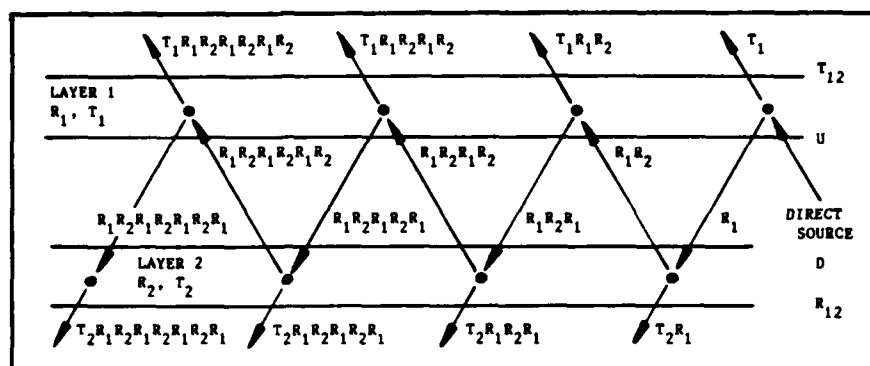

Figure B.4

Diagram of the components of radiation using the Adding
technique for combining two layers with known transmissions and
reflectivities with source between the layers.

EQUATIONS:

$$R_{12} = T_2 R_1 + T_2 R_1 R_2 R_1 + T_2 R_1 R_2 R_1 R_2 R_1 + \cdots$$

$$= T_2 R_1 (1 + R_2 R_1 + (R_2 R_1)^2 + \ldots)$$

$$= T_2 R_1 / (1 - R_1 R_2)$$

$$U = R_1 R_2 + R_1 R_2 R_1 R_2 + R_1 R_2 R_1 R_2 R_1 R_2 + \cdots$$

$$= R_1 R_2 (1 + R_1 R_2 + (R_1 R_2)^2 + \ldots)$$

$$= R_1 R_2 / (1 - R_1 R_2)$$

$$D = R_1 + R_1 R_2 R_1 + R_1 R_2 R_1 R_2 R_1 + \cdots$$

$$= R_1 (1 + R_1 R_2 + (R_1 R_2)^2 + \ldots)$$

$$= R_1 / (1 - R_1 R_2)$$

$$T_{12} = T_1 + T_1 R_1 R_2 + T_1 R_1 R_2 R_1 R_2 + T_1 R_1 R_2 R_1 R_2 R_1 R_2 + \cdots$$

$$= T_1 (1 + R_1 R_2 + (R_1 R_2)^2 + \ldots)$$

$$= T_1 / (1 - R_1 R_2)$$

APPENDIX C

GEOMETRIES ASSOCIATED WITH ILLUMINATING AN ARBITRARILY INCLINED PLANE ON THE EARTH

Adapted and condensed directly from: Solar Energy Engineering
                                          Edited by A.A.M. Sayigh
                                          Chapter 2 by Enrico Coffari
                                          Academic Press, New York, 1977

TERMS AND SYMBOLS:

A – Azimuth measured from true (geographical) north, positive in the eastward (clockwise) direction.
        Range: 0 to 360 degrees
                  0 to 2π radians

h – Hour angle
          (+) westward from the noon meridian
          (–) eastward from the noon meridian
        Range: +180 to –180 degrees
                + π to π radians

h_{sr} – Hour angle of sunrise

h_{ss} – Hour angle of sunset

i – Elevation angle of the incident radiation on the inclined plane measured from the surface of the plane to the position of the sun.
          (+) angle in front of plane's surface (sun illuminated)
          (–) angle behind the plane's surface
        Range: +90 to –90   degrees
                + $\pi/2$ to – $\pi/2$ radians

α – Azimuth angle the inclined plane is facing in the coordinate system used by E. Coffari
          (+) eastward azimuth from true north
          (–) westward azimuth from true north
        Range: +90 to –90   degrees
                + $\pi/2$ to – $\pi/2$ radians

      Note the range does not need to be larger due to the definition of the zenith angle.

β – Solar elevation angle
        Range: +90 to –90   degrees
                – $\pi/2$ to $\pi/2$ radians

    z – Zenith angle of the inclined plane measured from the local vertical to the normal vector of the plane's surface.
           (+) southward facing plane
           (−) northward facing plane
      Range: +90 to −90 degrees
              +$\pi/2$ to −$\pi/2$ radians

    δ – Declination of the sun
           (+) north
           (−) south
      Range: +90 to −90 degrees
              +$\pi/2$ to −$\pi/2$ radians

    φ – Latitude
           (+) north
           (−) south
      Range: +90 to −90 degrees
              +$\pi/2$ to − $\pi/2$ radians

SOLAR ALTITUDE (ELEVATION):

$$\sin \beta = \sin \delta \sin \varphi + \cos \delta \cos h \cos \varphi \tag{C.1}$$

At solar noon the hour angle is zero and Eqn (C.1) reduces to:

$$\sin \beta = \sin \delta \sin \varphi + \cos \delta \cos \varphi = \cos (\delta - \varphi) = \cos (\varphi - \delta) \tag{C.2}$$

$$\beta = \arcsin (\cos(\delta - \varphi)) = \arcsin (\cos(\varphi - \delta)) \tag{C.3}$$

Beta (β) ranges from 0 to 90 degrees with negative values of meaning that the sun is below the horizon (polar night).

SOLAR AZIMUTH

The solar azimuth angle A measured from true (geographical) north positively in the eastward direction:

$$A = \arctan \left(\frac{\sin h}{- \cos \varphi \tan \delta + \sin \varphi \cos h} \right) \tag{C.4}$$

with   −90 $\geq$ A $\geq$ +90 degrees

To obtain the correct azimuth:

If h>0 (afternoon azimuth) and A<180   then   A = A + 180
If h<0 (morning azimuth)   and A>180   then   A = A − 180

SUNRISE AND SUNSET TIMES

$$h = \arccos (- \tan \delta \tan \varphi) \tag{C.5}$$

$$h_{ss} = h \qquad\qquad h_{sr} = -h$$

But if:

$- \tan \delta \ \tan \varphi$	$+1$	The sun will neither rise nor set for the day, polar night.
	$= +1$	The sun will be on the horizon for an instant only (at solar noon). This occurs the last day before a polar night and the first day after.
	$= -1$	The sun will be on the horizon for an instant only (at midnight, h= $\pm$ 180). This occurs the day before and the day after a polar day.
	< -1	The sun will neither rise nor set for the day; polar day.

SUNRISE AND SUNSET AZIMUTHS

$$A = \arcsin (- \sin h \cos \delta) \qquad (C.6)$$

If $\delta > 0$ then the sun rises and sets in the northern quadrants.
If $\delta = 0$ then the sun rises due east and sets due west.
If $\delta < 0$ then the sun rises and sets in the southern quadrants.

CALCULATION OF THE ANGLE OF INCIDENCE OF DIRECT RADIATION ON AN INCLINED PLANE

$$\cos i = (\cos z \sin \varphi - \sin z \cos \varphi \cos \alpha) \ \sin \delta \qquad (C.7)$$
$$+ (\cos z \cos \varphi + \sin z \sin \varphi \cos \alpha) \ \cos \delta \cos \ h$$
$$+ \sin z \sin \alpha \cos \delta \sin \ h$$

$$\cos i = C_1 \ \sin \delta + C_2 \cos \delta \ \cos h + C_3 \cos \delta \sin h$$

where

$$C_1 = \cos z \sin \varphi - \sin z \cos \varphi \cos \alpha$$

$$C_2 = \cos z \cos \varphi + \sin z \sin \varphi \cos \alpha$$

$$C_3 = \sin z \sin \alpha$$

ZERO IRRADIATION SOLAR TIMES, ALTITUDES, AND AZIMUTHS OF AN INCLINED PLANE

From Eqn (C.7), E. Coffari developed a solution by transforming the

sines and cosines into tangents, and because of the one-to-one

correspondence of tangent functions wihtin their period, the

mathematical solutions coincide with the physical positions of the hour
angle of the sun at zero-irradiation times.

The two zero-irradiation hour angles of a given day and for a given
tilted plane divide the circle representing the 24 hours of the day into
two sectors: in one the sun is above the plane, in the other it lies
under the plane. The lack of real solutions indicate that the sun is
above or below the tilted plane for the whole day. To determine which
sector represents the time of day when the sun is above (or under) the
tilted plane, or, in the latter case, to determine whether the plane is
in the sun or in the shade for the day, it is sufficient to calculate
the angle of incidence of the solar radiation for any hour angle except
for the hour angles of the zero-irradiation times. This is most
conveniently done for solar noon as Eqn (C.7) reduces to:

$$\cos i = (\cos z \sin \varphi - \sin z \cos \varphi \cos \alpha) \sin \delta \qquad (C.8)$$
$$+ (\cos z \cos \varphi + \sin z \sin \varphi \cos \alpha) \cos \delta$$

and if $\cos i > 0$, the sector in which the selected hour angle lies will
be the sector in which the sun is above the tilted plane.
If $\cos i < 0$, the will be under the tilted plane in the other sector.

Sunrise and sunset also divide the circle representing the 24 hours
of a day into two sectors. The sector(s) in which the sun is above
both the tilted plane and the horizon is (are) the one(s) in which the
surface is exposed to the sun.

Eqn (C.7) may be reduced to a form simpler to handle by letting:

$$x = \sin z \sin \alpha \cos \delta$$

$$y = (\cos z \cos \omega - \sin z \sin \omega \cos \alpha) \cos \delta$$

$$z = (\cos z \sin \omega - \sin z \cos \omega \cos \alpha) \sin \delta$$

$$\cos i = x \sin h - y \cos h - z \qquad \qquad$$

The condition of parallelism is reached when the solar beam lies on the plane of the slope, i.e. the angle of incidence is equal to 90 degrees, or cos i = 0:

$$x \sin h \quad + \quad y \cos h \quad + \quad z = 0 \qquad (C.10)$$

and the hour angles h of the zero-irradiation times may be calculated as follows, letting $h = 2\omega$:

$$\sin h = \sin 2\omega = 2 \sin\omega\cos\omega = 2 \, \frac{\tan\omega}{\sqrt{1 + \tan^2\omega}} \, \frac{1}{\sqrt{1 + \tan^2\omega}}$$

$$= 2 \, \frac{\tan\omega}{\sqrt{1 + \tan^2\omega}}$$

$$\cos h = \cos 2\omega = \cos^2\omega - \sin^2\omega = \frac{1}{1 + \tan^2\omega} - \frac{\tan^2\omega}{1 + \tan^2\omega}$$

$$= \frac{1 - \tan^2\omega}{1 + \tan^2\omega}$$

Substituting the above equations in Eqn (C.10), we obtain

$$2x \; \frac{\tan \omega}{1 + \tan^2 \omega} \; + \; Y \; \frac{1 - \tan^2 \omega}{1 + \tan^2 \omega} \; + \; z \; = \; 0$$

and rearranging, we have

$$(z - y) \tan^2 \omega \; + \; 2x \tan \omega \; + \; (y + z) \; = \; 0$$

$$\tan \omega \; = \; \frac{-x \; \pm \; \sqrt{x^2 - (z^2 - y^2)}}{z - y}$$

$$\tan \omega_1 = \frac{-x + \sqrt{x^2 + y^2 - z^2}}{z - y} \; , \qquad \tan \omega_2 = \frac{+x - \sqrt{x^2 + y^2 - z^2}}{z - y} \; ,$$

$$h_1 \; = \; 2 \arctan(\tan \omega_1) \qquad h_2 = 2 \arctan(\tan \omega_2) \quad (C.11)$$

The hour angles h_1 and h_2, are the angles at which the sun's rays are parallel to the inclined plane; complex and conjugate solutions indicate that the sun's rays are never parallel to the given plane for the day.

The next step involves calculating the cosine of the angle of incidence for an hour angle that is not a zero-irradiation hour angle, by using Eqn (C.9). For simplicity, we shall calculate the angle of incidence of the solar radiation for an hour angle of 0 degrees, corresponding to solar noon.

If $\cos i > 0$, the plane will be exposed to solar radiation at solar noon and hence, the sun will shine on it from h_1 or from sunrise, whichever occurs later, and until h_2 or sunset whichever occurs earlier (from sunrise to sunset if h_1 and h_2 are complex numbers).

If $\cos i < 0$, the tilted plane is in the shade at solar noon (all day if h_1 and h_2 are complex numbers), and will be exposed to the sun from h_2 to h_1 (clockwise direction) except, of course, for the interval of time between sunrise and sunset.

The solar altitude and azimuth at the hour angle corresponding to the zero-irradiation times may be calculated from Eqns (C.1) and (C.4).

APPENDIX D

TWO STREAM SOLUTION OF THE EQUATION OF RADIATIVE TRANSFER

(Adapted From Radiation Commission, 1975)

TERMS AND SYMBOLS:

A = Albedo

b = Backscattered radiation

E^+ = Downward radiation flux

E^- = Upward radiation flux

f = Forward scattered radiation

$\rho(\mu)$ = Scattering phase function

T = Transmission

τ = Optical thickness of parallel slab

$\overline{\omega_0}$ = Single scattering albedo

TWO-STREAM APPROXIMATION (OR SHUSTER-SCHWARZSCHILD METHOD)

The two-stream approximation has been used by many authors to achieve a quick approximate solution to the equation of transfer by decomposing the radiation field into two opposing streams. The treatments vary slightly, and a comparison of the various methods follow.

Chu and Churchill (1955) consider a beam passing through a parallel slab of optical thickness τ_1, incident on the surface at an angle θ_0. The radiation is broken into two fluxes: the first is in the direction of the incident beam, while the second is in the backwards direction.

For these fluxes the equation of transfer integrated over azimuth yields the two equations

$$\mu_0 \frac{dE^+}{d\tau} = -E^+ + \overline{\omega}_0 \, fE^+ + \overline{\omega}_0 bE^- \quad ,$$

$$-\mu_0 \frac{dE^-}{d\tau} = -E^- + \overline{\omega}_0 \, fE^- + \overline{\omega}_0 bE^+ \quad ,$$

$$\mu_0 = |\cos \theta_0|$$

Here, is assumed positive for the downwards directions and the factors b and f represent the fraction of radiation scattered backward and forward, respectively. Clearly, we have

$$b + f = 1 \quad ,$$

and Chu and Churchill make the logical choice

$$f = \frac{1}{2} \int_0^1 p(u) \, du$$

These equations are a two-dimensional linear system, easily solved by a number of methods, with the boundary conditions

$$E^+ (o) = 1 \quad , \text{ downward radiation at top of atmosphere}$$

$$E^- (\tau_1) = o \quad , \text{ upward radiation at bottom of atmosphere}$$

This gives the results

$$E^+ = \frac{e^{-k\tau} - G^2 e^{-(2k\tau_1 - k\tau)}}{1 - G^2 e^{-2k\tau_1}} \quad ,$$

$$E^- = \frac{Ge^{-k\tau} - Ge^{-(2k\tau_1 - k\tau)}}{1 - G^2 e^{2k\tau_1}} \quad ,$$

$$G = (r-s)(r+s)^{-1} \quad ,$$

$$r = 1 - \omega_o f + \omega_o b \quad ,$$

$$k = s/\mu_o$$

$$s = \left[(1 - \overline{\omega}_o f)^2 - \overline{\omega}_o^2 b^2 \right]^{\frac{1}{2}}$$

For the albedo, we find

$$A = \frac{F^-(o)}{\mu_o} = E^-(o) = \frac{G(1 - e^{-2K\tau_1})}{1 - G^2 e^{2k\tau_1}}$$

The transmission (including the incident beam) is given by

$$T = \frac{F^+(\tau_1)}{\mu_0} = E^+(\tau_1) = \frac{(1-G^2)e^{-k\tau_1}}{1-G^2 e^{-k\tau_1}}$$

For $\overline{\omega}_0 = 1$, the secular equation give $k^2 = 0$. The analysis must be repeated for this case. We easily find

$$E^- = \frac{b(\tau_1 - \tau)\mu_0}{1 + b\tau_1/\mu_0}$$

$$E^+ = \frac{1 + b(\tau_1 - \tau)/\mu_0}{1 + b\tau_1/\mu_0}$$

This yields

$$A = \frac{b\tau_1/\mu_0}{1 + b\tau_1/\mu_0}$$

$$T = 1 - \frac{b\tau_1/\mu_0}{1 + b\tau_1/\mu_0}$$

APPENDIX E

CALCULATION OF SOLID ANGLE AS RELATED TO A LAMBERTIAN SURFACE

Figure E.1 shows the illustration of the solid angle and its representation in polar coordinates. Under this formulation the solid angle is:

$$\Omega = \frac{\sigma}{R^2}$$

where

σ - Surface area on the spherical surface

R - Radius of the sphere

From the diagram, it an be seen that:

$$d\sigma = (R\, d\theta)\, (R\, \sin\theta\, d\varphi)$$

$$\Omega = \frac{d\sigma}{R^2} = \sin\theta\, d\theta\, d\varphi$$

the irradiance is defined by the normal component of the radiance integrated over the entire solid angle and may be written:

$$E = \int_{\Omega} L(\theta, \varphi)\, \cos\theta\, d\Omega$$

$$E = \int_{0}^{2\pi} \int_{0}^{\pi/2} L(\theta, \varphi)\, \cos\theta\, \sin\theta\, d\theta\, d\varphi$$

For isotropic radiation, L is not a function of angle and the value of the irradiance becomes:

$$E = \pi L$$

When a Lambertian surface is assumed, the surface is presumed to reflect isotropically in all directions. Hence, the solid angle is weighted by

the cosine factor as above. To determine the radiance of a Lambertian surface, multiply the incident irradiance by the surface reflectivity and divide by π .

$$L = \frac{\rho E}{\pi}$$

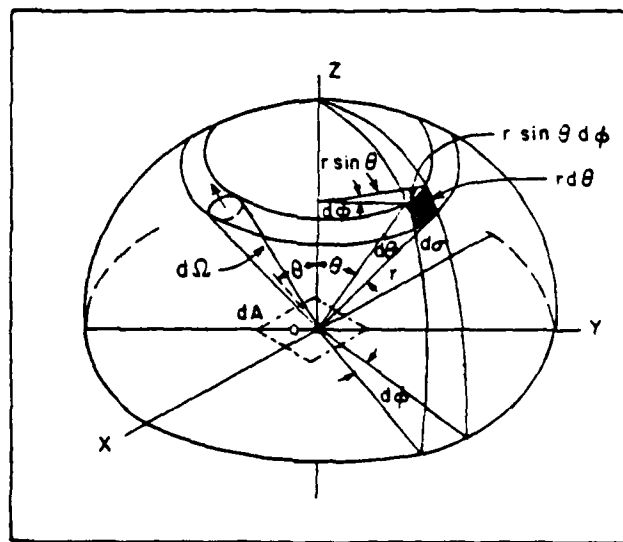Figure E.1

Illustration of a solid angle and its representation in polar coordinates. Also shown is a pencil of radiation through an element of area dA in directions confined to an element of solid angle $d\Omega$.

GLOSSARY OF TERMS

Terms with a first or second subscript, λ , are spectral quantities or functions of wavelength.

A   – Area of (object) in m^2

$a_{o\lambda}$ – Absorption coefficient for ozone

$a_{u\lambda}$ – Absorption coefficient for the uniformly mixed gases

$a_{w\lambda}$ – Absorption coefficent for water vapor

C_λ – Correction factor for Bird model formulation of the diffuse radiation on a horizontal surface

d_n – Day of the year (Jan 1 = 0; Dec 31 = 364)

E   – Irradiance on (object) in (W/m^2)

F_a – Forward to total scattering ratio for the aerosol

$H_{o\lambda}$ – Solar irradiance at the top of the atmosphere (W/m^2)

I   – Intensity in (W/Sr)

$I_{a\lambda}$ – Aerosol scattered component on a horizontal surface

$I_{d\lambda}$ – Direct normal component of solar radiation

$I_{r\lambda}$ – Rayleigh scattered component on a horizontal surface

$I_{s\lambda}$ – Scattered or diffuse component on a horizontal surface

L   – Radiance of (object) in $(W/m^2\text{-}Sr)$

M   – Relative air mass in atmosphere

    or Reflected irradiance from (object) in (W/m^2)

M_o – Relative air mass for ozone in atmosphere

M'   – Pressure corrected relative air mass in atmosphere

O_3 – Ozone amount in a vertical path (cm)

P   – Surface pressure in millibars (mb)

P_o – Reference surface pressure, 1013.0 mb

R   – Actual Earth-Sun distance

R_m – Mean Earth-Sun distance

R_s – The distance between the target location and the satellite location

T_{a_λ} – Transmittance function for aerosol extinction

T_{o_λ} – Transmittance function for ozone absorption

T_{u_λ} – Transmittance function for the uniformly mixed gases (Oxygen and carbon dioxide)

T_{w_λ} – Transmittance function for water vapor

W_o – Single scattering albedo

w – Precipitable water in a vertical path (cm)

α_n – Turbidity exponent (Angstrom formalism)

β_n – Turbidity coefficient (Angstrom formalism)

θ_o – Expression defined in terms of the day of the year for use in computing the astronomical factors

θ_1 – Solar zenith angle relative to a flat surface

θ_2 – Solar zenith angle relative to the normal of a tilted plane

θ_3 – Satellite zenith angle relative to the normal of a tilted plane

θ_4 – Satellite zenith angle relative to a flat surface

λ – Wavelength in micrometers

    or   Longitude

π – Pi (3.14159)

ρ – Albedo or reflectance of (object)

ρ_g – Albedo of the ground

ρ_s – Albedo of the air

Φ – Flux in (Watts)

BIBLIOGRAPHY

Aida, M. "Scattering Of Solar Radiation As A Function Of Cloud
    Dimensions And Orientation". Journal of Quantitative Spectroscopy
    And Radiative Transfer, 17, 1977, pp. 303-310.

Air Weather Service (AWS), U.S. Air Force. Use of the Skew T Log P
    Diagram in Analysis and Forecasting. AWS Manual 15 July 1969,
    pp. 105-124.

Anderson, A. (Editor) The Raman Effect; Volume 1: Principles. Marcel
    Dekker, Inc., New York, 1971.

Angstrom, A. "Techniques Of Determining The Turbidity Of The
    Atmosphere. Tellus, 13, 1961, pp. 214-223.

Angstrom, A. "The Parameters Of Atmospheric Turbidity". Tellus, 16,
    1964, pp. 64-75.

Atwater, M.A. and Ball, J.T. "Review Paper, A Numerical Solar Radiation
    Model Based On Standard Meteorological Observations". Solar Energy,
    21, 1978, pp. 163-170.

Atwater, M.A. and Ball, J.T "A Surface Solar Radiation Model For Cloudy
    Atmospheres". Monthly Weather Review, April 1981, pp. 878-888.

Atwater, M.A. and Ball, J.T. "Effects Of Clouds On Insolation Models".
    Solar Energy, 27, 1981, pp. 37-44.

Atwater, M.A. and Brown, P.S. "Numerical Computations Of The Latitudinal
    Variation Of Solar Radiation For An Atmosphere Of Varying Opacity".
    Journal Of Applied Meteorology, 13, March 1974, pp. 289-297.

Ball, J.T.; Atwater, M.A.; and Thoren, S.J. "Sensitivity Of Computed
    Incoming Solar Radiation At The Surface To Cloud Analyses". Monthly
    Weather Review, April 1981, pp. 889-894.

Barbaro, S.; Coppolino, S.; Leone, C.; and Sinagra, E. "An Atmospheric
    Model For Computing Direct and Diffuse Solar Radiation". Solar
    Energy, 22, 1979, pp. 225-228.

Bendt, P.; Collares-Pereira, M.; and Rabl, A. "The Frequency
    Distribution Of Daily Insolation Values". Solar Energy, 27, 1981,
    pp. 1-5.

Bird, R.E. "A Simple Solar Spectral Model For Direct-Normal And
    Diffuse Horizontal Irradiance". Solar Energy, 32(4), 1984,
    pp. 461-471.

Bird, R.E. and Riordan, C. Simple Solar Spectral Model for Direct and Diffuse Irradiance on Horizontal and Tilted Planes at the Earth's Surface for Cloudless Atmospheres. Solar Energy Research Institute, Golden, Colorado; SERI/TR-215-2436, December 1984.

Bird, R.E. and Hulstrom, R.L. TECHNICAL NOTE, "Availability of SOLTRAN 5 Solar Spectral Model". Solar Energy, 30(4), 1983, p. 379.

Bird, R.E.; Hulstrom, R.L.; and Lewis, L.J. "Terrestrial Solar Spectral Data Sets". Solar Energy, 30(6), 1983, pp. 563-573.

Bird, R.E. and Hulstrom, R.L. "Solar Spectral Measurements And Modelling", January 1981, Solar Research Institute (SERI), SERI/TR-642-1013. Prepared for the U.S. Department of Energy; Contract No. EG-77-C-01-4042

Bird, R.E. and Hulstrom, R.L. "A Simplified Clear Sky Model for Direct and Diffuse Insolation on Horizontal Surfaces". February 1981, Solar Energy Research Institute (SERI), SERI-TR-642-7611. Prepared for the U.S. Department of Energy; Contract No. EG-77-C-01-4042

Bird, R.E. and Hulstrom, R.L. "Review, Evaluation, and Improvement of Direct Irradiance Models". Journal of Solar Energy Engineering, 103, August 1981, pp. 182- 192

Bird, R.E. and Hulstrom, R.L. "Application of Monte Carlo Techniques to Insolation Characterization and Prediction", July 1979, Solar Energy Research Institute (SERI), RR-36-306. Prepared for the U.S. Department of Energy; Contract No. EG-77-C-01-4042

Bird, R.E.; Hulstrom, R.L.; Kliman, A.W.; and Eldering, H.G. "Solar Spectral Measurements in the Terrestrial Environment. Applied Optics, 21(8), 15 April 1982, pp. 1430-1436.

Bird, R.E. and Riordan, C. "Simple Solar Spectral Model for Direct and Diffuse Irradiance on Horizontal and Tilted Planes at the Earth's Surface for Cloudless Atmospheres". Journal of Climate and Applied Meteorology, 25(1), January 1986, pp. 87-97.

Bott, A. and Zdunkowski, W. "A Fast Solar Radiation Transfer Code for Application in Climate Models". Archives of Meteorology, Geophysics, and Bioclimatology, Series B, 33, 1983, pp. 163-174.

Bowker, D.E.; Davis, R.E.; Myrick, D.L.; Stacy, K. and Jones, W.T. "Spectral Reflectances of Natural Targets for Use in Remote Sensing Studies". NASA Reference Publication 1139, June 1985; NASA Scientific and Technical Information Branch.

Braun, J.E. and Mitchell, J.C. "Solar Geometry for Fixed and Tracking Surfaces". Solar Energy, 31(5), 1983, pp. 439-444.

Brine, D.T. and Iqbal, M. "Diffuse and Global Solar Spectral Irradiance Under Cloudless Skies". Solar Energy, 30(5), 1983, pp. 447-453.

Bruhl and Zdunkowski, W. "An Approximate Calculation Method for Parallel and Diffuse Solar Irradiance on Inclined Surfaces in the Presence of Obstructing Mountains or Buildings". Archives for Meteorology, Geophysics, and Climatology, Series B, 32, 1983, pp. 111-129.

Bruno, R. TECHNICAL NOTE: "A Correction Procedure for Separating Direct and Diffuse Insolation on a Horizontal Surface". Solar Energy, 20(1), 1978, pp. 97-100.

Buckius, R.O. and King, R. "Diffuse Solar Radiation on a Horizontal Surface for a Clear Sky". Solar Energy, 21, 1978, pp. 503-509.

Castagnoli, C; Giraud, C; Longhetto, A.; Morra, O. and Civitano, L. "Correlation Between Normal Direct Radiation and Global Radiation Depending on Cloudiness". Solar Energy, 28(4), 1982, pp. 289-292.

Chen, T.S. and Ohring, G. "On the Relationship Between Clear-Sky Planetary and Surface Albedos". Journal of the Atmospheric Sciences, 41(1), January 1984, pp. 156-158.

Choudhury, B.J. "A Parameterized Model for Global Insolation Under Partially Cloudy Skies". Solar Energy, 29(6), 1982, pp. 479-486.

Choudhury, B.J. and Chang, A.T.C. "The Albedo of Snow for Partially Cloudy Skies". Boundary-Layer Meteorology, 20, 1981, pp. 371-389.

Cole, R.J. TECHNICAL NOTE: "The Longwave Radiation Incident Upon Inclined Surfaces". Solar Energy, 22, 1979, pp. 459-462.

Crosigani, B; Paolo, D.P; and Bertolotti, M. Statistical Properties of Scattered Light. Academic Press, New York, 1975, p. 212.

Danielson, R.E. and Moore, D.R. "The Transfer of Visible Radiation Through Clouds". Journal of the Atmospheric Sciences, 26, September 1969, pp. 1078-1987.

Dave, J.V. "Extensive Datasets of the Diffuse Radiation in Realistic Atmospheric Models with Aerosols and Common Absorbing Gases". Solar Energy, 21, 1978, pp. 361-369.

Dave, J.V. and Braslau, N. "Effect of Cloudiness on the Transfer of Solar Energy Through Realistic Model Atmospheres". Journal of Applied Meteorology, 14, April 1975, pp. 388-395.

Dave, J.V. "Validity of the Isotropic-Distribution Approximation in Solar Energy Estimations". Solar Energy, 19, 1977, pp. 331-333.

Davies, J.A. and McKay, D.C. "Estimating Solar Irradiance and Components". Solar Energy, 29(1), 1982, pp. 55-64.

Davies, R. "The Effect of Finite Geometry on the Three-Dimensional Transfer of Solar Irradiance in Clouds". Journal of the Atmospheric Sciences, 35, September 1978, pp. 1712-1725.

Davis, J.M.; Cox, S.K.; and McKee, T.B. "Total Shortwave Characteristics of Absorbing Finite Clouds". Journal of the Atmospheric Sciences, 36, March 1979, pp. 508-509.

Davis, J.M.; Cox, S.K.; and McKee, T.B. "Vertical and Horizontal Distributions of Solar Absorption in Finite Clouds". Journal of the Atmospheric Sciences, 36, October 1979, pp. 1976-1984.

Deirmendjian, D. "Scattering and Polarization Properties of Water, Clouds and Hazes in the Visible and Infrared". Applied Optics, 3(2), February 1964, pp. 187-196.

Department of Atmospheric and Oceanic Science, University of Michigan. Solar Energy Measurements and Instrumentation Summer Training Course, July 9-10, 1979.

Dogniaux, R.; Grueter, J.W.; Kasten, F.; Page, J.K.; C. Perrin De Brichambaut; Treble, F.C. and Palz, W. "Solar Meteorology (Units and Symbols)". International Journal of Solar Meteorology, 2, 1984, pp. 249-255.

Duggin, M.J. "Simultaneous Measurement of Irradiance and Reflected Radiance in Field Determination of Spectral Reflectance". Applied Optics, 20(22), 15 November 1981, pp. 3816-3818.

Engels, J.D.; Clark, J.A. and Pollack, S.M. LETTERS TO THE EDITOR: "The Probability Distribution of Terrestrial Irradiation", Solar Energy, 26, 1981, p. 471.

Engels, J.D.; Pollack, S.M. and Clark, J.A. TECHNICAL NOTE: "Observations on the Statistical Nature of Terrestrial Irradiation". Solar Energy, 26, 1981, pp. 91-92.

Ezeilo, C.C. TECHNICAL NOTE: "Effective Radiative Disc Radius of the Sun". Solar Energy, 19, 1977, p. 387.

Fiegelson, E.M. (Editor) Radiation in a Cloudy Atmosphere. D. Reidel Publishing Company, Dordrecht, Holland, 1984, p. 293.

Fiegelson, E.M. "Preliminary Radiation Model of a Cloudy Atmosphere: Part I - Structu e of Clouds and Solar Radiation". Atmospheric Physics, 51, 1978, pp. 203-229.

Fleagle, R.G. and Businger, J.A. An Introduction to Atmospheric Physics, Academic Press, New York, 1963, p. 345.

Goldberg, B. and Klein, K.H. "A Model for Determining the Spectral Quality of Daylight on a Horizontal Surface at Any Geographic Location". Solar Energy, 24, 1980. pp. 351-357.

Goldberg, B. and Klein, K.H. "Variations in the Spectral Distribution of Daylight at Various Geographical Locations on the Earth's Surface". Solar Energy, 19, 1977, pp. 3-13.

Green, A.E.S.; Sawada, T. and Shettle, E.P. "The Middle Ultraviolet Reaching the Ground". Photochemistry and Photobiology, 19, 1974, p. 251.

Grether, D.; Evans, D.; Hunt, A; and Wahlig, M. "The Effect of Circumsolar Radiation on the Accuracy of Pyrheliometer Measurements of the Direct Solar Radiation": Report prepared for the U.S. Department of Energy by Lawrence Berkeley Laboratory, University of California, Energy and Environment Division, May 1981.

Griggs, M. "Aircraft Measurements of Albedo and Absorption of Stratus Clouds, and Surface Albedos". Journal of Applied Meteorology, 7, December 1968, pp. 1012-1017.

Gube, M.; Schmetz, J. and Raschke, E. "Solar Radiative Transfer in a Cloud Field". Contribution to Atmospheric Physics, 53(1), February 1980, pp. 24-34.

Guzzi, R; Veccho, G.L.; Rizzi, R. and Scalabrin, G. "Experimental Validation of a Spectral Direct Solar Radiation Model", Solar Energy, 31(4), 1983, pp. 359-363.

Hansen, J.E. "Exact and Approximate Solutions for Multiple Scattering by Cloudy and Hazy Planetary Atmospheres". Journal of the Atmospheric Sciences, 26, May 1969, pp. 478-487.

Hansen, J.E. "Multiple Scattering of Polarized Light in Planetary Atmospheres, Part I: The Doubling Method". Journal of the Atmospheric Sciences, 28, January 1971, pp. 120-125.

Hansen, J.E. "Multiple Scattering of Polarized Light in Planetary Atmospheres, Part II: Sunlight Reflected by Terrestrial Water Clouds". Journal of the Atmospheric Sciences, 28, November 1971, pp. 1400-1426.

Hansen, J.E. and Travis, L.D. "Light Scattering in Planetary Atmospheres". Space Science Reviews, 16, 1974, pp. 527-610.

Hansen, V. "Determination of Atmospheric Turbidity Parameters from Spectral Solar Radiation Measurements". Archives of Meteorology, Geophysics, and Bioclimatology, Series B, 22, 1974, pp. 301-308.

Hatfield, J.L.; Giorgis, R.B.; and Flocchini, R.G. "A Simple Solar Radiation Model for Computing Direct and Diffuse Spectral Fluxes". Solar Energy, 27(4), 1981, pp. 323-329.

Haurwitz, Bernhard. "Insolation in Relation to Cloud Type". Journal of Meteorology, 3, December 1946, pp. 123-124.

Haurwitz, Bernhard. "Insolation in Relation to Cloud Type". Journal of Meteorology, 5, June 1948, pp. 110-113.

Hay, J.E. "A Revised Method for Determining the Direct and Diffuse Components of the Total Short-wave Radiation". Atmosphere, 14(4), 1976, pp. 278-287.

Hering, W.S. "An Operational Technique for Estimating Visible Spectrum Contrast Transmittance", June 1981, Prepared for Air Force Geophysics Laboratory, Hanscom AFB, Massachusetts 01731, AFGL-TR-81-0198, p. 26.

Hobbs, P.V. and Deepak, A. Clouds Their Formation, Optical Properties, and Effects. Academic Press, New York, 1981.

Hood, J.M. and Cruse, T.J. "A Sun and Moon Ephemeris Generation Computer Program for Geophysical Use"; Research and Development Report 1104, U.S. Navy Electronics Laboratory, San Diego, California, 2 April, 1962.

Hooper, F.C. and Brunger, A.P. "A Model for the Angular Distribution of Sky Radiance". Journal of Solar Energy Engineering, 102, August 1980, pp. 196-202.

Ideriah, F.J.K. "A Model for Calculating Direct and Diffuse Solar Radiation". Solar Energy, 26, 1981, pp. 447-452.

Iqbal, M. An Introduction to Solar Radiation. Academic Press, New York, New York, 1983, p. 386.

Iqbal, M. TECHNICAL NOTE: "Estimation of the Monthly Average of the Diffuse Component of Total Insolation on a Horizontal Surface". Solar Energy, 20, 1977, pp. 101-105.

Iqbal, M. "Hourly vs. Daily Method of Computing Insolation on Inclined Surfaces". Solar Energy, 21, 1978, pp. 485-489.

Iqbal, M. "Prediction of Hourly Diffuse Solar Radiation from Measured Hourly Global Radiation on a Horizontal Surface". Solar Energy, 24, 1980, pp. 491-503.

Iribarne, J.V. and Godson, W.L. Atmospheric Thermodynamics. D. Reidel Publishing Company, Boston, Massachusetts, 1973, p. 222.

Janssen, L.H. anc van Shie, J. "Frequency of Occurrence of Transmittance in Several Wavelength Regions During a Three-year Period". Applied Optics, 21(12), 15 June 1982, pp. 2215-2223.

Jess, S.L. Introduction to Theoretical Meteorology. Holt, Rinehart, and Winston, New York, 1959, p. 362.

Jimenez, J.I. and Castro, Y. "Solar Radiation on Sloping Surfaces With Different Orientations in Granada, Spain". Solar Energy, 28(3), 1982, pp. 257-262.

Joseph, J.H. and Wiscombe, W.J. "The Delta-Eddington Approximation for Radiative Flux Transfer". Journal of Atmospheric Sciences, 33, December 1976, pp. 2452-2459.

Justus, C.G. and Paris, M.V. "A Model for Solar Spectral Irradiance and Radiance at the Bottom and Top of a Cloudless Atmosphere". Journal of Climate and Applied Meteorology, 24(3), March 1985, pp. 193-205.

Justus, C.G. and Paris, M.V. "A Model for Solar Spectral Irradiance at the Bottom and Top of a Cloudless Atmosphere", submitted to Journal of Climate and Applied Meteorology, 1984.

Kattawar, G.W. and Plass, G.N. "Influence of Particle Size Distribution on Reflected and Transmitted Light from Clouds". Applied Optics, 7(5), May 1968, pp. 869-878.

Kasten, F. and Czeplak, G. "Solar and Terrestrial Radiation Dependent on the Amount and Type of Cloud". Solar Energy, 24, 1980, pp. 177-189.

Kerker, M. The Scattering of Light and Other Electromagnetic Radiation, Academic Press, New York, 1969, p. 666.

Khrgian, A.K. Cloud Physics. Translated from Russian, Israel Program for Scientific Translations, Jerusalem, 1962. Published by U.S. Department of Commerce and the National Science Foundation, Washington, D.C., 1963.

Kimes, D.S. "Dynamics of Directional Reflectance Factor Distributions for Vegetation Canopies". Applied Optics, 22(9), 1 May 1983, pp. 1364-1372.

King, R. and Buckius, R.O. TECHNICAL NOTE: "Direct Solar Transmittance for a Clear Sky". Solar Energy, 22, 1979, pp. 297-301.

Kitchen, M. and Squires, E.C. "Aircraft Observations of Solar Radiation in Cloud-Free Atmospheres". Boundary-Layer Meteorology, 29, 1984, pp. 321-342.

Klein, S.A. REVIEW PAPER: "Calculation of Monthly Average Insolation on Tilted Surfaces". Solar Energy, 19, 1977, pp. 325-329.

Kondratev, K.Y. Radiation Characteristics of the Atmosphere and the Earth's Surface. Translated from Russian. Published for the National Aeronautics and Space Administration and the National Science Foundation by Amerind Publishing Company, New Delhi, India, 1973, p. 580. (NASA TTF-678).

Kondratev, K.Y. "Radiation Regime of Inclined Surfaces". World Meteorological Organization, TECHNICAL NOTE No. 152, 1977, p. 82.

Kondratev, K.Y. and Manolova, M.P. "The Radiation Balance of Slopes". Solar Energy, 4(1), 1960, pp. 14-19.

Kneizys, F.X.; Shettle, E.P.; Gallery, W.O.; Chetwynd, J.H.; Abreu, L.W.; Selby, J.E.A.; Fenn, R.W.; and McClatchey, R.A. "Atmospheric Transmittance/Radiance: Computer Code LOWTRAN5". 21 February 1980. Optical Physics Division, Air Force Geophysics Laboratory, Hanscom AFB, Massachusetts 01731. AFGL-TR-80-0067.

Labs, Dietrich, Neckel, and Heinz. "Transformation of the Absolute Solar Radiation Data Into the 'International Practical Temperature Scale of 1968'". Solar Physics, 15, 1970, pp. 79-87.

Lacis, A.A. and Hansen, J.E. "A Parameterization for the Absorption of Solar Radiation in the Earth's Atmosphere". Journal of the Atmospheric Sciences, 31, January 1974, pp. 118-138.

Lamm, L.O. TECHNICAL NOTE: "A New Analytic Expression for the Equation of Time". Solar Energy, 26, 1981, p. 465.

LeBaron, B.L. and Dirmhirn, I. "Strengths and Limitations of the Liu and Jordan Model to Determine Diffuse from Global Irradiance". Solar Energy, 31(2), 1983, pp. 167-182.

Leckner, B. "The Spectral Distribution of Solar Radiation at the Earth's Surface - Elements of a Model". Solar Energy, 20, 1978, pp. 143-150.

Leighton, P.A. Photochemistry of Air Pollution. Academic Press, New York, 1961, p. 300.

Liou, Kuo-Nan. An Introduction to Atmospheric Radiation. Academic Press, New York, 1980, p. 392.

Liou, Kuo-Nan. "A Numerical Experiment on Chandrasekhar's Discrete-Ordinate Method for Radiative Transfer: Applications to Cloudy and Hazy Atmospheres". Journal of the Atmospheric Sciences, 30, October 1973, pp. 1303-1326.

Liou, Kuo-Nan. "On the Absorption, Reflection and Transmission of Solar Radiation in Cloudy Atmospheres". Journal of the Atmospheric Sciences, 33, May 1976, pp. 798-805.

Liou, Kuo-Nan and Sasamori, T. "On the Transfer of Solar Radiation in Aerosol Atmospheres". Journal of the Atmospheric Sciences, 32, November 1975, pp. 2166-2177.

Liou, Kuo-Nan and Wittman, G.D. "Parameterization of the Radiative Properties of Clouds". Journal of the Atmospheric Sciences, 36, July 1979, pp. 1261-1273.

Lillesand, T.M. and Kiefer, R.W. Remote Sensing and Image Interpretation. John Wiley and Sons, New York, 1979, p. 612.

Liu, B.Y.H. and Jordan, R.C. "The Interrelationship and Characterisctic Distribution of Direct, Diffuse, and Total Solar Radiation". Solar Energy, 4(3), 1960, pp. 1-19.

Lumb, F.E. "The Influence of Cloud on Hourly Amounts of Total Solar Radiation at the Sea Surface". Quarterly Journal of the Royal Meteorological Society, 90, 1964, pp. 493-495.

Ma, C.C.Y. and Iqbal, M. "Statistical Comparison of Models for Estimating Solar Radiation on Inclined Surfaces". Solar Energy, 31(3), 1983, pp. 313-317.

Major, G. "A Method for Determining the Circumsolar Sky Function". Tellus, 32, 1980, pp. 340-347.

Major, G. "On the Spectral Composition of Global Radiation". Solar Energy, 31(1), 1983, pp. 73-78.

Manes, A. and Ianetz, A. "Solar Irradiance on Non-Horizontal Surfaces at the East-Mediterranean Coastal Plain of Israel". Solar Energy, 31(1), 1983, pp. 3-19.

Mani, A. and Chacko, O. "Attenuation of Solar Radiation in the Atmosphere". Solar Energy, 24, 1980, pp. 347-349.

McCartney, E.J. Optics of the Atmosphere, Scattering by Molecules and Particles. John Wiley and Sons, New York, 1976.

McClatchey, R.A.; Fenn, R.W.; Selby, J.E.A.; Volz, F.E and Garing, J.S. "Optical Properties of the Atmosphere (Revised)". Air Force Cambridge Research Laboratories, AFCRL-71-0279, 10 May 1971, Environmental Research Papers, No. 354.

McKee, T.B. and Cox, S.K. "Scattering of Visible Radiation by Finite Clouds". Journal of the Atmospheric Sciences, 31, October 1974, pp. 1885-1892.

Mecherikunnel, A.T.; Gatlin, J.A.; and Richmond, J.C. "Data on Total and Spectral Solar Irradiance". Applied Optics, 22(9), 1 May 1983, pp. 1354-1359.

Mecherikunnel, A.T. and Duncan, C.H. "Total and Spectral Solar Irradiance Measured at Ground Surface". Applied Optics, 21(3), 1 February 1982, pp. 554-556.

Monteith, J.L. Principles of Environmental Physics. American Elsevier Publishing Company, New York, 1973.

Nack, M.L. and Curran, R.J. "Transformation of Surface Albedo to Surface-Atmosphere Albedo and Irradiance, and their Spectral and Temporal Averages". NASA Technical Memorandum 78057, August 1978, National Aeronautics and Space Administration, Goddard Space Flight Center, Greenbelt, Maryland 20771.

Neckel, H. and Labs, D. "Improved Data on Solar Spectral Irradiance from .33 to 1.25u". Solar Physics, 74, 1981, pp. 231-249.

Newell, T.A. TECHNICAL NOTE: "Simple Models for Hourly to Daily Radiation Ratio Correlations". Solar Energy, 31(3), 1983, pp. 339-342.

Norris, D.J. "Correlation of Solar Radiation with Clouds". Solar Energy, 12, 1968, pp. 107-112.

Norris, D.J. "Solar Radiation on Inclined Surfaces". Solar Energy, 10(2), 1966, pp. 72-76.

Otterman, J. "Plane With Protrusions as an Atmospheric Boundary". PREPRINT DRAFT

de Packh, D.C. TECHNICAL NOTE: "Transmission of Sunlight Through a Uniform Water-Drop Atmosphere". Solar Energy, 20, 1978, pp. 93-95.

Paltridge, G.W. and Barton, I.J. "Erythemal Ultraviolet Radiation Distribution Over Australia - The Calculations, Detailed Results and Input Data Including Frequency Analysis of Observed Australian Cloud Cover". Commonwealth Scientific and Industrial Research Organization (CSIRO), Division of Atmospheric Physics, Technical Paper No. 33, 1978, p. 48.

Paltridge, G.W. and Platt, C.M.R. Radiative Process in Meteorology and Climatology. Development in Atmospheric Science 5. Elsevier Scientific Publishing Company, New York, 1976, p. 318.

Parikh, J. "A Comparative Study of Cloud Classification Techniques". Remote Sensing of Environment, 6, 1977, pp. 67-81.

Penndorf, R. "Tables of the Refractive Index for Standard Air and the Rayleigh Scattering Coefficient for the Spectral Region Between 0.2 and 20.0 micrometers and Their Application to Atmospheric Optics". Journal of the Optical Society of America, 47(2), February 1957, pp. 176-182.

Plass, G.N. and Kattawar, G.W. "Influence of Single Scattering Albedo on Reflected and Transmitted Light from Clouds". Applied Optics, 7(2), February 1968, pp. 361-367.

Plass, G.N. and Kattawar, G.W. "Radiant Intensity of Light Scattered from Clouds". Applied Optics, 7(4), April 1986, pp. 699-704.

Radiation Commission; J. Noble (Editor). Standard Procedures To Compute Atmospheric Radiative Transfer in a Scattering Atmosphere. International Association of Meteorology and Atmospheric Physics (IAMAP), World Meteorological Organization (WMO), Geneva: Published by National Center for Atmospheric Research (NCAR), Boulder, Colorado, July 1977.

Rangarajan, S.; Swaminathan, M.S.; and Mani, A. "Computation of Solar Radiation from Observations of Cloud Cover". Solar Energy, 32(4), 1984, pp. 553-556.

Rao, C.R.N.; Takashima, T; Bradley, W.A.; and Lee, T.Y. "Near Ultraviolet Radiation at the Earth's Surface: Measurements and Model Comparisons". Tellus, 36B, 1984, pp. 286-293.

Reddy, S.J. "An Empirical Method for Estimating Sunshine from Total Cloud Amount". Solar Energy, 15, 1974, pp. 281-285.

Reed, R.K. "Comparison of Measured and Estimated Insolation Over the Easterm Pacific Ocean". Journal of Applied Meteorology, March 1982, pp. 339-341.

Revfeim, K.J.A. TECHNICAL NOTE: "An Interpretation of the Coefficients of the Angstrom Equation". Solar Energy, 31(5), 1983, pp. 415-416.

Richardson, A.J. "Relating Landsat Digital Count Values to Ground Reflectance for Optically Thin Atmospheric Conditions". Applied Optics, 21(8), 15 April 1982, pp. 1457-1464.

Ridgway, W.L. and Davies, R. "Interpretation of Spectral Reflection from Cloud Tops". Fifth Conference on Atmospheric Radiation, October 31-November 4, 1983, Baltimore, Maryland, American Meteorological Society, pp. 524-527.

Riordan, C.J. Comparisons of Modelled and Measured Spectral Solar Irradiance Data. Solar Energy Research Institute, Golden, Colorado; SERI/TR-215-2809, February 1986.

Robinson, D.A. and Kukla, G. "Albedo of a Dissipating Snow Cover". Journal of Climate and Applied Meteorology, 23, December 1984, pp. 1626-1634.

Robinson, N. (Editor). Solar Radiation. Elsevier Publishing Company, New York, 1966.

Sassi, G. TECHNICAL NOTE: "Some Notes On Shadow and Blockage Effects". Solar Energy, 31(3), 1983, pp. 331-333.

Sayigh, A.A.M. (Editor). Solar Energy Engineering. Academic Press, New York, New York, 1977, p. 498.

Schmetz, J. "On the Parameterization of the Radiative Properties of Broken Clouds". Tellus, 36A, 1984, pp. 417-432.

Schmetz, J. and Raschke, E. "An Application of a Two-Stream Approximation to Calculations of the Transfer of Solar Radiation in an Atmosphere With Fractional Cloud Cover". Contributions To Atmospherics, 52(3), August 1979, pp. 151-160.

Schneider, S.H. and Dickinson, R.E. "Parameterization of Fractional Cloud Amounts in Climatic Models: The Importance of Modeling Multiple Reflections". Journal of Applied Meteorology, 15, October 1976, pp. 1050-1056.

Shaw, G.E. "Atmospheric Turbidity in the Polar Regions". Journal of Applied Meteorology, 21, August 1982, pp. 1080-1088.

Shaw, G.E. "Sun Photometry". Bulletin of the American Meteorological Society, 64(1), January 1983, pp. 4-10.

Shaw, G.E. "Solar Spectral Irradiance and Atmospheric Transmission at Mauna Loa Observatory". Applied Optics, 21(11), 1 June 1982, pp. 2006-2011.

Sherry, J.E. and Justus, C.G. "A Simple Hourly All-Sky Solar Radiation Model Based on Meteorological Parameters". Solar Energy, 32(2), 1984, pp. 195-204.

Sherry, J.E. and Justus, C.G. "A Simple Hourly Clear-Sky Solar Radiation Model Based on Meteorological Parameters". Solar Energy, 30(5), 1983, pp. 425-431.

Stanhill, G. "Diffuse Sky and Cloud Radiation in Israel". Solar Energy, 10(2), 1966, pp. 96-101.

Stanhill, G. "The Distribution of Global Solar Radiation Over the Land Surfaces of the Earth". Solar Energy, 31(1), 1983, pp. 95-104.

Stephans, G.L. "The Transfer of Radiation Through Vertically Non-uniform Stratoculumus Water Clouds". Contributions To Atmospheric Physics, 49, 1976, pp. 237-253.

Stephans, G.L. "Radiation Profiles in Extended Water Clouds. I: Theory". Journal of the Atmospheric Sciences, 35, 1978, pp. 2111-2122.

Stephans, G.L. "Radiation Profiles in Extended Water Clouds. II: Parameterization Schemes". Journal of the Atmospheric Sciences, 35, 1978, pp. 2123-2132.

Stephans, G.L.; Paltridge, G.W. and Platt, C.M.R. "Radiation Profiles in Extended Water Clouds, III: Observations". Journal of the Atmospheric Sciences, 35, 1978, pp. 2133-2141.

Stephans, G.L. and Webster, P.J. "Cloud Decoupling of the Surface and Planetary Radiative Budgets". Journal of the Atmospheric Sciences, 41(4), February 1984, pp. 681-686.

Suckling, P.W. and Hay, J.E. "Modelling Direct, Diffuse and Total Solar Radiation for Cloudless Days". Atmosphere, 14(4), 1976, pp. 298-308.

Suckling, P.W. and Hay, J.E. "A Cloud Layer-Sunshine Model for Estimating Direct Diffuse and Total Solar Radiation". Atmosphere, 15(4), 1977, pp. 194-207.

Swain, P.H. and Davis, S.M. (Editors). Remote Sensing: The Quantitative Approach, McGraw-Hill Inc., New York, 1978, p. 396.

Sweat, M.E. and Carroll, J.J. "On the Use of Spectral Radiance Models to Obtain Irradiances on Surfaces of Arbitrary Orientation". Solar Energy, 30(4), 1983, pp. 373-377.

Szeicz, G. "Solar Radiation for Plant Growth". Journal of Applied Ecology, 11, 1974, p. 617.

Temps, R.C. and Coulson, K.L. "Solar Radiation Incident Upon Slopes of Different Orientations". Solar Energy, 19, 1977, pp. 179-184.

Thekaekara, M.P. "Extraterrestrial Solar Spectrum, 3000-6100 A at 1-A Intervals". Applied Optics, 13(3), March 1974.

Thomalla, E.; Kopke, P.; Muller, H. and Quenzel, H. "Circumsolar Radiation Calculated for Various Atmospheric Conditions". Solar Energy, 30(6), 1983, pp. 575-587.

Tsay, S. and Jayaweera, K. "Dependence of Radiative Properties of Arctic Stratus Clouds on Cloud Microstructure". Geophysical Research Letters, 10(12), December 1983, pp. 1188-1191.

Tschunko, H.F.A. "Derivation of the Point Spread Function". Applied Optics, 22(9), 1 May 1983, pp. 1413-1414.

Twomey, S. "The Effect of Cloud Scattering on the Absorption of Solar Radiation by Atmospheric Dust". Journal of the Atmospheric Sciences, 29, 1972, pp. 1156-1159.

Twomey, S. "Computations of the Absorption of Solar Radiation by Clouds:. Journal of the Atmospheric Sciences, 33, 1976, pp. 1087-1091.

Ulaby, F.T.; Moore, R.K.; Fung, A.K. Microwave Remote Sensing, Volumes I and II; Addison-Wesley Publishing Company, Reading, Massachusetts, 1981

U.S. Department of Energy. An Introduction to Meteorological Measurements and Data Handling for Solar Energy Applications, October 1980; U.S. Department of Commerce, National Technical Information Service.

Valovcin, F.R. "Spectral Radiance of Snow and Clouds in the Near Infrared Spectral Region", Air Force Geophysics Laboratory, Hanscom AFB, Massachusetts 01731, Optical Physics Division, Project 7670, 17 November 1978, AFGL-TR-78-0289, p. 46.

van de Hulst, H.C. Light Scattering by Small Particles. Chapman and Hill, New York, 1957.

Van Hemelruck, E. "The Oblateness Effect on the Extraterrestrial Solar Radiation". Solar Energy, 31(2), 1983, pp. 223-228.

Van Heuklon, T.K. "Estimating Atmospheric Ozone for Solar Radiation Models". Solar Energy, 22, 1979, pp. 63-68.

Walraven, R. "Calculating the Position of the Sun". Solar Energy, 20, 1978, pp. 393-397.

Weinman, J.A. and Guetter, P.J. "Penetration of Solar Irradiances Through the Atmosphere and Plant Canopies". Journal of Applied Meteorology, 11, February 1971, pp. 136-140.

Welch, R.M. "Radiation Calculations Based Upon Detailed Cloud Microphysics". Fifth Conference on Atmospheric Radiation, October 31-November 4, 1983, Baltimore, Maryland. Published by the American Meteorological Society, pp. 505-507.

Welch, R.M.; Cox, S.K. and Davis, J.M. Solar Radiation and Clouds, Meteorological Monographs Number 39, American Meteorological Society, Boston, Massachusetts 02108, May 1980, p. 96.

Welch, R.M.; Geleyn, J.F.; Zdunkowski, W.G.; and Korb, G. "Radiative Transfer of Solar Radiation in Model Clouds". Contributions to Atmospheric Physics, 49, 1976, pp. 128-146.

Welch, R.M. and Wielicki, B.A. "Stratocumulus Cloud Field Fluxes: The Effect of Cloud Shape". Journal of the Atmospheric Sciences, 41 (21), 1 November 1984, pp. 3085-3103.

Welch, R.M. and Zdunkowski, W.G. "The Radiative Characteristics of Noninteracting Cumulus Cloud Fields Part I: Parameterization for Finite Clouds". Contributions to Atmospheric Physics, 54(2), May 1981, pp. 258-272.

Welch, R.M. and Zdunkowski, W.G. "The Radiative Characteristics of Noninteracting Cumulus Cloud Fields Part II: Calculations for Cloud Fields". Contributions to Atmospheric Physics, 54(2), May 1981, pp. 273-285.

Welch, R.M. and Zdunkowski, W.G. "The Effect of Cloud Shape on Radiative Characteristics". Contributions to Atmospheric Physics, 54(4), November 1981, pp. 482-491.

Wendling, P. "Albedo and Reflected Radiance of Horizontally Inhomogeneous Clouds". Journal of the Atmospheric Sciences, 34, April 1977, pp. 642-650.

Weseley, M.L. "Simplified Techniques to Study Components of Solar Radiation Under Haze and Clouds". Journal of Applied Meteorology, 21, March 1982, pp. 373-383.

Wielicki, B.A. "Cloud Fraction and Size Distributions Derived Using Landsat Multispectral Scanner Data". Fifth Conference on Atmospheric Radiation, October 31-November 4, 1983, Baltimore, Maryland, American Metereological Society, pp. 268-271.

Wilkinson, B.J. TECHNICAL NOTE: "An Improved FORTRAN Program for the Rapid Calculation of the Solar Position". Solar Energy, 27, 1981, pp. 67-68.

Wiscombe, W.J. "The Delta-M Method: Rapid Yet Accurate Radiative Flux Calculations for Strongly Asymmetric Phase Functions". Journal of the Atmospheric Sciences, 34, 1977, pp. 1408-1422.

Wiscombe, W.J.; Welch, R.M. and Hall, W.D. "The Effects of Very Large Drops on Cloud Absorption. Part I: Parcel Models", Journal of the Atmospheric Sciences, 41(8), 15 April 1984, pp. 1336-1355.

Yamada, T. "A Review of Direct Solar Radiation to Inclined Surfaces". Radiological and Environmental Research Division Annual Report, Argonne National Laboratory, Atmospheric Physics, January-December, 1978, ANL-78-65, Part IV.

Yamamoto, G. "Direct Absorption of Solar Radiation by Atmospheric Water Vapor, Carbon Dioxide and Molecular Oxygen". Journal of the Atmospheric Sciences, 19, 1962, pp. 182-188.

Zdunkowski, W.G. "An Approximation Method for the Determination of Short-Wave Radiative Fluxes in Scattering and Absorbing Media". Contributions to Atmospheric Physics, 47, 1974, pp. 129-144.

Zdunkowski, W.G. and Korb, G. "An Approximative Method for the Determination of Short Wave Radiative Fluxes in Scattering and Absorbing Media". Contributions to the Atmospheric Physics, 49, 1974, pp. 129-144.

Zdunkowski, W.G.; Welch, R.M.; and Korb, G. "An Investigation of the Structure of Typical Two-Stream Methods for the Calculation of Solar Fluxes and Heating in Clouds". Contributions to Atmospheric Physics, 53(2), May 1980, pp. 147-166.